DEVELOPMENT OF SMALL MOLECULE PROBES FOR FLUORESCENCE AND PHOTOACOUSTIC MOLECULAR IMAGING

BY

HAO LI

THESIS

Submitted in partial fulfillment of the requirements
for the degree of Master of Science in Chemistry
in the Graduate College of the
University of Illinois at Urbana-Champaign, 2017

Urbana, Illinois

Adviser:

Assistant Professor Jefferson Chan

ABSTRACT

Molecular imaging enables the visualization, characterization and quantification of biochemical processes taking place at the molecular levels within intact living subjects. As such, it has become an indispensable tool for both basic research and biomedical applications. In particular, fluorescence imaging allows us to study molecular processes at the cellular level in real time because of its excellent sensitivity, high resolution and non-invasive nature. The use of reaction-based small-molecule fluorescent probes, a class of probes that exhibit differential fluorescence signals upon reacting with their intended target, has further rendered fluorescence imaging with good selectivity and higher sensitivity. Such reaction-based small-molecule fluorescent probes is often comprised of at least two components: a dye capable of generating a large fluorescence signal upon excitation and a target-specific reactive handle. The selection of both components are important as the dye often determines the spacial resolution as well as biocompatibility, whereas the reactive handle dictates selectivity and sensitivity. As such, finding new dye platforms as well as new reactive handles are essential to expanding the repertoire of reaction-based probes for non-invasive real-time fluorescence imaging. In Chapter 1, I will describe the development of a formaldehyde (FA)-responsive small-molecule fluorescent probe, formaldehyde probe 1 (FP1). Specifically, we utilized a FA-specific biorthogonal chemical transformation to render FP1 FA-specific. Moreover, we also developed a neutral, red-shifted fluorophore platform with exceptional photostability to enable the

real-time tracking of FA and in the hope of studying the long-term effect of FA in living systems.

While fluorescence imaging excels at studying cellular systems, its usage *in vivo* is challenging due to the limited imaging depth up to 1 mm as a result of light scatting. In other word, if the imaging target resides deeper than 1 mm, the outcoming fluorescence will scatter and hence erodes the resolution. As the thickness of the human skin varies from 0.5 to 4 mm depending on different parts of the human body, most optical methods including fluorescence imaging can only be applied *ex-vivo* or to study superficial subjects such as skin. On the other hand, photoacoustic imaging (PAI), an imaging technique based on the detection of ultrasonic waves generated by light absorption, circumvents this problem because it detects ultrasonic waves which scatters 3000 times less than light. As a result, PAI can reach several centimeters of depth penetration while retaining high special resolution. When coupled with small-molecule stimuli-responsive photoacoustic probes that yield a different PA signal upon activation by the molecular target, PAI becomes a versatile molecular imaging technique that holds great promise for both animal models studies and human diagnostics. In Chapter 2, I will describe the development of two copper(II)-responsive small-molecule photoacoustic probes APC-1 and APC-2. Specifically, we equipped both APCs with a 2-picolinic ester sensing module that is readily hydrolysed in the presence of Cu(II) but not by other divalent metal ions. Additionally, APC-1 and APC-2 were explicitly designed for ratiometric photoacoustic imaging by using an aza-

BODIPY dye scaffold exhibiting two spectrally resolved near-infrared absorbance bands, one below 700 nm and the other above, that are associated with the 2-picolinic ester capped and uncapped phenoxide forms, respectively. The ratiometric photoacoustic turn-on responses for APC-1 and APC-2 were verified using tissue-mimicking phantoms.

ACKNOWLEDGEMENTS

First I would like to thank my advisor Prof. Jefferson Chan whom I have learned much from. He is a knowledgeable and fearless scientist who guided me throughout my thesis process. Additionally, I want to thank Dr. Junlong Geng, Aaron Roth, Chelsea Anorma and Lukas Smaga for working with me on varies projects and offering me help as well as constructive insights. The same goes to the rest of the team who have been insightful colleges and great friends.

Next, I want to thank my girlfriend Jianing Li for her unconditional supports and help on both professional and personal levels. I appreciate her spending countless nights in the lab with me and coming to visit for most the weekends knowing that I was too busy to do the same. I thank her for the sacrifice she had to make so that I can pursue my dream and passion. The same goes to my families especially my parents and my grandparents. Without them this thesis would not have been possible,

I would also like to thank Dr. Keith Hoffman for helping me to get through the darkest time during my stay at UIUC. He is a great chemist and more importantly a great friend. He showed me through example how one could do such an amazing job at balancing the intrinsically conflicting roles of being a hardworking chemist and a father of four children. The content of what I learned from him is much beyond a thesis or any degree that is available.

Last but not least, I appreciate the professional insights I received from my former committee members, Prof. Wilfred van der donk, Prof. Yi Lu and Prof. Ralph Nuzzo. I also want to thank Dr. Dean Olson, Dr. Lingyang Zhu for their technical

assistant on using NMR, Dr. Furong Sun and Dr. Haijun Yao for their technical assistant on using MS. Finally, I want to thank our chemical biology staff members, Kara Metcalf, Lori Johnson, Jamison Lowe and Gayle Adkisson for their generous help at various occasions.

TABLE OF CONTENTS

CHAPTER 1: A REACTION-BASED FLUORESCENT PROBE FOR IMAGING OF FORMALDEHYDE IN LIVING CELLS 1

CHAPTER 2: PHOTOACOUSTIC PROBES FOR RATIOMETRIC IMAGING OF COPPER(II) 10

FIGURES, TABLES AND SCHEMES 18

REFERENCES 31

APPENDIX A-MATERIAL AND METHODS FOR CHAPTER 1 35

APPENDIX B-SYNTHESES FOR CHAPTER 1 39

APPENDIX C-SUPPLEMENTARY FIGURES FOR CHAPTER 1 53

APPENDIX D-MATERIAL AND METHODS FOR CHAPTER 2 80

APPENDIX E-SYNTHESES FOR CHAPTER 2 84

APPENDIX F-SUPPLEMENTARY FIGURES FOR CHAPTER 2..... 102

CHAPTER 1: A REACTION-BASED FLUORESCENT PROBE FOR IMAGING OF FORMALDEHYDE IN LIVING CELLS

1.1 BACKGROUND

Formaldehyde (FA) is a highly reactive carbonyl species that has potent capacity to crosslink DNA and proteins through the formation of stable methylene bridges and is often used as a tissue fixative and embalming agent. Exposure to exogenous FA via inhalation or ingestion poses a significant threat to human health. For instance, FA overload can damage the central nervous system leading to reduced performance in memory and cognitive abilities.[1] On the other hand, the endogenous production of FA is a normal physiological process mediated by enzymatic systems such as semicarbazide-sensitive amine oxidase (SSAO) that generate FA as well as opposing molecular mechanisms that remove it.[2,3] In the brains of healthy individuals, FA concentration is in the 0.2-0.4 mM range[4] and has been proposed to play a role in the storage, preservation, and retrieval of long-term memory through DNA demethylation cycles.[5] On the other hand, FA levels are known to be elevated in patients afflicted with neurodegenerative diseases such as Alzheimer's disease due to the overexpression of SSAO.[6] In this context, FA is neurotoxic and has been shown to degrade neuronal networks through the induction of hyperphosphorylation and polymerization of the tau protein.[7] Additionally, FA was proposed to induce *β*-amyloid misfolding and aggregation via crosslinking lysine residues (LyC6 and LyF8) present in *β*-amyloid.[8]

The material in Chapter 1 includes previously published work: Roth, A.; Li, H.; Anorma, C.; Chan, J. *J Am Chem Soc* **2015**, *137*, 10890. Figures and tables are adapted with permission from the authors.

To date, an assortment of methods including HPLC and radiometric assays have been developed to analyze levels of endogenous FA, albeit only from body fluids such as blood and urine.[9,10] Optical imaging is a powerful alternative because it can be used to image living systems noninvasively with excellent spatial resolution. Small-molecule probes that make use of biorthogonal chemical transformations have been employed to detect a variety of bioanalytes[11] ranging from gasotransmitters such as carbon monoxide[12,13] and hydrogen sulfide[14] to metal ions including iron[15] and zinc,[16] as well as carbonyl metabolites like methylglyoxal.[17] Such imaging agents exhibit high sensitivity, excellent selectivity, rapid response, good stability and negligible cytotoxicity; hence, they greatly facilitate the detection and tracking of the target analyte in living systems with minimal perturbation. However, prior to this work, no such imaging agents were available for live cell imaging of FA due to a lack of FA-specific biorthogonal chemical transformation.[18] For this reason, developing such chemical reaction was a crucial first step towards the development of a FA-responsive fluorescent probe. Moreover, we also aimed to develop a neutral, red-shifted fluorophore platform with exceptional photostability to enable the real-time tracking of FA and to study the long-term effect of FA in living systems.

1.2 RESULTS AND DISCUSSION

To this end, we present a new approach for the detection of FA in live cells through the development of Formaldehyde Probe 1 (FP1), a FA-responsive

fluorescent probe comprised of a fluorescent core (Figure 1.1, in black) and a FA reactive moiety (Figure 1.1, in blue).[19]

My main contribution towards this chapter was the development of a new julolidine-based silicon rhodol fluorescent scaffold for the construction of FP1. Rhodol dyes are privileged dye platforms because of their large extinction coefficient, high quantum yield, pH-insensitive emission and most importantly excellent photostability.[20] Rhodols that have absorption maxima at the 488- and 514-nm lines of the argon ion laser as well as the 546-nm line of the mercury arc lamp have been reported and used to develop reaction-based fluorescence probes.[21] However, a more red-shifted rhodol that absorbs at the 633-nm lines of the helium-neon laser was unavailable. The use of far-red excitation light is desirable for bioimaging because of the high penetration depth, minimal phototoxicity, and low autofluorescence.

The synthesis began with the choloromethylation of **1** in the presence of formaldehyde and hydrochloride gas, affording benzyl chloride **2** in 66% yield. *m*-Bromojulolidine **4** was synthesized by double alkylation of **3** with 1-bromo-3-chloropropane followed by cyclization. After screening varying amounts of different Lewis acids as well as optimizing reaction temperature, we found that **5** could be obtained in satisfactory yield via Friedel-Crafts alkylation of compound **4** with **2** in the presence of one equivalent of aluminum trichloride at low temperature. Finally, lithium-halogen exchange reaction afforded the double lithium adduct, which was then reacted with dimethyldichlorosilane and subsequently oxidized in air to give the desired silicon-xanthone **6** (Scheme 1.1).

The construction of the bottom indole moiety **12** began with the methyl carbamate formation from **7** in the presence of methyl choloroformate. Iodination of **8** with *N*-iodosuccinimide afforded **9**, which was then coupled to trimethylsilylacetylene via Sonogashira coupling. In the presence of sodium ethoxide, **10** was cyclized to give indole **11** which was methylated with methyl iodide to afford **12** (Scheme 1.2).

With both building blocks in hand, FP1 was synthesized beginning with the reaction between indole **12** and *tert*-butyllithium to afford a lithium adduct which was subsequently reacted with silicon xanthone **6**. Silicon rhodol **13** was obtained after sequential acid-mediated dehydration and BBr_3 demethylation reactions. The indole moiety was subjected to Vilsmeier-Haack formylation conditions to furnish carboxaldehyde **14** which was transformed to the homoallylic amine **15** with potassium allyltrifluoroborate in methanolic ammonia. Lastly, reductive amination with 4-nitrobenzaldehyde and triacetoxyborohydride yielded FP1 (Scheme 1.3). The photophysical properties of FP1 and the FA-turned-over product **14** were summarized in table 1.1. As expected, **14** absorbs right at the 633-nm line of the helium-neon laser with a large extinction coefficient and relatively high quantum yield. We further examined the photostability of FP1 towards repeated irradiation cycles and no decrease in fluorescence was observed after 100 scans at 25% laser power with a pinhole size of 1 airy unit (Figure C.1). Of note, imaging experiments described in this study were done using 3% laser power and thus, FP-1 exhibited negligible photobleaching under these conditions.

We then evaluated the fluorescence response of FP1 to FA. Prior to FA treatment, a 1 μM solution of FP1 is almost non-fluorescent, presumably due to the donor-excited photoinduced electron transfer (d-PeT) quenching effect of the 4-nitrobenzyl moiety; however, upon addition of FA, a dose-dependent fluorescence increase was observed (Figure C.2).[22] For example, upon treatment with 0.1 mM FA, a concentration below reported physiological levels in the brain, FP1 showed *ca.* 3.9-fold fluorescence increase after 3 hrs at 37 °C (Figure C.2), whereas 5 mM FA triggered a *ca.* 33.5-fold enhancement (Figure C.2a). To show the high selectivity of FP-1 towards formaldehyde over other biologically relevant aldehyde-containing species such as acetaldehyde, glucose, methylglyoxal, and pyridoxal, we incubated 1 μM FP1 with 1 mM of the various carbonyl species and observed only minimal cross-reactivity. Interestingly, FP1 exhibited a mere 1.9-fold fluorescence increase upon incubation with 1mM acetaldehyde after 3 hrs (Figure 1.2b), while 12.8-fold signal enhancement was observed when FP1 was treated with FA under the same conditions. Moreover, the stability of FP-1 in the presence of various cellular reductants and reactive oxygen species was examined and minimal fluorescence change was observed.

After demonstrating the excellent response to FA and exceptional selectivity *in vitro*, we tested the ability of FP1 to visualize FA in live cells. To this end, HEK293TN cells were incubated with 2 μM FP1 at 37 °C for 8 min and then treated with buffer alone or buffer containing FA at 1, 2.5, or 5 mM for 3 hrs. Prior to imaging, cells were allowed to recover in FA-free buffer for 30 min. As shown in Figure 1.3a-d and

quantified in Figure 1.3e, treatment of HEK293TN cells with FA resulted in a dose-dependent increase in fluorescence. At 5 mM FA, a nearly 3-fold fluorescence increase was observed. Likewise, a time-dependent turn-on response at each FA concentration was observed (Figures C.3 & C.4). Having established the utility of FP1 in live HEK293TN cells, we turned our attention to Neuroscreen-1 (NC) cells, a subclone of the PC12 cell line recognized as a standard neuronal model system.[23] As was the case with HEK293TN cells, incubation of NC cells with 1, 2.5, or 5 mM FA at 37 °C for 3 hrs gave rise to a robust dose-dependent signal enhancement of up to 2.3-fold (Figure 1.4a-d), as well as a time-dependent turn-on response at each concentration (Figures C.5 & C.6). We confirmed via HR-MS that the fluorescence increase resulted from conversion of FP1 to carboxyaldehyde **4** by reacting FP1 with 5 mM FA in the presence of cellular lysates (Figure C.7). Because FA is a powerful fixative, we performed cell viability assays to determine the cytotoxicity of FA under our experimental conditions. We employed a dye exclusion protocol utilizing trypan blue to selectively stain and distinguish dead cells from those that were viable. At 1 mM FA, only 5% of the HEK293TN cells were dead after 3 hrs, whereas nearly 35% of cells were no longer viable at 5 mM FA (Figure C.8a). NC cells on the other hand, were remarkably resilient when incubated with FA up to 2.5 mM. Specifically, at this concentration there was only *ca.* 12% loss in viability after 3 hrs. However, incubation with 5 mM FA resulted in considerable cell death (Figure C.8b). To further verify that the cell populations under investigation were indeed alive, DAPI, a cell permeable nuclear and chromosome counterstain, was employed to identify intact nuclei (Figure C.9). Owning to the

positive imaging results, we were motivated to perform a real-time imaging experiment in live NC cells. For this experiment, NC cells were stained with 1 μM FP1 as previously described followed by on-stage addition of 1 mM FA at 25 °C. Images were then acquired every min for 2 hrs. Under these conditions we observed a 1.3-fold fluorescence increase; however, we also noted a FA-induced cell rounding effect which could be reversed during a 30 min recovery period. It is essential to determine the cellular distribution of FP1 because enzymes that produce endogenous FA exhibit unique subcellular localization patterns. For example, SSAO is primarily localized to the plasma membrane.[24] Thus, we co-stained both HEK293TN and NC cells with ER-Tracker Green, LysoTracker Green DND-26, and MitoTracker Green FM, fluorescent indicators that are known to selectively stain the endoplasmic reticulum, lysosome, and mitochondria, respectively (Figures C.10 & C.11). From these imaging experiments, it was evident that FP1 stained the cytoplasm and the endoplasmic reticulum in both cell lines as shown by excellent fluorescence overlay with ER-Tracker Green. In contrast, FP1 did not co-localize with the lysosomal or mitochondrial stains. Additionally, we performed an assay to determine dye efflux properties. HEK293TN and NC cells were stained with 1 μM FP1 for 8 min and then washed with fresh dye-free buffer. Images were acquired after a 30 min recovery period and then again after 8 hrs. We found that there was no statistically significant decrease in fluorescence suggesting that FP1 is chemically stable and does not efflux into the cell media (data not shown).

To corroborate our confocal imaging data, we turned to flow cytometry because this high-throughput technique allows for the rapid quantification of large cell populations. As such, HEK293TN and NC cells were stained with FP1 as previously described and then incubated with 1, 2.5, and 5 mM FA for up to 3 hrs. As with confocal imaging, we observed a concentration- and time-dependent fluorescence signal enhancement (Figures C.12 & C.13). Indeed, there was a clear shift in the live cell population when FA was applied. Based on the median APC-A fluorescence intensity values (an APC-A filter set was used), treatment of HEK293TN cells with 5 mM FA at 37 °C for 3 hrs resulted in nearly a 2.5-fold turn-on, which is in agreement with the 2.9-fold turn-on from confocal imaging assays (Figure 1.3e). In contrast, NC cells incubated with 5 mM FA afforded a 4.2-fold increase by flow cytometry, whereas, only a 2.3-fold turn-on was noted using confocal microscopy (Figure 1.3e). This discrepancy can be attributed to the cytotoxicity of FA at this concentration which reduces the fluorescence of dead cells due to dye leakage. Thus, a lower apparent turn-on was recorded because it is difficult to image only viable cells in the presence of those that are dead.

1.3 CONCLUSIONS AND PERSPECTIVES

In summary, we have developed a new fluorescent probe, FP1, for imaging FA using the 2-aza-Cope sigmatropic rearrangement. FP1 is highly sensitive and selective towards FA wand was used to detect FA *in vitro* at concentrations below physiologically relevant concentrations. Additionally, FP1 is based on a new julolidine-

based silicon rhodol fluorescent scaffold which features an absorption maxima centered at 633 nm. This property enabled us to excite FP1 with the 633 nm helium-neon laser in both confocal microscopy and flow cytometry experiments. Because FP1 exhibits excellent photostability, metabolic stability and slow efflux, we were able to monitor intracellular FA concentration in real time. We envision that with the improvement on the relatively slow reaction kinetics of FP-1, our strategy will be able to elucidate the physiological roles of FA in live cells. Moreover, since our work was published, other groups have developed two-photon FA probes and positron emission tomography probes that have shown satisfactory results for the *in vivo* imaging of FA.[25,26] Ongoing efforts in our group are working towards the development of FA photoacoustic probes which will be reported in subsequent works.

CHAPTER 2: PHOTOACOUSTIC PROBES FOR RATIOMETRIC IMAGING OF COPPER(II)

2.1 BACKGROUND

The photoacoustic (PA) effect is a “light in, sound out” phenomenon where light absorption by an optical absorber thermoelastically generates pressure waves (sound). Based on the PA effect, photoacoustic tomography (PAT) was developed to construct high-resolution tomographic images by detecting the pressure wave resulting from light absorption event.[27,28] PAT holds great promise for medical diagnostic applications because it synergistically combines the excellent contrast of optical imaging with the deep-tissue penetration of ultrasonic imaging. In contrast to most of the purely optical methods such as fluorescence microscopy where the imaging depth is limited to 1 mm as defined by optical diffusion limit, PAT can reach several centimeter of depth penetration while retaining high special resolution. The increased penetration depth is achievable with PAT because sound scatters much less than light in biological tissues. Compared to ultrasonic imaging that relies on the relatively small difference in acoustic impedance which often leads to weak contrast in soft tissue, PAT offers much higher sensitivity of detection due to the high variance in the optical properties in different soft tissues. Moreover, because PAT does not involve ionizing radiation, it is less invasive compared to x-ray computed tomography (CT) or positron emission tomography (PET), for medical diagnostic applications.

The material in Chapter 2 includes published work: Li, H.; Zhang. P.; Smaga, L.; Hoffman. R.; Chan, J. J Am Chem Soc **2015**, 137, 15628. Figures are adapted with permission from the authors.

Indeed, PAT has been applied non-invasively to visualize and study various types of cancer,[29] cardiovascular diseases,[30] and abnormalities of microcirculation.[31]

Initially, endogenous contrasts such as hemoglobin, melanin and lipids were used in PAT to identify diseases such as cancer and to study physiological processes *in vivo*.[32,33] However, many diseases and processes have little or insufficient intrinsic PA contrast. As the demand for greater sensitivity and selectivity grew, exogenous contrasts based on small-molecule dyes, metal-based nanoparticles and carbon nanotubes have been developed.[34] These contrast agents enhance the PA signal of the target by specific localization via passive diffusion or receptor-mediated uptake pathways. While these contrast agents are able to provide structural and functional information, they can rarely reveal information at the molecular level. Indeed, there have only been several reports of PA probes that can be activated by a molecular target to elicit a change in the signal intensity.[35-37] We termed this versatile class of PA agents “acoustogenic probes” (APs), defined as small-molecule-based activatable imaging agents that respond selectively to stimuli (e.g., tumor biomarkers) to afford a PA signal enhancement. The molecular information obtained by these APs are invaluable for both basic research and personalized biomedicine such as tailoring treatment to a specific individual. As such, our goal was to develop new APs that will offer the unique opportunity to interrogate the complex biological role of a given molecular target in its native environment with minimal perturbation.

2.2 RESULTS AND DISCUSSION

To this end, we have developed two APs, APC-1 and APC-2 (Acoustogenic Probe for Copper(II)-1 and -2), for the ratiometric photoacoustic imaging of Cu(II).[38] For this project, we chose to detect Cu(II) because dysregulation of this important transition metal ion has been implicated in numerous diseases including Alzheimer's disease, an area studied by our group. [39] APC-1 comprised of a Cu(II)-responsive 2-picolinic ester moiety that can selectively chelates Cu(II) and activates the ester bond for hydrolysis (Figure 2.1a, in blue),[40,41] as well as a near-infrared (NIR) absorbing aza-BODIPY dye platform to generate the PA signal (Figure 2.1a, in black); while APC-2 has three extra sulfated ethylene glycol functional groups compared to APC-1 to enhance water solubility (Figure 2.1a, in red). We chose aza-BODIPY as the dye platform because it has maximum absorption in the NIR range (650-900 nm), a large extinction coefficient (> 10^4 $M^{-1}cm^{-1}$) and high photostability which are all desirable properties for bioimaging.

Additionally, we tuned the acidity of the aza-BODIPY phenol moiety by installing two ortho-chloro substituents. The resulting compound has an apparent pKa value of 4.35 which ensures full deprotonation of the phenol after APCs react with Cu(II) at physiological pH (Figure 2.1b). Compared to the phenol capped with 2-picolinic ester, the uncapped phenoxide product 6 has a much stronger electron donating capability and can red-shift the absorption maximum of the aza-BODIPY via internal charge transfer. Indeed, our aza-BODIPY dye exhibits dual-wavelength absorbance bands, one below 700 nm and the other above, which correspond to the capped 2-picolinic

ester probe (Figure 2.2, dotted line) and the uncapped phenoxide product **21**, respectively (Figure 2.2, solid line), thereby enabling ratiometric imaging of Cu(II).[42,43] This is very valuable because ratiometric response can account for artifacts such as undesirable variability in the signal intensity due to non-uniform dye accumulation or photobleaching. Our strategy involves irradiating APC-1 at both the blue-shifted (680 nm) and red-shifted (755 nm) absorbance maxima to generate two corresponding PA signals from which a ratio can be determined (Figure 2.1b). In the absence of Cu(II), the 2-picolinic ester moiety remains intact and thus, the absorbance at 680 nm will be larger than the signal at 755 nm resulting in a small 775/680 PA ratio. In contrast, when APC-1 is treated with Cu(II), the hydrolyzed product 6 will exhibit a decrease in the 680 nm band and a concomitant increase in the 755 nm absorbance maximum leading to a large 775/680 PA ratio. Normalization of the two PA ratios will result in the ratiometric turn-on response.

First, we synthesized APC-1 via an EDC-mediated coupling reaction between 2-picolinic acid and the dichlorophenol precursor **21** in 53% yield (Scheme E.1). However, because APC-1 is extremely hydrophobic, organic co-solvents or surfactants were required to achieve sufficient solubility to avoid dye aggregation in aqueous buffers since aggregation abolishes the dual-wavelength character requisite for ratiometric imaging. As such, we sought to develop a water soluble analog, first by employing previously reported strategies for enhancing the hydrophilicity of aza-BODIPY dyes such as PEGylation and incorporation of amino sulfonic acid moieties.[44,45] Unfortunately, these approaches were insufficient. Instead, we found

that three PEG-3 sulfate groups endowed excellent water solubility. As such, APC-2, was synthesized beginning from the dimerization of 4-nitro-1,3-diphenylbutan-1-one precursors **26** and **29** to afford the tetraarylazadipyrromethene intermediate **30**. To facilitate purification of **30** from homodimers of **26** and **29**, it was necessary to convert the primary alcohols to the corresponding *tert*-butyldimethylsilyl ether groups using TBS-Cl. The fully TBS-protected tetraarylazadipyrromethene **31** underwent facile boron chelation which was followed by desilylation using TBAF to afford aza-BODIPY **32** in 64% yield. Sulfation of 18 with SO_3-NMe_3 complex in DMF gave the PEG-3 sulfate intermediate **33** which was subjected to standard Tsuji-Trost deallylation conditions to give **34** in 74% yield over two steps. Lastly, the 2-picolinic ester was installed using EDC in water to afford APC-2 in 53% yield (Scheme 2.1).

We subsequently characterized the photophysical properties of APCs as summarized in table 2.1. Unless noted otherwise, all subsequent assays were done in PBS with 0.1% CrEL, a potent surfactant used as a vehicle to solubilize poorly-water soluble drugs. The absorbance maximum of APC-2 was centered at 697 nm (ε = 3.6 × 10^4 $M^{-1}cm^{-1}$), whereas the corresponding maximum of the phenoxide product **34** was at 767 nm (3.7 × 10^4 $M^{-1}cm^{-1}$) (Table 2.1). Because both compounds were non-fluorescent in PBS, there would be a greater extent of non-radiative decay which correlates to an overall stronger PA signal.[46] APC-2 was exceptionally photostable and only photobleached ~15% after continuous irradiation with 90% light intensity for 1 hr (Figure F.1).

We then turned our attention to evaluating the response of APC-2 to Cu(II) supplementation using UV-Vis spectroscopy. The absorbance of APC-2 and its phenoxide product **34** differ dramatically owing to the extended π-conjugation of the product. Specifically, APC-2 exhibits a large bathochromic shift (70 nm) of the λ_{max} from 697 nm to 767 nm (Figure 2.3a). As a consequence, the extinction coefficient at 767 nm increased from 0.2 × 10^4 $M^{-1}cm^{-1}$ to 3.7 × 10^4 $M^{-1}cm^{-1}$. This bathochromic shift enabled ratiometric imaging via irradiating APC-2 and its phenoxide product **34** at 697 nm and 767 nm. Indeed, APC-2 exhibited a normalized ratiometric turn-on response of 91.3- and 100.5-fold when treated with 1 and 10 equivalents of Cu(II), respectively (Figure 2.3b). Specifically, upon addition of Cu(II), we observed a slight decrease in the PA output at 697 nm and a large increase in the PA signal at 767 nm as a result if the Cu(II)-mediated hydrolysis of the 2-picolinic ester moiety (Figure 2.3c). Having established excellent responsiveness to Cu(II), we then evaluated the metal ion selectivity by treating solutions of APC-2 with various biologically relevant metal ions. The PA response of APC-2 was not affected by the presence of physiologically relevant concentrations of alkaline earth metals such as Mg(II) and Ca(II). Moreover, divalent transition metal ions like Mn(II), Fe(II), Co(II), Ni(II), and Zn(II) also did not induce a change in the PA signal. Finally, APC-2 was selective for Cu(II) over Cu(I), verifying its excellent metal and redox specificity (Figure 2.3d).

Lastly, we compared the PA and fluorescence emission properties of APC-2 as a function of imaging depth for potential deep-tissue imaging experiments. To this end, we developed a tissue-mimicking phantom made from milk, water and agarose. We

varied the ratio of milk to water to obtain a phantom where the scattering and absorption properties were at least 2x greater than that of an authentic biological tissue. Solutions of APC-2 in fluorinated ethylene propylene tubes were inserted into phantoms that cut to 1 cm thickness above and below the sample, and were then imaged with PA tomographer. In comparison to samples analyzed without the phantom overlay, the PA signal intensity only decreased by ~15% at this imaging depth (data not shown). In contrast, when a solution of APC-2 in 2:3 v/v EtOH:PBS (conditions that favor fluorescence emission) was imaged using an epi-fluorescence microscope, a 1 cm thick phantom overlay completely abolished the fluorescence signal (Figure F.10).

2.3 CONCLUSIONS AND PERSPECTIVES

In closing, we have developed the first small-molecule-based probe exclusively designed for ratiometric photoacoustic imaging. APC-2 displays an absorbance maximum in the NIR window, a large extinction coefficient (> 10^4 $M^{-1}cm^{-1}$), and is highly photostable. The unique dual-wavelength absorbance profile and low apparent pKa of the dichlorophenol moiety produces a large normalized turn-on response of 100.5-fold upon Cu(II) treatment, but not to other biologically relevant metal ions. We also highlight the strength of PA imaging by performing imaging experiments in the centimeter range using a highly scattering and absorbing tissue-mimicking phantom. APC-2 has the potential to enable deep-tissue molecular imaging with high resolution which is difficult to achieve with other imaging modalities. Additionally, the highly modular aza-BOPIDY platform used in the current study can be easily adapted to

sense other biologically important analytes beyond Cu(II) by simply installing alternative reactive triggers in the last step of the synthesis. Ongoing efforts in our group focused on developing other strategies to solubilize aza-BODIPY platform without adding charged residues, as well as expanding our platform to image other biologically important analytes that are also involved in the progression of Alzheimer's disease.

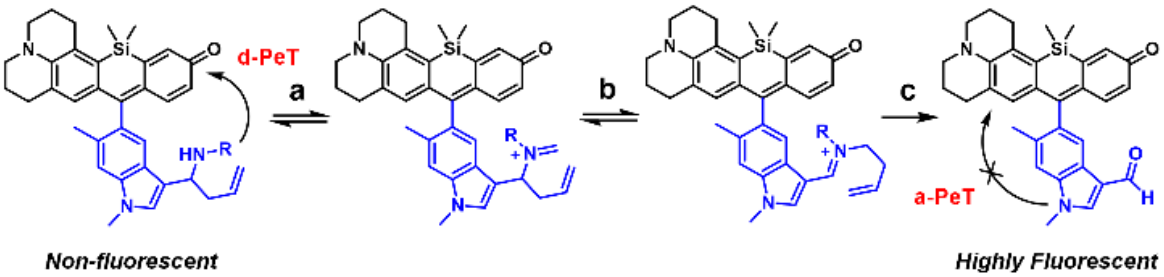

Figure 1.1. A new formaldehyde detection strategy based on the 2-aza-Cope sigmatropic rearrangement. The R group designates the 4-nitrobenzyl quencher moiety. Labels a, b, and c represent condensation, rearrangement, and hydrolysis steps, respectively.

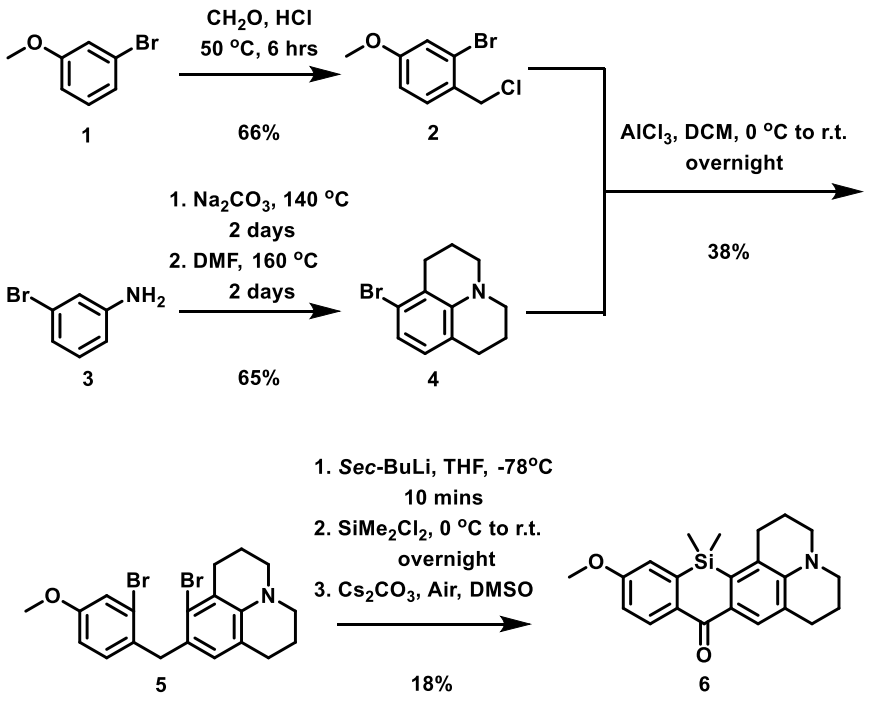

Scheme 1.1. Synthesis of julolidine-based silicon xanthone **6**.

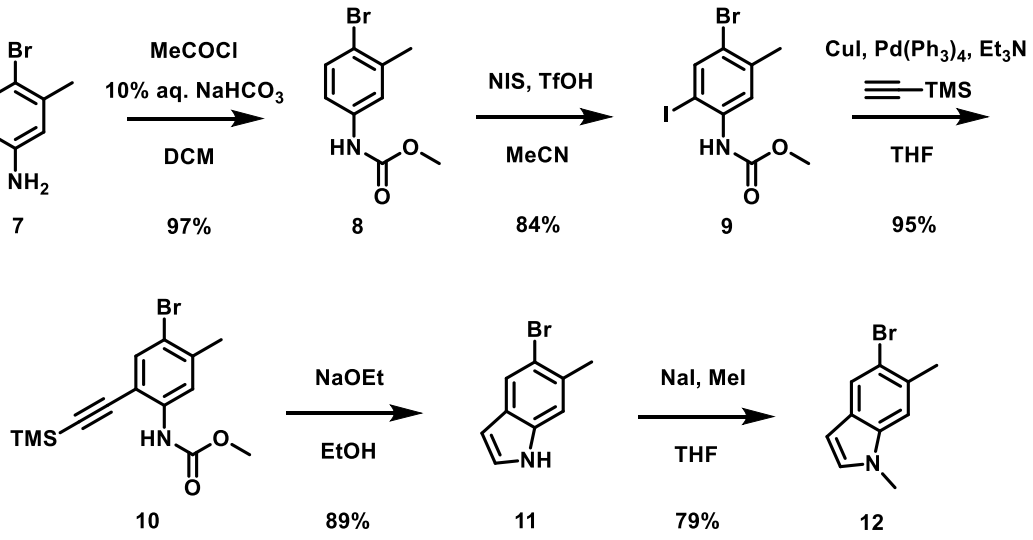

Scheme 1.2. Synthesis of indole **12**.

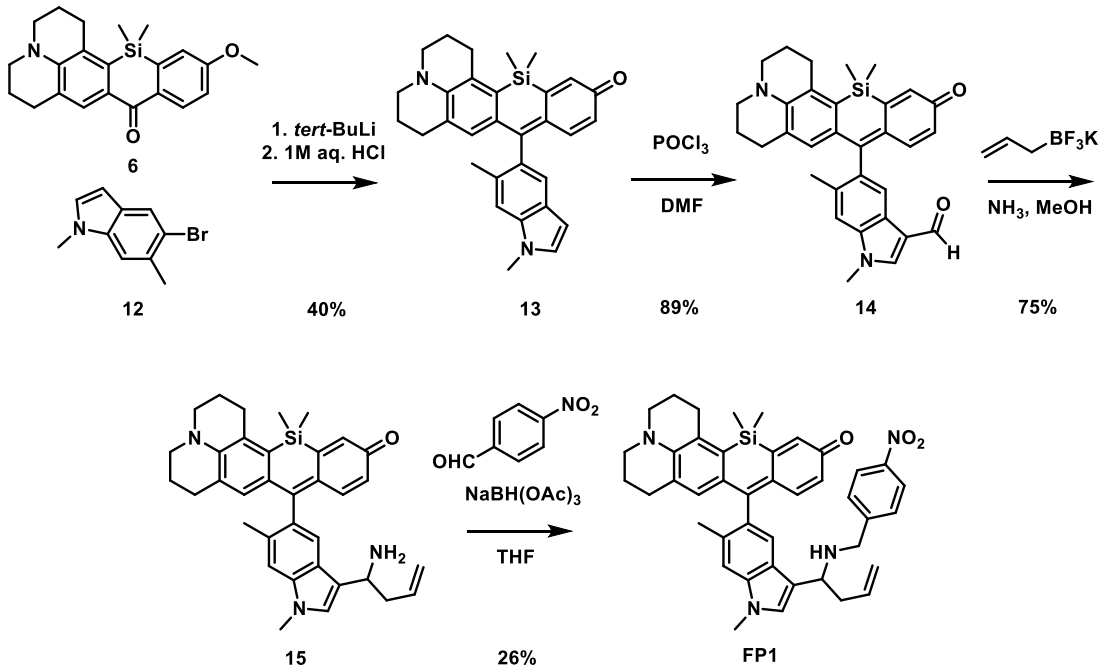

Scheme 1.3. Synthesis of FP1.

Compound	Φ	ε ($M^{-1}·cm^{-1}$)	λ_{abs} (nm)	λ_{em} (nm)
13	ND[a]	8.6×10^4	633	649
14	0.13	10.6×10^4	633	649
15	0.02	10.0×10^4	633	649
FP1	ND[a]	2.9×10^4	620	649

Table 1.1. Photophysical properties of compound **13**, **14**, **15** and FP1. a) ND = not determinable.

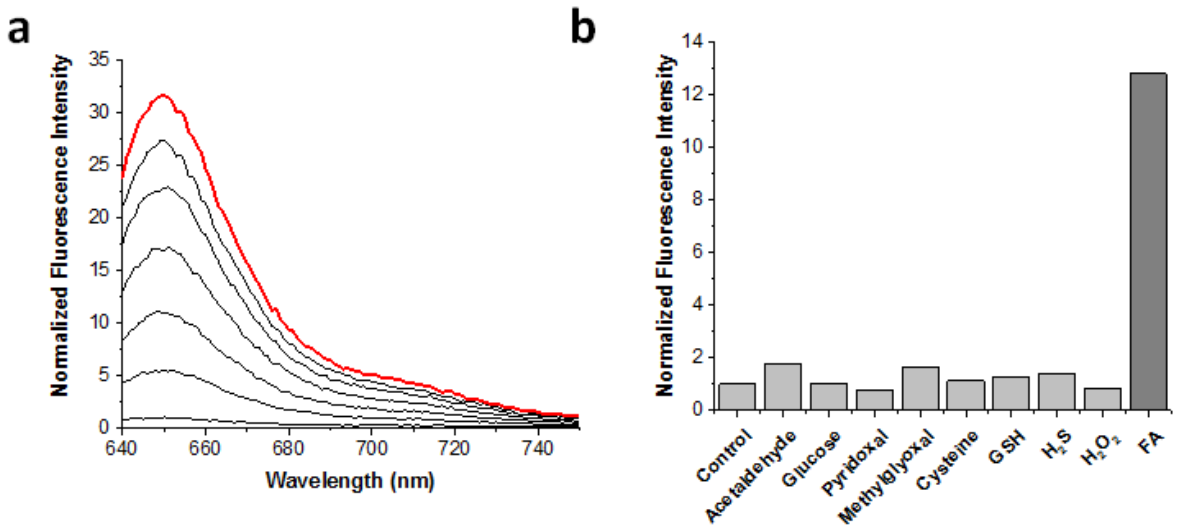

Figure 1.2. a) Fluorescence response of 1 µM FP1 to 5 mM FA in PBS buffer (pH 7.4) at 37 °C. FP1 was excited at 633 nm and the emission was collected between 640 and 750 nm. Time points on graph are 0, 30, 60, 90, 120, 150, and 180 min. b) Fluorescence response of 1 µM FP1 to biologically relevant aldehydes, reactive sulfur species, and hydrogen peroxide. Bars represent normalized fold-changes in response to treatment with each analyte listed at 1 mM for 3 hrs.

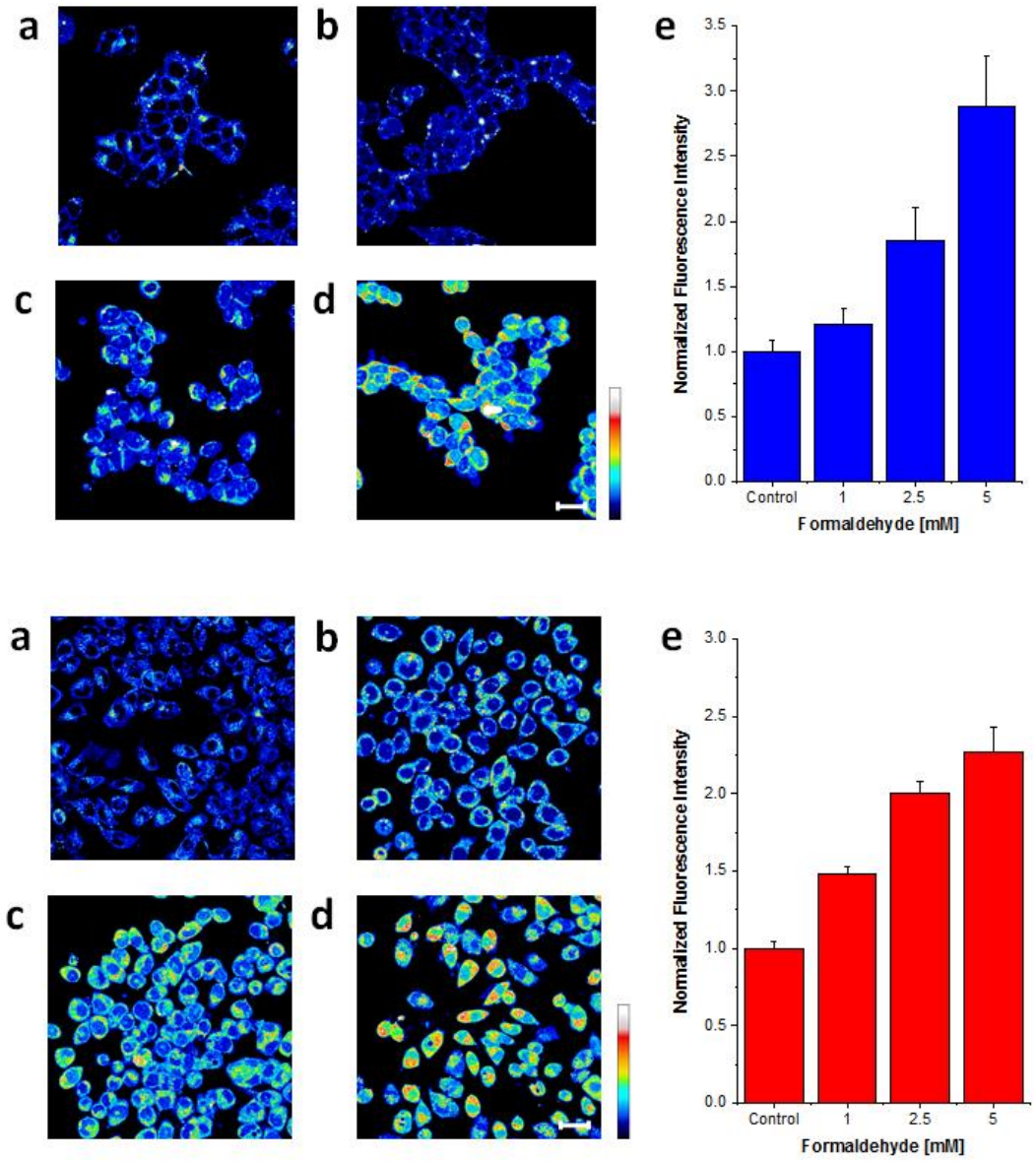

Figure 1.3. Confocal microscopy images acquired by irradiation of HEK293TN cells (top) and NC cells (bottom) treated with a) a DMEM vehicle control, b) 1 mM, c) 2.5 mM, and d) 5 mM FA for 3 hrs at 37 °C with the 633 nm HeNe laser. Scale bar represents 20 µm. e) Quantification of imaging data.

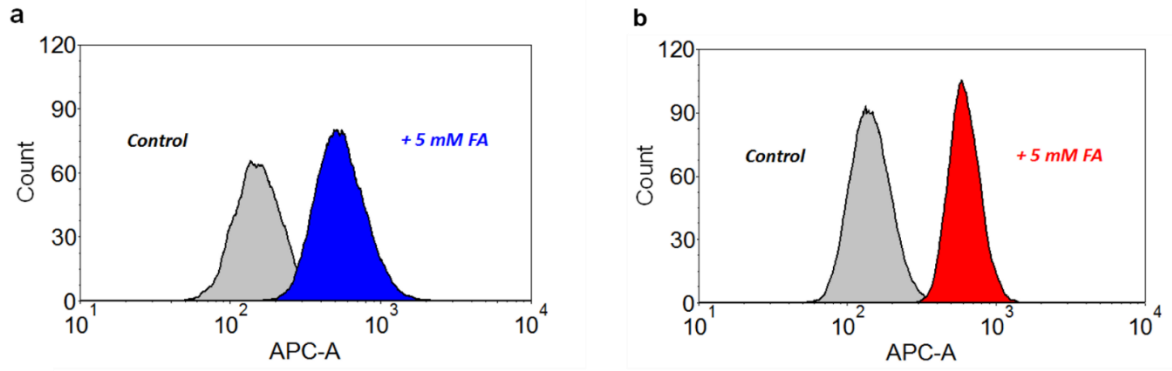

Figure 1.4. Flow cytometry analysis of a) HEK293TN and b) NC cells stained with 1 µM FP1 and incubated with 5 mM FA at 37 °C for 3 hrs. Excitation was provided by the 633 nm HeNe laser and a APC-A filter set was applied. Only live cells were counted.

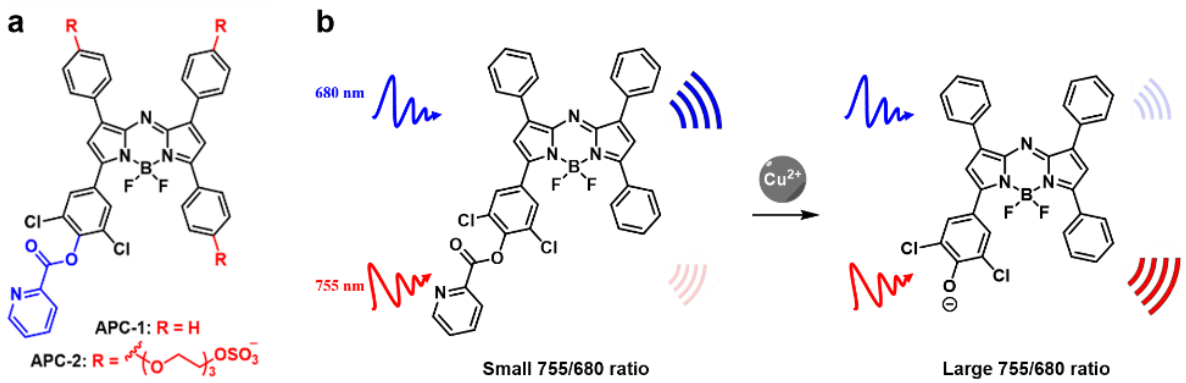

Figure 2.1. a) Chemical structure of APC-1 and APC-2. b) Proposed mechanism for ratiometric PA imaging of Cu(II). APC-1 (left) is excited at 680 nm (blue) and 755 nm (red) to afford two PA signals. In the presence of Cu(II), the 2-picolinic ester moiety is removed to yield **21**, resulting in a weaker PA signal at 680 nm and stronger PA signal 755 nm.

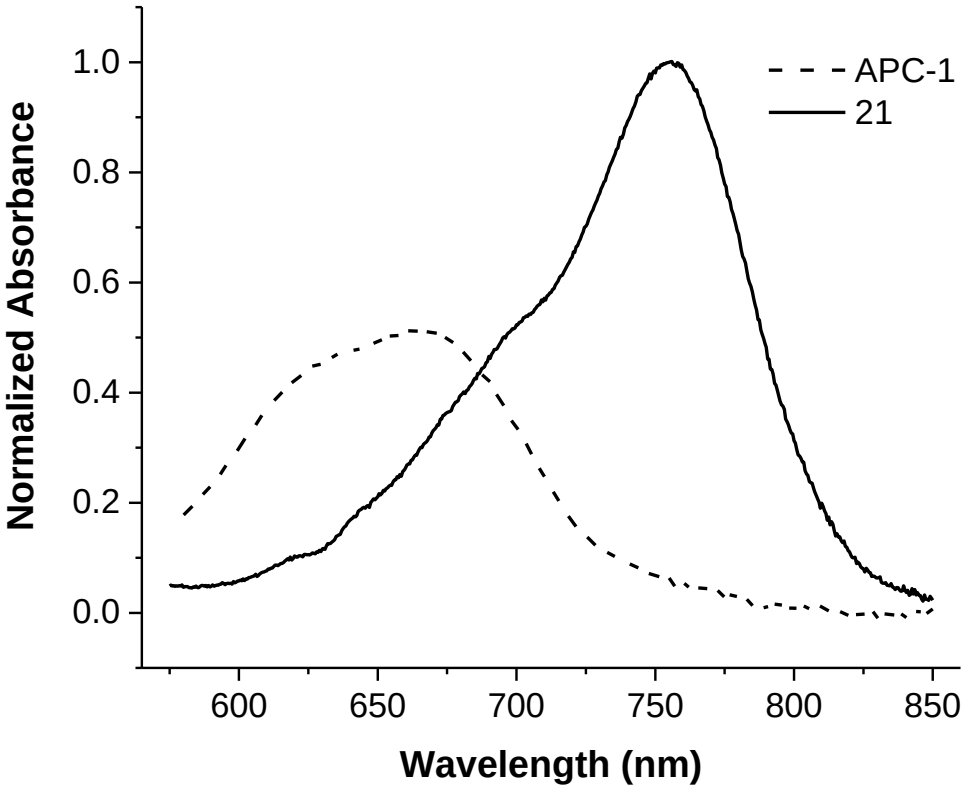

Figure 2.2. Normalized absorbance spectra of 2 μM APC-1 (dashed line) and 2 μM **21** (solid line) in PBS + 0.1% CrEL (pH 7.4).

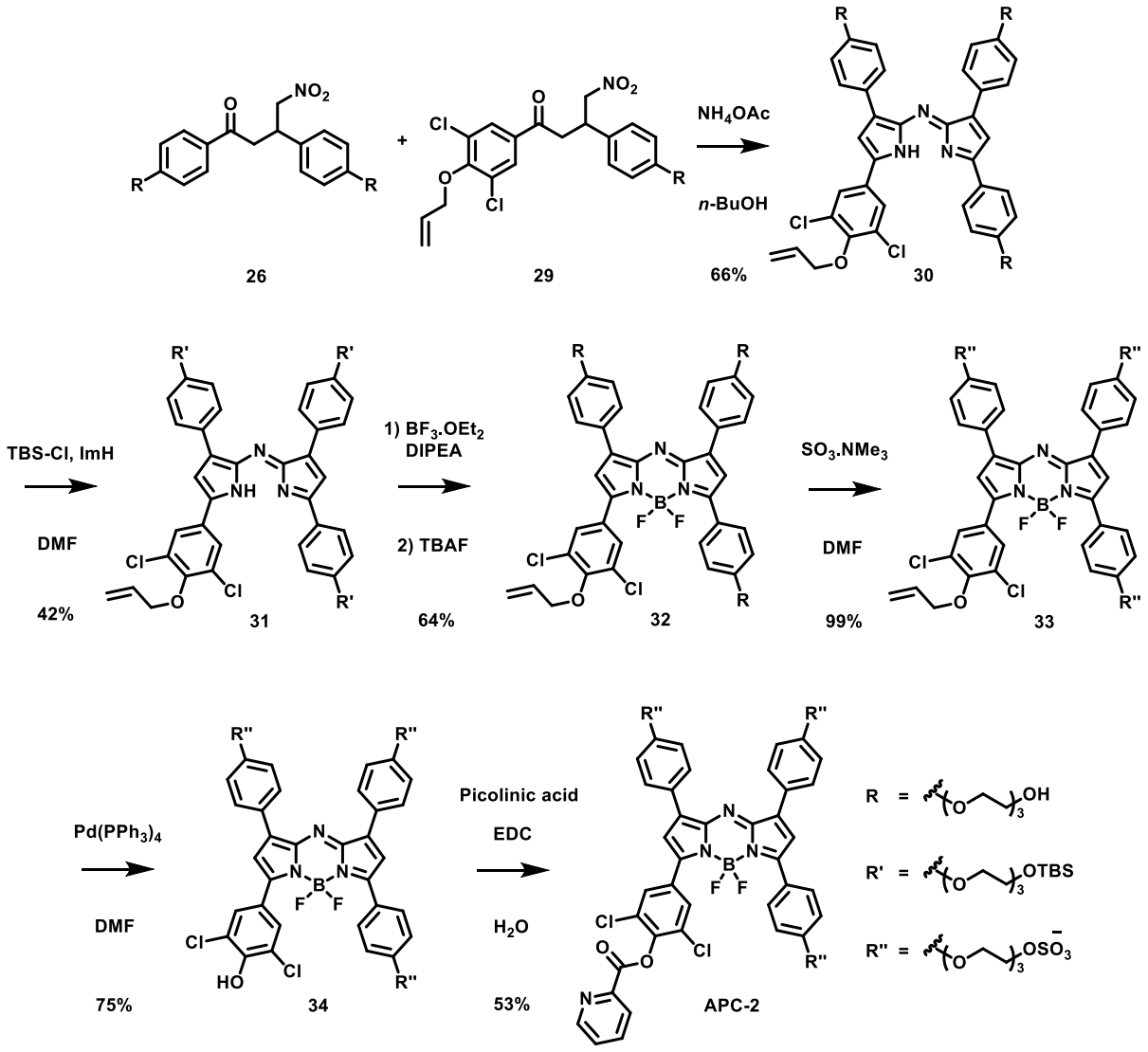

Scheme 2.1. Synthesis of Acoustogenic Probe for Copper(II)-2 (APC-2).

Compound	ε ($M^{-1} \cdot cm^{-1}$)	λ_{abs} (nm)	Φ
21	3.9×10^4	755	5.0% [a]
APC-1	1.9×10^4	675	2.8% [a]
34	3.7×10^4	767	1.2 [b]
APC-2	3.6×10^4	697	5.4% [b]

Table 2.1. Photophysical properties of compound **21**, APC-1, **34** and APC-2 measured in PBS (pH 7.4) + 0.1% CrEL. a) Quantum efficiencies determined in THF. b) Quantum efficiencies determined in 2:3 v/v EtOH:PBS.

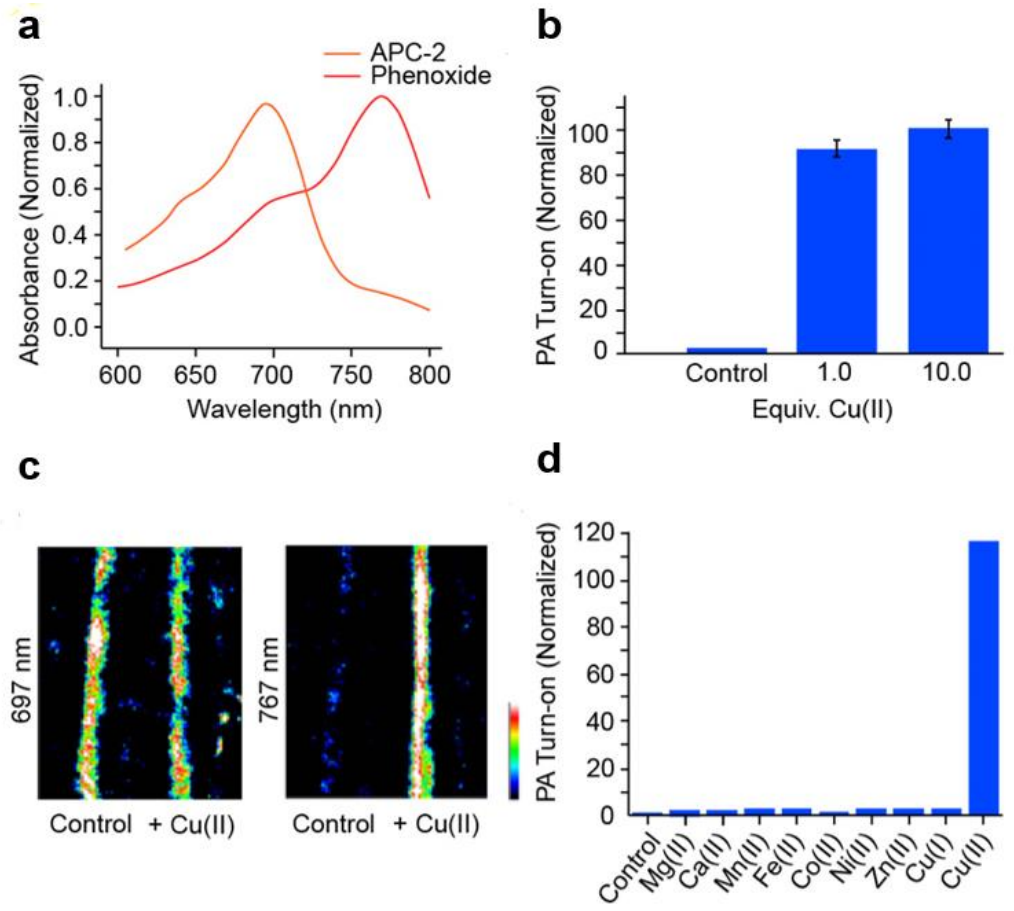

Figure 2.3. (a) Normalized absorbance spectra of APC-2 and the phenoxide **34** at 2 μM. (b) Normalized PA turn-on responses of APC-2 in the presence of 1 and 10 equivalents of Cu(II). (c) PA images (λ = 697 nm, left; λ = 767 nm, right) of APC-2 treated with 0 and 10 equivalents of Cu(II) in a phantom. (d) PA responses of APC-2 to various metal ions (2 mM for Ca(II) and Mg(II), 50 μM for all other cations).

REFERENCES

(1) Bahar, I.; Wallqvist, A.; Covell, D. G.; Jernigan, R. L. *Biochemistry* **1998**, *37*, 1067.

(2) Yu, P. H.; Cauglin, C.; Wempe, K. L.; Gubisne-Haberle, D. *Anal Biochem* **2003**, *318*, 285.

(3) Iborra, F. J.; Renaupiqueras, J.; Portoles, M.; Boleda, M. D.; Guerri, C.; Pares, X. *J Histochem Cytochem* **1992**, *40*, 1865.

(4) Tong, Z. Q.; Han, C. S.; Luo, W. H.; Wang, X. H.; Li, H.; Luo, H. J.; Zhou, J. N.; Qi, J. S.; He, R. Q. *Age* **2013**, *35*, 583.

(5) Tong, Z. Q.; Han, C. S.; Luo, W. H.; Li, H.; Luo, H. J.; Qiang, M.; Su, T.; Wu, B. B.; Liu, Y.; Yang, X.; Wan, Y.; Cui, D. H.; He, R. Q. *Sci Rep-Uk* **2013**, *3*.

(6) Unzeta, M.; Sole, M.; Boada, M.; Hernandez, M. *J Neural Transm* **2007**, *114*, 857.

(7) Lu, J.; Miao, J. Y.; Su, T.; Liu, Y.; He, R. Q. *Bba-Gen Subjects* **2013**, *1830*, 4102.

(8) Chen, K.; Maley, J.; Yu, P. H. *J Neurochem* **2006**, *99*, 1413.

(9) Su, T.; Wei, Y.; He, R. Q. *Prog Biochem Biophys* **2011**, *38*, 1171.

(10) Szarvas, T.; Szatloczky, E.; Volford, J.; Trezl, L.; Tyihak, E.; Rusznak, I. *J Radioan Nucl Ch Le* **1986**, *106*, 357.

(11) Chan, J.; Dodani, S. C.; Chang, C. J. *Nat Chem* **2012**, *4*, 973.

(12) Wang, J.; Karpus, J.; Zhao, B. S.; Luo, Z.; Chen, P. R.; He, C. *Angew Chem Int Ed* **2012**, *51*, 9652.

(13) Michel, B. W.; Lippert, A. R.; Chang, C. J. *J Am Chem Soc* **2012**, *134*, 15668.

(14) Lin, V. S.; Lippert, A. R.; Chang, C. J. *P Natl Acad Sci USA* **2013**, *110*, 7131.

(15) Hirayama, T.; Okuda, K.; Nagasawa, H. *Chem Sci* **2013**, *4*, 1250.

(16) Chyan, W.; Zhang, D. Y.; Lippard, S. J.; Radford, R. J. *P Natl Acad Sci USA* **2014**, *111*, 143.

(17) Wang, T. N.; Douglass, E. F.; Fitzgerald, K. J.; Spiegel, D. A. *J Am Chem Soc* **2013**, *135*, 12429.

(18) Song, H.; Rajendiran, S.; Kim, N.; Jeong, S. K.; Koo, E.; Park, G.; Thangadurai, T. D.; Yoon, S. *Tetrahedron Lett* **2012**, *53*, 4913.

(19) Roth, A.; Li, H.; Anorma, C.; Chan, J. *J Am Chem Soc* **2015**, *137*, 10890.

(20) Whitaker, J. E., Haugland, R. P., and Prendergast, F. G. *Anal Biochem* **1991**, *194*, 330

(21) Peng, T.; Yang, D. *Org Lett* **2010**, *12*, 496.

(22) Ueno, T.; Urano, Y.; Kojima, H.; Nagano, T. *J Am Chem Soc* **2006**, *128*, 10640.

(23) Greene, L. A.; Tischler, A. S. *P Natl Acad Sci USA* **1976**, *73*, 2424.

(24) Andres, N.; Lizcano, J. M.; Rodriguez, M. J.; Romera, M.; Unzeta, M.; Mahy, N. *J Histochem Cytochem* **2001**, *49*, 209.

(25) Tang, Y.; Kong, X.; Xu, A.; Dong, B.; Lin, W. *Angew Chem Int Ed* **2016**, *55*, 3356.

(26) Liu, W.; Truillet, C.; Flavell, R. R.; Brewer, T. F.; Evans, M. J.; Wilson, D. M.; Chang, C. J. *Chem Sci* **2016**, *7*, 5503.

(27) Wang, L. H. V.; Hu, S. *Science* **2012**, *335*, 1458.

(28) Xia, J.; Yao, J. J.; Wang, L. V. *Prog Electromagn Res* **2014**, *147*, 1.

(29) Mallidi, S.; Luke, G. P.; Emelianov, S. *Trends Biotechnol* **2011**, *29*, 213.

(30) Zemp, R. J.; Song, L.; Bitton, R.; Shung, K. K.; Wang, L. V. *Opt Express* **2008**, *16*, 18551.

(31) Luke, G. P.; Yeager, D.; Emelianov, S. Y. *Ann Biomed Eng* **2012**, *40*, 422.

(32) H. F. Zhang, K. Maslov, G. Stoica, L. V. Wang, *Nat Biotechnol* **2006**, *24*, 848.

(33) S. Mallidi, G. P. Luke, S. Emelianov, *Trends Biotechnol.* **2011**, *29*, 213.

(34) Cash, K. J.; Li, C. Y.; Xia, J.; Wang, L. H. V.; Clark, H. A. *Acs Nano* **2015**, *9*, 1692.

(35) Dragulescu-Andrasi, A.; Kothapalli, S. R.; Tikhomirov, G. A.; Rao, J. H.; Gambhir, S. S. *J Am Chem Soc* **2013**, *135*, 11015.

(36) Pu, K. Y.; Shuhendler, A. J.; Jokerst, J. V.; Mei, J. G.; Gambhir, S. S.; Bao, Z. N.; Rao, J. H. *Nat Nanotechnol* **2014**, *9*, 233.

(37) Levi, J.; Kothapalli, S. R.; Ma, T. J.; Hartman, K.; Khuri-Yakub, B. T.; Gambhir, S. S. *J Am Chem Soc* **2010**, *132*, 11264.

(38) Li, H.; Zhang. P.; Smaga, L.; Hoffman. R.; Chan, J. *J Am Chem Soc* **2015**, *137,* 15628*.*

(39) Manto, M. *Toxics* **2014**, *2*, 327.

(40) Fife, T. H.; Przystas, T. J. *J Am Chem Soc* **1985**, *107*, 1041.

(41) Kierat, R. M.; Kramer, R. *Bioorg Med Chem Lett* **2005**, *15*, 4824.

(42) Strobl, M.; Rappitsch, T.; Borisov, S. M.; Mayr, T.; Klimant, I. *Analyst* **2015**, *140*, 7150.

(43) Jokic, T.; Borisov, S. M.; Saf, R.; Nielsen, D. A.; Kuhl, M.; Klimant, I. *Anal Chem* **2012**, *84*, 6723.

(44) Collado, D.; Vida, Y.; Najera, F.; Perez-Inestrosa, E. *Rsc Adv* **2014**, *4*, 2306.

(45) Kamkaew, A.; Burgess, K. *Chem Commun* **2015**, *51*, 10664.

(46) Kim, C.; Favazza, C.; Wang, L. H. V. *Chem Rev* **2010**, *110*, 2756.

APPENDIX A-MATERIAL AND METHODS FOR CHAPTER 1

This appendix includes information about the source of materials, general, spectroscopic methods as well as cell culture and imaging materials and methods used for Chapter 1.

A.1 MATERIALS

Thin-layer chromatography (TLC) was performed on glass-backed TLC plates pre-coated with silica gel containing an UV_{254} fluorescent indicator (Macherey-Nagel). Compounds were visualized with a 254/365nm, handheld UV lamp (UVP). Flash chromatography was performed using 230-400 mesh silica gel P60 (SiliCycle Inc). Solvents used for anhydrous reactions were dried over 3 Å molecular sieves activated via heating under vacuum at 300 °C. All glassware used in anhydrous reactions were flame-dried or heated overnight in an oven at 160 °C and cooled immediately prior to use. 3-Bromoaniline, 3-bromoanisole, 4-bromo-3-methylaniline, 4-nitrobenzaldehyde, *N*-iodosuccinimide, potassium allyltrifluoroborate, sodium triacetoxyborohydride, tetrakis(triphenylphosphine)palladium(0), trifluoromethanesulfonic acid, and trimethylacetylene were purchased from Oakwood Products and used as received. 1-Bromo-3-chloropropane, aluminum trichloride, boron tribromide, copper iodide, dichlorodimethylsilane, formaldehyde solution, methyl chloroformate, phosphorous oxychloride, *sec*-butyllithium solution, and *tert*-butyllithium solution were purchased from Sigma-Aldrich and used without purification. Deuterated solvents were purchased from Cambridge Isotope Laboratories. ER-Tracker™ Green, LysoTracker® Green DND-26, MitoTracker® Green FM, DAPI, Trypan Blue solution were purchased from Life Technologies.

All buffers used for pH titrations were prepared in deionized water and brought to the appropriate pH with aqueous HCl or NaOH. The buffers used were 50 mM glycine (pH range 2.00-3.50), 50 mM NaOAc (pH range 4.00-5.60), 50 mM MES (pH range 5.60-6.80), 50 mM HEPES (pH range 6.80-8.20), 50 mM Tris (pH range 8.20-9.50) and 50 mM glycine (pH range 9.50-10.40). A 10 mM stock solution of formaldehyde for in vitro titration experiments was prepared by heating a suspension of paraformaldehyde (>88% w/w, 17.6 mg, 0.50 mmol, TCI, lot #NXR2B) in phosphate buffered saline (PBS) buffered to pH 7.4 (50mL) at 88 °C for 1 hr. The solution was cooled to room temperature and filtered through a 0.22 µm syringe filter (Millex).

A.2 SPECTROSCOPIC METHODS

NMR spectra were recorded on Varian 400 or 500 MHz spectrometers at 25 °C. Chemical shifts are reported in ppm (δ) and are referenced to residual protic peaks. The following abbreviations are used to describe coupling constants: singlet (s), doublet (d), triplet (t), quartet (q), doublet doublet (dd), doublet triplet (dt), doublet quartet (dq), doublet doublet triplet (ddt), multiplet (m), and broad singlet (bs). IR spectra were recorded with a PerkinElmer Spectrum Two IR spectrometer. High-resolution mass spectra were acquired with a Waters Q-TOF Ultima ESI mass spectrometer and a Waters Synapt G2-Si ESI/LC-MS mass spectrometer. UV-visible spectra were recorded on a Cary 60 spectrometer. Fluorescence spectra were acquired on a QuantaMaster-400 scanning spectrofluorometer with micro

fluorescence quartz cuvettes (Science Outlet). Flow cytometry was performed on a BD Biosciences LSR II (San Jose, CA, USA), and the data were analyzed as described using FACSDiva software.

A.3 CELL CULTURE AND IMAGING MATERIALS AND METHODS

HEK293TN cells were obtained from Prof. Paul Hergenrother (UIUC, Chemistry) and cultured in phenol-red free Dulbecco's modified eagle medium (DMEM, Corning) supplemented with 10% fetal bovine serum (FBS, Sigma Aldrich), and 1% penicillin/streptomycin (Corning). Neuroscreen-1 cells were obtained from Prof. Kai Zhang (UIUC, Biochemistry) and cultured in Ham's F-12K medium (Sigma Aldrich) supplemented with 15% horse serum (Hyclone), 2.5% fetal bovine serum (FBS, Sigma Aldrich), and 1% penicillin/streptomycin (Corning). Cells were incubated at 37°C and 5% CO_2. One day before imaging, cells were passed and plated on 8-well chambered coverglasses (Lab-Tek) at a density of 40,000 cells per mL (or 20,000 cells per well). Cells would reach 70-80% confluency before imaging. Immediately before the experiments, cells were washed with serum-free DMEM, incubated with FP1 in serum-free DMEM, rinsed with fresh media and imaged. Samples of HEK293TN and NC cells for flow cytometry were prepared by passaging and seeding each well of a 6-well cluster culture dish (Cyto-One) with 300,000 cells one day before experiments. Cells had reached 70% confluency before staining with 2 µM FP1 for 8 mins. Stained cells were aspirated and serum-free DMEM added. Subsequently, a 10x concentrated FA solution was added to give a final concentration of 1.0 mM. 2.5 mM and 5 mM.

After incubation cells with FA, the media was removed and replaced with serum-free DMEM. Finally, cells were trypsinized, pelleted via centrifugation, resuspended in PBS for flow cytometric analysis.

APPENDIX B-SYNTHESES FOR CHAPTER 1

This appendix includes the detailed synthetic methods and spectroscopic characterizations for compounds synthesized in Chapter 1.

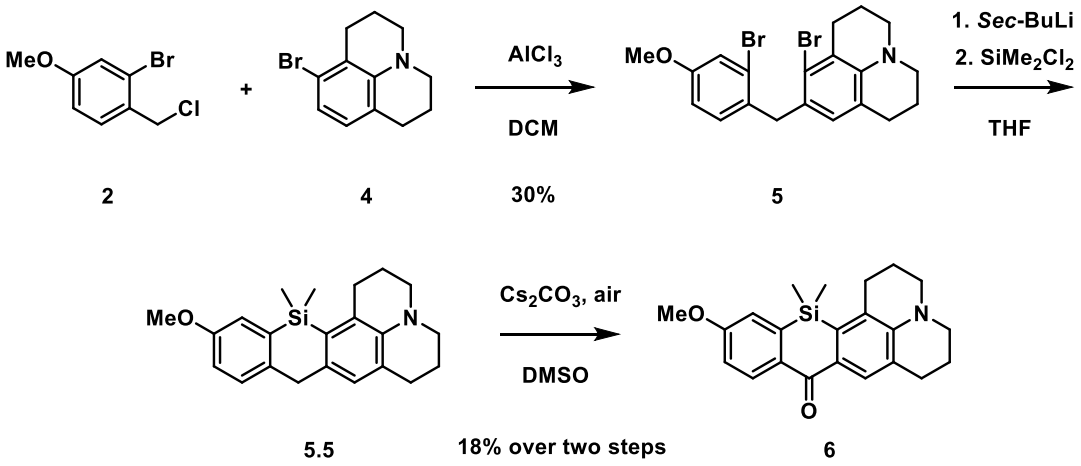

Scheme B.1. Synthesis of Si-xanthone **6**.

2-Bromo-4-methoxybenzyl chloride (2). A two-neck round-bottom flask was charged with 3-bromoanisole (35.0 mL, 276.5 mmol, 1.0 eq.) and formaldehyde (37 wt % in H_2O, 38.0 mL, 1.38 mol, 5.0 eq.). Hydrogen chloride gas, generated from conc. hydrochloric acid and conc. sulfuric acid, was bubbled through the reaction mixture which was stirred at 50 °C for 6 hrs. Upon cooling to room temperature, the reaction was diluted with H_2O (50 mL) and extracted with CH_2Cl_2 (3 × 50 mL). The combined organic fractions were washed with brine (100 mL), dried (Na_2SO_4), filtered and concentrated under reduced pressure. The crude residue was purified by fractional distillation to afford the title compound as a colorless oil (43.1 g, 183.1 mmol, 66.3% yield). ^{1}H NMR (500 MHz, $CDCl_3$) δ 7.36 (d, *J* = 8.5 Hz, 1H), 7.13 (d, *J* = 2.6 Hz, 1H),

6.85 (dd, *J* = 8.5, 2.6 Hz, 1H), 4.68 (s, 2H), 3.79 (s, 3H). ^{13}C NMR (125 MHz, $CDCl_3$) δ 160.5, 132.0, 129.0, 125.0, 118.6, 114.0, 55.8, 46.5. IR (neat): 3008, 2966, 2937, 1602, 1492, 1263, 1242, 1028, 865, 843, 729, 661 cm^{-1}. HR-MS calculated for C_8H_8BrClO $[M\text{-}HCl]^+$ *m/z* 198.9753, found 198.9759.

8-Bromo-1,2,3,5,6,7-hexahydropyrido[3,2,1-ij]quinoline (4). A round-bottom flask was charged with 3-bromoaniline (8.0 mL, 73.1 mmol, 1.0 eq.), 1-bromo-3-chloropropane (58.5 mL, 584.6 mmol, 8.0 eq.), and Na_2CO_3 (31.0 g, 292.3 mmol, 4.0 eq.). After stirring at 140 °C for 48 hrs, the reaction cooled to room temperature, transferred to a separatory funnel, and extracted with CH_2Cl_2 (3 × 100 mL). The combined organic fractions were dried (Na_2SO_4), filtered, and concentrated under reduced pressure. Residual 1-bromo-3chloropropane was removed at 60 °C, 1 Torr. The crude dialkylated intermediate was dissolved in DMF (15.0 mL) and stirred at 160 °C for 24 hrs. After cooling to room temperature, the solution was concentrated under reduced pressure, washed with H_2O (200 mL), and extracted with CH_2Cl_2 (3 × 100 mL). The combined organic fractions were dried (Na_2SO_4), filtered, and concentrated under reduced pressure. The crude residue was purified via flash chromatography on a silica column (1:99 v/v EtOAc:Hexanes) to afford the title compound as a light yellow oil (12.0 g, 47.6 mmol, 65.1% yield). ^{1}H NMR (400 MHz, $CDCl_3$) δ 6.78 (d, *J* = 8.0 Hz, 1H), 6.66 (d, *J* = 8.0 Hz, 1H), 3.14 (dt, *J* = 12.5, 5.7 Hz, 4H), 2.80 (t, *J* = 6.7 Hz, 2H), 2.72 (t, *J* = 6.5 Hz, 2H), 2.07–1.87 (m, 4H). ^{13}C NMR (100 MHz, $CDCl_3$) δ 144.8, 128.0, 123.2, 120.9, 120.8, 119.6, 50.2, 49.9, 28.8, 27.8, 22.2, 22.1. IR (neat): 3009, 2935,

1583, 1488, 1456, 1440, 1388, 1327, 1207, 1186, 1067, 1038, 792, 755, 578, 463 cm^{-1}. HR-MS calculated for $C_{12}H_{14}BrN$ $[M+H]^+$ *m/z* 252.0388, found 252.0393.

8-Bromo-9-(2-bromo-4-methoxybenzyl)-2,3,6,7-tetrahydro-1H,5H-pyrido[3,2,1-ij]quinoline (5). A flame-dried round-bottom flask was charged with compound **8** (5.0 g, 19.8 mmol, 1.0 eq.) and anhydrous CH_2Cl_2 (200 mL). $AlCl_3$ (3.17 g, 23.8 mmol, 1.2 eq.) was added to the reaction in one portion. The resultant mixture was sonicated under a nitrogen atmosphere for 30 min. A solution of compound **8** (6.07 g, 25.8 mmol, 1.4 eq.) in anhydrous CH_2Cl_2 (7.0 mL) was transferred to the reaction via dropwise syringe addition. After overnight stirring at room temperature, the reaction was quenched by slow addition of sat. $NaHCO_3$ (~200 mL) and filtered through a bed of celite which was washed with CH_2Cl_2 (100 mL). The aqueous phase was separated and extracted with CH_2Cl_2 (3 × 100 mL). The combined organic fractions were washed with brine (100 mL), dried (Na_2SO_4), filtered, and concentrated under reduced pressure. The crude product was purified via flash chromatography on a silica column (4:96 v/v EtOAc:Hexanes) to afford the title compound as a brown oil. (2.71 g, 6.0 mmol, 30.0% yield). Unreacted compound **8** was recovered via flash chromatography on a silica column. ^{1}H NMR (500 MHz, $CDCl_3$) δ 7.18 (d, *J* = 2.6 Hz, 1H), 6.93 (d, *J* = 8.5 Hz, 1H), 6.79 (dd, *J* = 8.5, 2.6 Hz, 1H), 6.51 (s, 1H), 4.04 (s, 2H), 3.80 (s, 3H), 3.22–3.13 (m, 2H), 3.13–3.08 (m, 2H), 2.86 (t, *J* = 6.7 Hz, 2H), 2.67 (t, *J* = 6.6 Hz, 2H), 2.07–2.00 (m, 2H), 2.00–1.94 (m, 2H). ^{13}C NMR (125 MHz, $CDCl_3$) δ 158.6, 143.4, 132.3, 131.1, 128.9, 126.5, 125.9, 125.2, 121.6, 121.0, 118.0, 113.7, 55.7, 50.3, 49.8,

41.4, 29.7, 27.8, 22.5, 22.2. IR (neat): 3006, 2938, 2834, 1488, 1458, 1441, 1331, 1305, 1283, 1233, 1205, 1183, 1037, 858, 751, 725, 667, 547, 463 cm^{-1}. HR-MS calculated for $C_{20}H_{21}Br_2NO$ $[M+H]^+$ *m/z* 450.0068, found 450.0055.

12-methoxy-14,14-dimethyl-2,3,6,7,9,14-hexahydro-1H,5H-benzo[5,6]silino[2,3-f]pyrido[3,2,1-ij]quinolone (5.5). A flame-dried round-bottom flask was charged with compound **9** (2.71 g, 6.0 mmol, 1.0 eq.) and anhydrous THF (100 mL). An oven-dried addition funnel was attached to the flask and the system was flushed with nitrogen. The reaction was cooled to -78 °C and treated with 1.4 M *sec*-butyllithium in cyclohexane (12.9 mL, 18.0 mmol, 3.0 eq.) via funnel addition over 30 min. After stirring at the same temperature for 10 min, a solution of $SiMe_2Cl_2$ (1.36 mL, 11.5 mmol, 1.9 eq.) in anhydrous THF (11.5 mL) was added dropwise over 20 min. The reaction was warmed to room temperature and stirred overnight. The volatiles were removed under reduced pressure to obtain the crude product which was washed with sat. $NaHCO_3$ (100 mL) and extracted with CH_2Cl_2 (3 × 50 mL). The combined organic fractions were washed with brine (100 mL), dried (Na_2SO_4), filtered, and concentrated under reduced pressure to afford the title compound as a brown oil which was sufficiently pure to use without further purification. ^{1}H NMR (400 MHz, $CDCl_3$) δ 7.23 (d, *J* = 8.3 Hz, 1H), 7.17 (d, *J* = 2.7 Hz, 1H), 6.88 (dd, *J* = 8.3, 2.7 Hz, 1H), 6.85 (s, 1H), 4.00 (s, 2H), 3.86 (s, 3H), 3.16 (s, 2H), 2.99 (s, 1H), 2.81 (s, 1H), 2.20 – 1.96 (m, 4H), 0.56 (d, *J* = 1.3 Hz, 4H). ^{13}C NMR (100 MHz, $CDCl_3$) δ 157.5, 141.4, 138.6, 137.4, 134.2, 131.3, 128.6, 127.9, 127.7, 123.9, 118.6, 114.3, 55.5, 50.8, 50.2, 40.3, 29.9,

28.2, 22.9, 22.4, -0.4. IR (neat): 2933, 2833, 1682, 1596, 1548, 1304, 1246, 1039, 820, 768, 649, 453 cm^{-1}. HR-MS calculated for $C_{22}H_{27}NOSi$ $[M+H]^+$ *m/z* 350.1940, found 350.1940.

12-Methoxy-14,14-dimethyl-2,3,5,6,7,14-hexahydro-1H,9H-benzo[5,6]silino[2,3-f]pyrido[3,2,1-ij]quinolin-9-one (6). A round-bottom flask was charged with compound **10** (2.1 g, 6.0 mmol, 1.0 eq.), $CFCO_3$ (5.9 g, 18.0 mmol, 3.0 eq.), and DMSO (20 mL). The reaction mixture was heated at 90 °C with the flask open to the atmosphere for 3 days. After cooling to room temperature, the reaction was diluted with CH_2Cl_2 (50 mL) and filtered through a bed of celite. The filtrate was diluted with brine (150 mL) and extracted with CH_2Cl_2 (3 × 100 mL). The combined organic fractions were washed with brine (100 mL), dried (Na_2SO_4), filtered, and concentrated under reduced pressure. The crude product was purified via flash chromatography on a silica column to afford the title compound as a yellow powder (412 mg, 1.1 mmol, 18.3% yield over two-steps beginning from compound **3**). ^1H NMR (400 MHz, $CDCl_3$) δ 8.43 (d, *J* = 8.9 Hz, 1H), 8.09 (s, 1H), 7.08 (d, *J* = 2.8 Hz, 1H), 7.02 (dd, *J* = 8.9, 2.8 Hz, 1H), 3.90 (s, 3H), 3.30 (m, 4H), 2.93 (t, *J* = 6.3 Hz, 2H), 2.83 (t, *J* = 6.4 Hz, 2H), 2.13–1.88 (m, 4H), 0.53 (s, 6H). ^{13}C NMR (100 MHz, $CDCl_3$) δ 185.7, 170.6, 161.8, 145.7, 142.2, 135.4, 134.2, 131.9, 130.6, 128.6, 124.8, 123.1, 117.6, 115.1, 55.5, 50.6, 50.1, 29.1, 28.4, 22.0, 21.7, -0.1. m.p. = 130 °C (decomp). IR (neat): 3012, 2972, 1739, 1585, 1366, 1231, 834, 765 cm^{-1}. HR-MS calculated for $C_{22}H_{25}NO_2Si$ $[M+H]^+$ *m/z* 364.1733, found 364.1740.

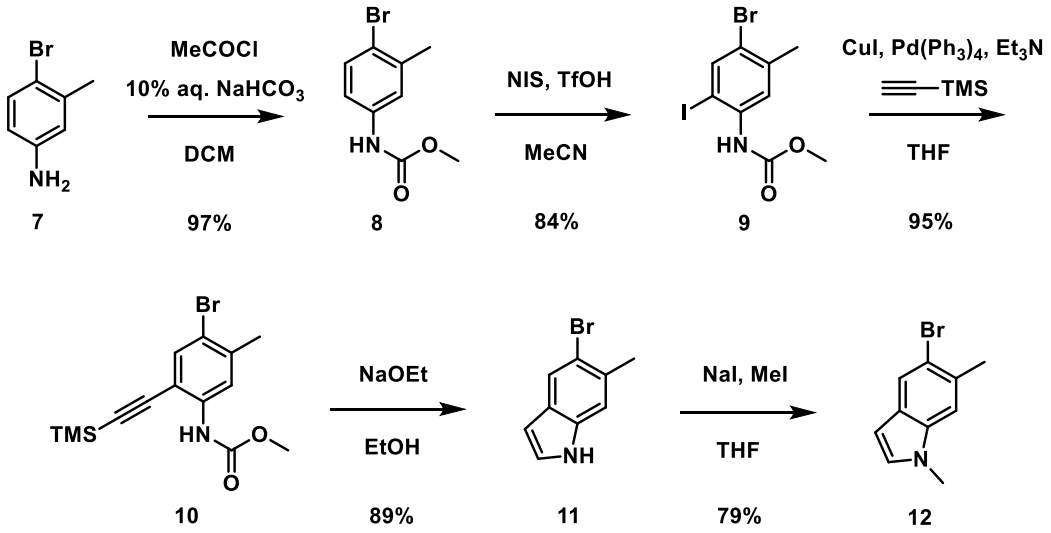

Scheme B.2. Synthesis of 5-Bromo-1,6-dimethyl-1*H*-indole **12**.

Methyl (4-bromo-3-methylphenyl)carbamate (8). A solution of 4-bromo-3-methylaniline (5.25 g, 28.2 mmol, 1.0 eq.), CH_2Cl_2 (50 mL), and 10% aq. $NaHCO_3$ (40 mL) was cooled in an ice-bath. Methyl chloroformate (4.0 mL, 51.8 mmol, 1.8 eq.) was added dropwise to the rapidly stirred solution. The reaction was subsequently warmed to room temperature and stirred for 2 hrs. The reaction was then diluted with CH_2Cl_2 (50 mL) and sequentially washed with sat. NH_4Cl (50 mL), sat. $NaHCO_3$ (50 mL) and brine (50 mL). The organic fraction was dried (Na_2SO_4), filtered and concentrated to afford the crude residue as a brown solid which was purified via flash chromatography on a silica column (1:1 v/v EtOAc:Hexanes) to afford the title compound as a white solid (6.65 g, 27.3 mmol, 96.6% yield). ^{1}H NMR (500 MHz, $CDCl_3$) δ 7.39 (d, *J* = 8.6 Hz, 1H), 7.28 (s, 1H), 7.18 (s, 1H), 7.12 (d, *J* = 8.6 Hz, 1H), 3.75 (s, 3H), 2.31 (s, 3H). ^{13}C NMR (125 MHz, $CDCl_3$) δ 154.5, 138.7, 137.4, 132.8, 121.3, 118.8, 118.1, 77.7,

77.4, 77.2, 52.7, 23.2. m.p. = 71-72 °C. IR (neat): 3328, 1705, 1584, 1275, 1233, 1071, 1023, 826, 765, 679, 653 cm^{-1}. HR-MS calculated for $C_9H_{10}BrNO_2$ $[M+H]^+$ *m/z* 243.9973, found 243.9977.

Methyl (4-bromo-2-iodo-5-methylphenyl)carbamate (9). A solution of compound **8** (32.0 g, 131.1 mmol, 1.0 eq.) in MeCN (150 mL) was cooled to 0°C in an ice-bath. *N*-iodosuccinimide (30.1 g, 137.6 mmol, 1.05 eq.) was added in one portion to the stirred solution. Trifluoromethanesulfonic acid (1.2 mL, 13.1 mmol, 0.1 eq.) was then added dropwise. The reaction was subsequently warmed to room temperature and stirred overnight. After overnight stirring, the resulting white solid was filtered, washed with cold MeCN, and dried under reduced pressure (42.2 g, 110.1 mmol, 84.0% yield). The compound was used in the next step without further purification. ^{1}H NMR (500 MHz, $CDCl_3$) δ 7.94 (s, 1H), 7.85 (s, 1H), 6.87 (s, 1H), 3.80 (s, 3H), 2.35 (s, 3H). ^{13}C NMR (125 MHz, $CDCl_3$) δ 153.9, 141.0, 139.5, 137.8, 121.9, 119.5, 85.5, 52.9, 23.3. m.p. 130-131 °C. IR (neat): 3276, 2939, 1690, 1603, 1491, 1275, 1241, 1042, 873, 863, 772, 606 cm^{-1}. HR-MS calculated for $C_9H_{10}BrINO_2$ $[M+H]^+$ *m/z* 369.8940, found 369.8945.

Methyl (4-bromo-5-methyl-2-((trimethylsilyl)ethynyl)phenyl)carbamate (10). A flame-dried round-bottom flask was charged with compound **9** (5.38 g, 14.5 mmol, 1.0 eq.), CuI (0.28 g, 1.5 mmol, 0.1 eq.), and $Pd(PPh_3)_4$ (0.84 g, 0.7 mmol, 0.05 eq.) and then dried under vacuum for 30 min. The solids were then dissolved in anhydrous THF

(35 mL) and treated sequentially with trimethylsilylacetylene (2.3 mL, 16.0 mmol, 1.1 eq.) and anhydrous triethylamine (8.1 mL, 58.2 mmol, 4.0 eq.). The reaction was stirred at room temperature for 1 hr. All volatiles were removed under reduced pressure and the resultant residue was dissolved in EtOAc (50 mL) and washed with brine (3 × 50 mL). The organic fraction was dried (Na_2SO_4), filtered and concentrated to afford the crude product as a dark brown solid which was purified via flash chromatography on a silica column (3:97 v/v EtOAc:Hexanes) to afford the title compound as an orange solid (4.72g, 13.9 mmol, 95.4% yield). ^{1}H NMR (500 MHz, $CDCl_3$) δ 7.94 (s, 1H), 7.39 (s, 1H), 7.24 (s, 1H), 3.71 (s, 3H), 2.28 (s, 3H), 0.24 (s, 9H). ^{13}C NMR (125 MHz, $CDCl_3$) δ 153.4, 140.0, 138.7, 134.6, 119.4, 117.0, 110.6, 102.6, 99.0, 52.5, 23.6, 0.1. m.p. = 73-74 °C. IR (neat): 3394, 2959, 2150, 1740, 1509, 1220, 1070, 863, 839, 762, 574 cm^{-1}. HR-MS calculated for $C_{14}H_{18}BrNO_2Si$ $[M+Na]^+$ *m/z* 362.0182, found 362.0193.

5-Bromo-6-methyl-*1H*-indole (11). To a freshly prepared, 0.7 M sodium ethoxide solution (150 mL, 8.0 eq.) was added compound **10** (4.5 g, 13.3 mmol, 1.0 eq.) The reaction was stirred at 80°C until all starting material was consumed and then the solvent was removed under reduced pressure. The residue was dissolved in CH_2Cl_2 (50 mL) and washed with brine (3 × 50 mL). The organic fraction was dried (Na_2SO_4), filtered and concentrated to afford the crude residue as a dark brown solid which was purified via flash chromatography on a silica column (3:17 v/v EtOAc:Hexanes) to afford the title compound as a yellow solid (2.48 g, 11.8 mmol, 88.8% yield). ^{1}H NMR

(500 MHz, $CDCl_3$) δ 8.03 (bs, NH), 7.88 (s, 1H), 7.26 (s, 1H), 7.16 (t, 1H), 6.52-6.48 (m, 1H), 2.54 (s, 3H). ^{13}C NMR (125 MHz, $CDCl_3$) δ 135.5, 131.0, 128.0, 125.0, 124.0, 116.7, 112.7, 102.1, 23.8. m.p. = 85-86 °C. IR (neat): 2916, 1738, 1614, 1577, 1506, 1467, 1415, 1315, 1270, 1241, 1202, 964, 881, 842, 761, 730, 692 cm^{-1}. HR-MS calculated for C_9H_8BrN $[M+H]^+$ *m/z* 209.9918, found 209.9915.

5-Bromo-1,6-dimethyl-1H-indole (12). A flame-dried round-bottom flask was charged with compound **11** (5.41 g, 25.8 mmol, 1.0 eq.) and anhydrous THF (50 mL). The solution was cooled in an ice-bath and treated with NaH as a 60% dispersion in mineral oil (1.24 g, 30.9 mmol, 1.2 eq.) and methyl iodide (3.2 mL, 51.5 mmol, 2.0 eq.). After stirring at 0 °C for 2 hrs, the volatiles were removed under reduced pressure. The residue was dissolved with CH_2Cl_2 (100 mL) and washed with brine (50 mL). The organic fraction was (Na_2SO_4), filtered and concentrated to afford the crude product which was purified via flash chromatography on a silica column (7:193 v/v EtOAc:Hexanes) to afford the title compound as a yellow solid (4.56 g, 20.3 mmol, 79.1% yield**).** ^1H NMR (500 MHz, Acetone-d_6) δ 10.27 (bs, NH), 7.82 (s, 1H), 7.41 (s, 1H), 7.31 (dd, *J* = 3.2, 2.4 Hz, 1H), 6.45 (td, *J* = 2.1, 1.0 Hz, 1H), 2.48 (d, *J* = 0.8 Hz, 3H). ^{13}C NMR (125 MHz, Acetone-d_6) δ 136.1, 129.7, 128.5, 126.0, 123.5, 115.6, 113.2, 101.1, 23.1. m.p. = 90-91 °C. IR (neat): 33143118, 3095, 1467, 1338 1753, 1705, 1614, 1507, 1468, 1270, 993, 881, 842, 730, 693, 606 cm^{-1}. HR-MS calculated for $C_{10}H_{10}BrN$ $[M+H]^+$ *m/z* 224.0075, found 224.0079.

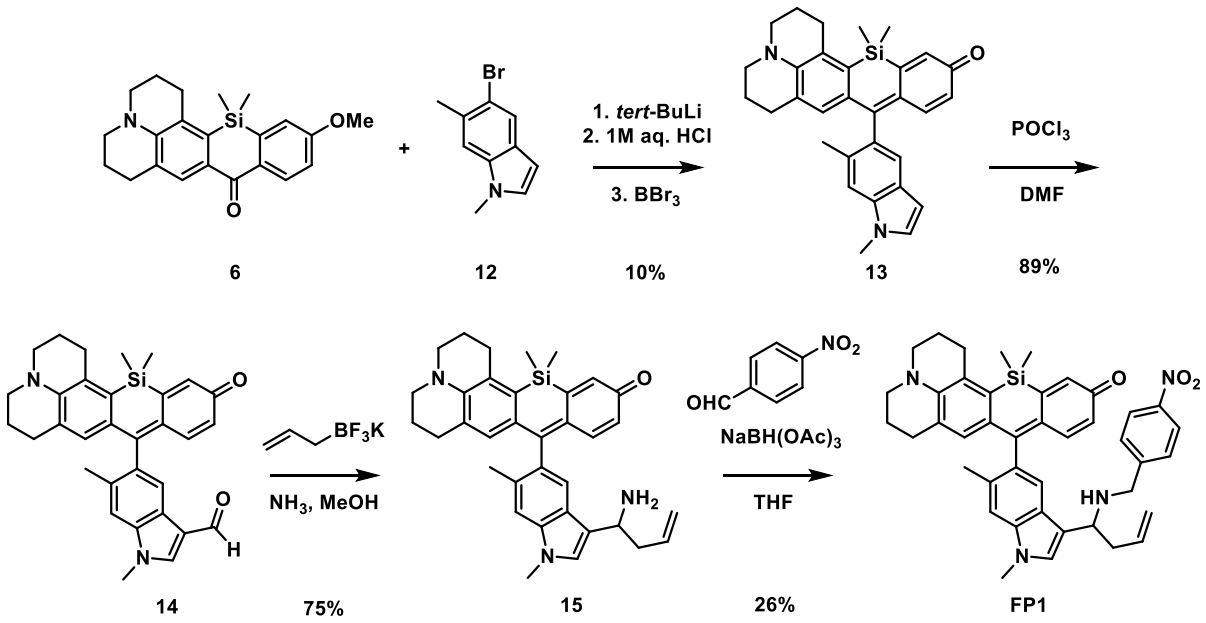

Scheme B.3. Synthesis of FP1.

9-(1,6-dimethyl-1H-indol-5-yl)-14,14-dimethyl-2,3,5,6,7,14-hexahydro-1H,12H-benzo[5,6]silino[2,3-f]pyrido[3,2,1-ij]quinolin-12-one (13). A solution of compound **12** (2.77 g, 12.4 mmol, 8.0 eq.) in 25 mL anhydrous THF was cooled to -78 °C and treated with a solution of *tert*-butyllithium in pentane (7.27 mL, 12.4 mmol, 8.0 eq.) which was added dropwise. The reaction was stirred at the same temperature for 8 min and then treated with a solution of compound **6** (556 mg, 1.5 mmol, 1.0 eq.) in anhydrous THF (15 mL). The reaction was warmed to room temperature and stirred for 3 hrs. The reaction was quenched by the addition of 10% aq. HCl (10 mL) and stirred at room temperature for 1 hr. The reaction was poured into sat. $NaHCO_3$ (25 mL) and extracted with CH_2Cl_2 (3 × 50 mL). The combined organic fractions were dried (Na_2SO_4), filtered, and concentrated under reduced pressure. The crude residue was eluted through a silica plug and concentrated to afford a blue film which was used without further purification. A solution of this intermediate in 20 mL anhydrous CH_2Cl_2

was cooled to 0 °C and treated with a solution of 1 M BBr_3 in CH_2Cl_2 (2.6 mL, 2.6 mmol, 6.0 eq.) which was added dropwise. The reaction was warmed to room temperature, stirred for 2 hrs, and then quenched by addition of sat. $NaHCO_3$ (100 mL) and extracted with CH_2Cl_2 (3 × 50 mL). The combined organic fractions were dried (Na_2SO_4), filtered, and concentrated under reduced pressure. The crude residue was purified by flash chromatography on a silica column (8:92 v/v MeOH/CH_2Cl_2) to afford the title compound as a blue film (45 mg, 0.1 mmol, 10% yield over two-steps beginning from compound **6**). ^{1}H NMR (500 MHz, $CDCl_3$) δ 7.30 (s, 1H), 7.23 (s, 1H), 7.08 (d, *J* = 3.1 Hz, 1H), 6.88 (d, *J* = 2.3 Hz, 1H), 6.84 (d, *J* = 9.9 Hz, 1H), 6.57 (s, 1H), 6.44 (d, *J* = 3.1 Hz, 1H), 6.20 (dd, *J* = 9.9, 2.3 Hz, 1H), 3.85 (s, 3H), 3.35 (t, *J* = 5.9 Hz, 2H), 3.30 (dt, *J* = 5.7, 2.9 Hz, 2H), 2.94 (t, *J* = 6.3 Hz, 2H), 2.41 (t, *J* = 6.2 Hz, 2H), 2.18 (s, 3H), 2.05 (q, *J* = 5.5 Hz, 2H), 1.84 (q, *J* = 6.1 Hz, 2H), 0.56 (d, *J* = 5.7 Hz, 6H). ^{13}C NMR (125 MHz, $CDCl_3$) δ 183.4, 162.3, 148.1, 145.5, 142.2, 136.9, 136.7, 136.1, 133.9, 132.3, 130.1, 129.2, 129.2, 128.7, 127.3, 126.2, 125.6, 122.0, 121.6, 109.9, 109.9, 100.8, 50.9, 50.3, 33.1, 29.9, 29.2, 28.1, 21.7, 21.2, 20.4, 0.0. IR (neat): 2924, 1612, 1578, 1509, 1228, 1210, 833, 765, 677, 556, 469 cm^{-1}. HR-MS calculated for $C_{31}H_{33}N_2OSi$ $[M+H]^+$ *m/z* 477.2362, found 477.2365

5-(14,14-dimethyl-12-oxo-2,3,6,7,12,14-hexahydro-1H,5H-benzo[5,6]silino[2,3-f]pyrido[3,2,1-ij]quinolin-9-yl)-1,6-dimethyl-1H-indole-3-carbaldehyde (14). Anhydrous DMF (3.0 mL) was cooled in an ice-bath and treated with dropwise addition of $POCl_3$ (10 uL, 0.11 mmol, 1.5 eq.). After 30 min, a solution of compound **13** (32 mg,

0.07 mmol, 1.0 eq.) in anhydrous DMF (2.0 mL) was added. The reaction was stirred 0 °C for 1 hr. The reaction was then syringed into a second reaction vessel where anhydrous DMF (3.0 mL) was cooled in an ice-bath and treated with dropwise addition of $POCl_3$ (10 uL, 0.11 mmol, 1.5 eq.). After 30 min, reaction was treated with additional $POCl_3$ (10 uL, 0.11 mmol, 1.5 eq.) and stirred for 3 hrs. The reaction was poured in $NaHCO_3$ (50 mL) and extracted wit EtOAc (4 × 30 mL). The combined organic fractions were dried (Na_2SO_4), filtered and concentrated under reduced pressure. The crude residue was purified by flash chromatography on a silica column (1:33 v/v MeOH/CH_2Cl_2) to afford the title compound as a dark blue film (30 mg, 0.06 mmol, 89.0 % yield). ^{1}H NMR (500 MHz, $CDCl_3$) δ 9.96 (s, 1H), 7.99 (s, 1H), 7.73 (s, 1H), 7.28 (s, 1H), 6.86 (d, *J* = 2.3 Hz, 1H), 6.72 (dd, *J* = 9.9, 0.8 Hz, 1H), 6.43 (s, 1H), 6.17 (dd, *J* = 10.0, 2.3 Hz, 1H), 3.94 (s, 3H), 3.31 (dt, *J* = 27.4, 5.9 Hz, 4H), 2.93 (dd, *J* = 7.4, 5.1 Hz, 2H), 2.39 (dd, *J* = 7.3, 5.2 Hz, 2H), 2.21 (s, 3H), 2.10–2.01 (m, 2H), 1.83 (p, *J* = 6.2 Hz, 2H), 0.55 (s, 6H). ^{13}C NMR (125 MHz, $CDCl_3$) δ 184.5, 183.8, 183.3, 147.9, 145.3, 141.6, 139.6, 138.0, 136.2, 135.6, 134.4, 132.9, 128.6, 128.2, 126.9, 126.0, 123.2, 122.6, 121.9, 118.2, 110.7, 50.8, 50.2, 34.0, 29.9, 29.2, 28.1, 21.7, 21.2, 20.5, 0.1, -0.1. IR (neat): 2927, 1737, 1574, 1353, 1301, 1203 cm^{-1}. HR-MS calculated for $C_{32}H_{32}N_2O_2Si$ $[M+H]^+$ *m/z* 505.2311, found 505.2319.

9-(3-(1-aminobut-3-en-1-yl)-1,6-dimethyl-1H-indol-5-yl)-14,14-dimethyl-2,3,5,6,7,14-hexahydro-1H,12H-benzo[5,6]silino[2,3-f]pyrido[3,2,1-ij]quinolin-12-one (15). Potassium allyltrifluoroborate (17.6 mg, 0.12 mmol, 2.0 eq.) was dissolved

in a 7N solution of NH_3 in MeOH (3.0 mL) and stirred at room temperature for 15 min. A solution of compound **14** (9 mg, 0.016 mmol, 1 eq.) in 7N solution of NH_3 in MeOH (2.0 mL) and H_2O (10 µL) were added sequentially to the reaction which was stirred for 16 hrs. The reaction was poured into sat. $NaHCO_3$ (50 mL) and extracted with EtOAc (4 × 30 mL). The combined organic fractions were dried (Na_2SO_4), filtered, and concentrated under reduced pressure. The crude residue was purified by flash chromatography on a silica column (1:19 v/v MeOH/CH_2Cl_2) to afford the title compound as a dark blue film (24 mg, 0.014 mmol, 74.5% yield). ^{1}H NMR (500 MHz, MeOD/$CDCl_3$) δ 7.24 (dd, *J* = 11.3, 8.6 Hz, 2H), 7.19 (s, 1H), 6.85–6.80 (m, 2H), 6.55 (d, *J* = 3.6 Hz, 1H), 6.15 (ddd, *J* = 10.1, 8.0, 2.4 Hz, 1H), 5.75–5.63 (m, 1H), 5.17–4.99 (m, 2H), 4.38 (td, *J* = 7.0, 4.7 Hz, 1H), 3.83 (s, 3H), 3.40 (t, *J* = 5.9 Hz, 2H), 3.35 (t, *J* = 6.1 Hz, 2H), 2.94 (t, *J* = 6.2 Hz, 2H), 2.74–2.66 (m, 1H), 2.61 (dd, *J* = 14.2, 7.2 Hz, 1H), 2.43–2.31 (m, 2H), 2.14 (s, 3H), 2.09–1.98 (m, 2H), 1.88–1.78 (m, 2H), 0.55 (s, 6H). ^{13}C NMR (125 MHz, $CDCl_3$) δ 184.4, 147.9, 144.8, 142.0, 137.4, 136.1, 136.0, 135.5, 134.7, 132.0, 131.1, 130.4, 129.0, 128.4, 127.2, 126.2, 125.7, 121.9, 119.9, 117.7, 110.0, 50.7, 50.2, 48.0, 43.7, 43.5, 33.0, 29.9, 29.2, 28.2, 21.8, 21.3, 20.4, 0.2, 0.0. IR (neat): 3012, 2972, 1739, 1585, 1366, 1231, 834, 765 cm^{-1}. HR-MS calculated for $C_{35}H_{39}N_3OSi$ $[M+H]^+$ *m/z* 546.2941, found 546.2947.

FP1. A solution of compound **15** (120.0 mg, 0.22 mmol, 1.0 eq.) in anhydrous THF (10.0 mL) was cooled in an ice-bath. To the solution, 4-nitrobenzaldehyde (100 mg, 0.66 mmol, 3.0 eq.), glacial AcOH (100 µL, 1.6 mmol, 10 eq.), and sodium

triacetoxyborohydride (186 mg, 0.88 mmol, 4.0 eq.) were added sequentially. The reaction was warmed to room temperature and stirred for 16 hrs. Upon completion, the reaction was poured into sat. $NaHCO_3$ (50 mL) and extracted with EtOAc (4 × 30 mL). The combined organic fractions were dried (Na_2SO_4), filtered, and concentrated under reduced pressure. The crude residue was purified by flash chromatography on a silica column (1:33 MeOH/CH_2Cl_2) to afford the title compound as a dark blue film. (32.0 mg, 0.057 mmol, 26.0 % yield). ^{1}H NMR (500 MHz, $CDCl_3$) δ 8.40 (d, *J* = 7.8 Hz, 1H), 8.20 (d, *J* = 8.7 Hz, 2H), 7.87 (dd, *J* = 8.6, 6.1 Hz, 2H), 7.38 (d, *J* = 51.2 Hz, 1H), 7.22 (s, 1H), 7.14 (d, *J* = 23.1 Hz, 1H), 6.88 (dd, *J* = 4.7, 2.3 Hz, 1H), 6.83 (dd, *J* = 22.0, 10.0 Hz, 1H), 6.53 (d, *J* = 50.1 Hz, 1H), 6.18 (ddd, *J* = 26.9, 9.9, 2.3 Hz, 1H), 5.79 (ddtd, *J* = 17.3, 10.1, 7.1, 4.5 Hz, 1H), 5.11–4.96 (m, 2H), 4.77 (td, *J* = 8.3, 5.5 Hz, 1H), 3.84 (d, *J* = 5.3 Hz, 3H), 3.43–3.33 (m, 2H), 3.3–3.21 (m, 2H), 2.96 (dt, *J* = 12.4, 5.9 Hz, 2H), 2.90–2.77 (m, 2H), 2.47–2.30 (m, 2H), 2.18 (d, *J* = 4.6 Hz, 3H), 2.14–2.02 (m, 2H), 1.91–1.71 (m, 2H), 0.59 (d, *J* = 7.1 Hz, 3H), 0.56 (d, *J* = 1.8 Hz, 3H).^{13}C NMR (125 MHz, $CDCl_3$) δ 183.9, 157.8, 157.7, 149.0, 148.0, 145.1, 142.1, 142.0, 137.3, 136.3, 135.8, 135.74, 135.70, 135.6, 134.4, 132.3, 132.2, 130.6, 129.1, 128.6, 128.5, 127.2, 126.6, 126.5, 126.0, 125.9, 124.5, 124.2, 123.97, 123.93, 121.9, 121.8, 120.5, 120.1, 117.7, 117.5, 116.6, 116.1, 110.25, 110.21, 68.1, 67.7, 50.8, 50.7, 50.29, 50.25, 42.2, 41.6, 33.16, 33.13, 29.9, 29.2, 29.2, 28.18, 28.10, 21.7, 21.28, 21.21, 20.5, 20.4, 0.15, 0.13, 0.06, 0.04. IR: 2925, 1737, 1571, 1347, 1301, 1204 cm^{-1}. HR-MS calculated for $C_{42}H_{44}N_4O_3Si$ $[M+H]^+$ *m/z* 681.3261, found 681.3272.

APPENDIX C-SUPPLEMENTARY FIGURES FOR CHAPTER 1

This appendix includes supplementary figures including ^{1}H and ^{13}C NMR spectrum for the compounds synthesized in Chapter 1.

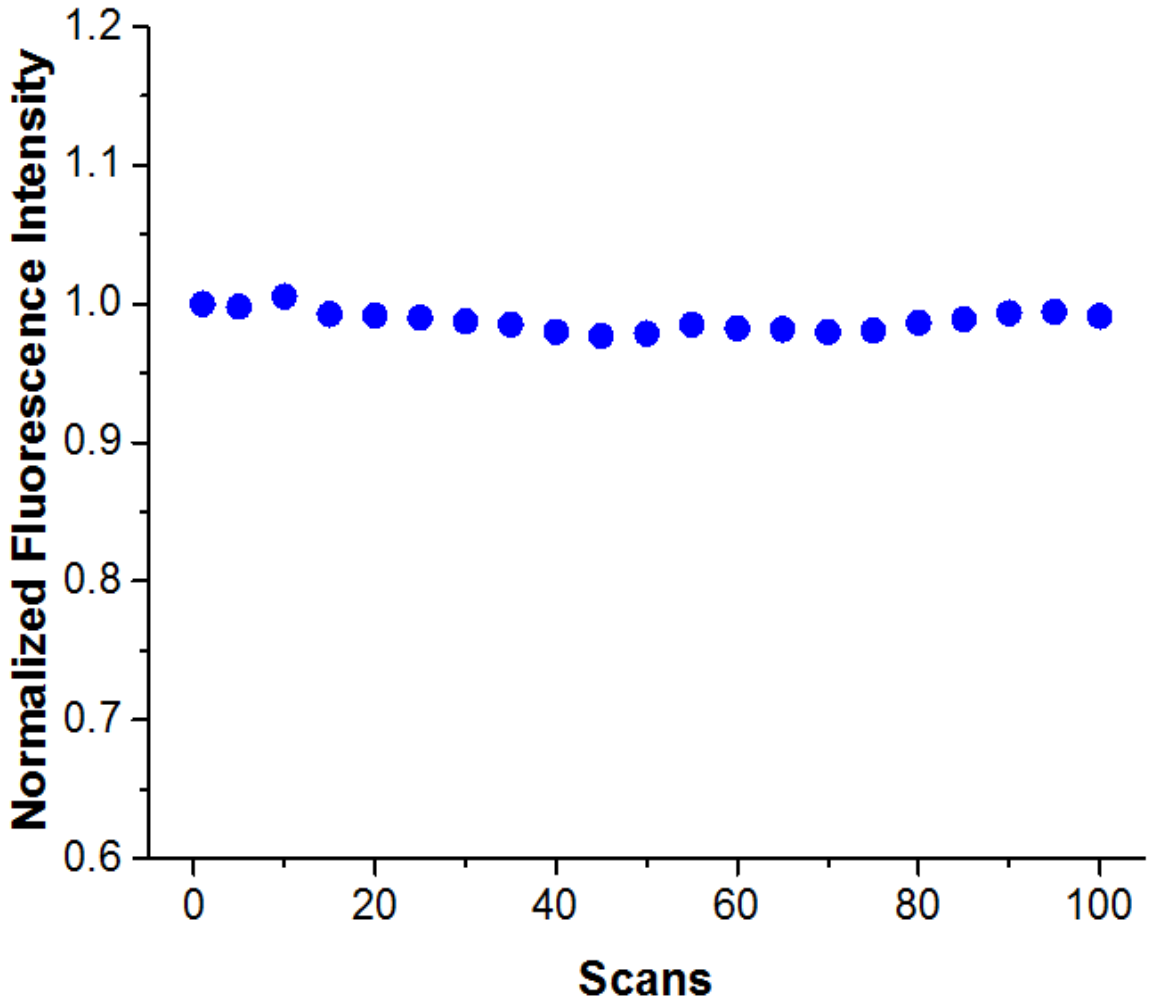

Figure C.1. Photobleaching assay of FP1 in live cells. HEK293TN cells were stained with a solution of 2 µM FP1 in DMEM for 8 min, rinsed with fresh DMEM. After 30 min, a field of cells were subjected to irradiation for 100 scans with the 633 nm HeNe laser set at 25% power with a pinhole size of 1 airy unit. A data point is plotted for every 5 scans.

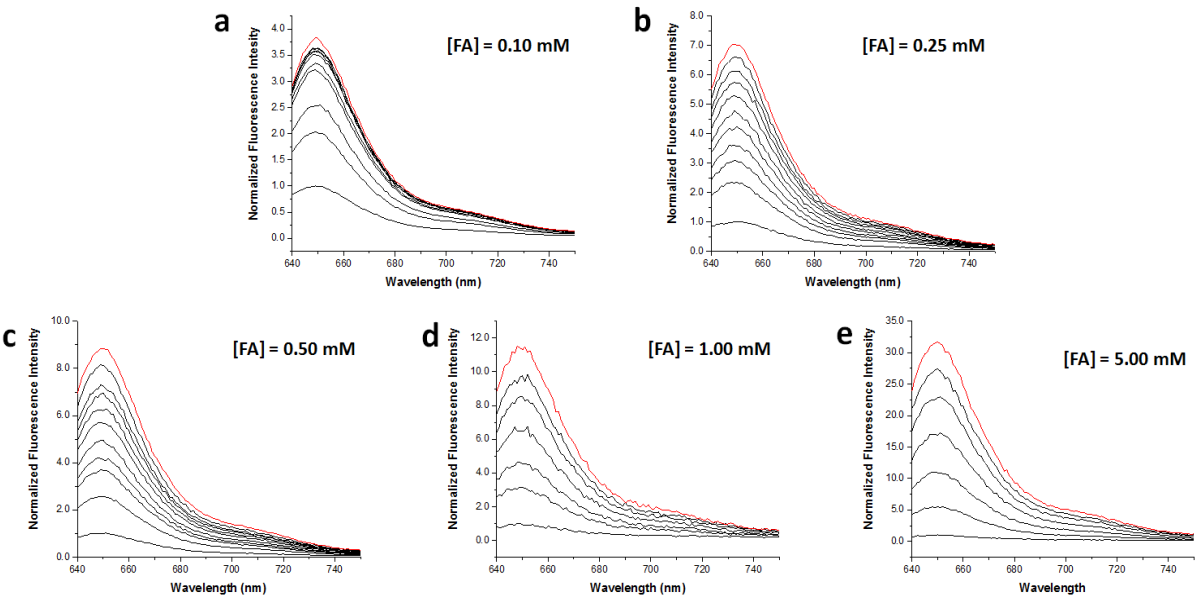

Figure C.2. Normalized fluorescence emission of 1 µM FP1 in PBS (pH 7.4) reacted with a) 0.1 mM, b) 0.25 mM, c) 0.5 mM, d) 1 mM, and e) 5 mM FA. FP1 was excited at 633 nm and the emission was collect between 640 and 750 nm. All experiments were performed at 37 °C for 3 h. Time points on graphs a-c are recorded every 15 min. The time points for graphs d-e represent every 30 min. A concentration dependent increase in fluorescence intensity was observed with a fold increase of 3.9, 7.0, 8.5, 11.6, and 33.5 for 0.1 mM, 0.25 mM, 0.5 mM, 1 mM, and 5 mM FA, respectively.

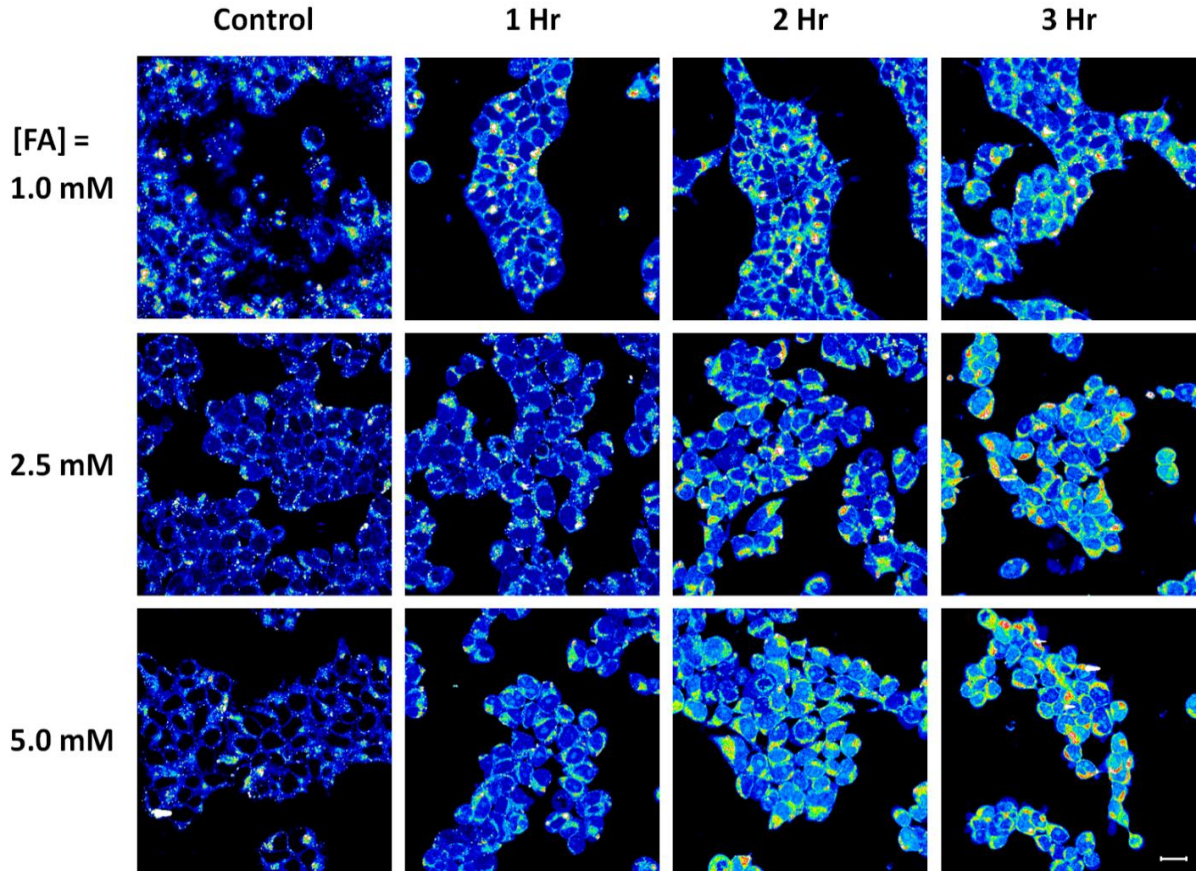

Figure C.3. Live-cell imaging of HEK293TN cells. Cells were stained with a solution of 2 µM FP_1 in serum-free DMEM for 8 min, washed with fresh DMEM to remove excess dye and then incubated with 1, 2.5, or 5 mM FA at 37 °C for 1, 2, and 3 h. Cells were irradiated with the 633 nm HeNe laser set at 3% power with a pinhole size of 1 airy unit. The emission was collected between 645 and 800 nm. Scale bar represents 20 µm.

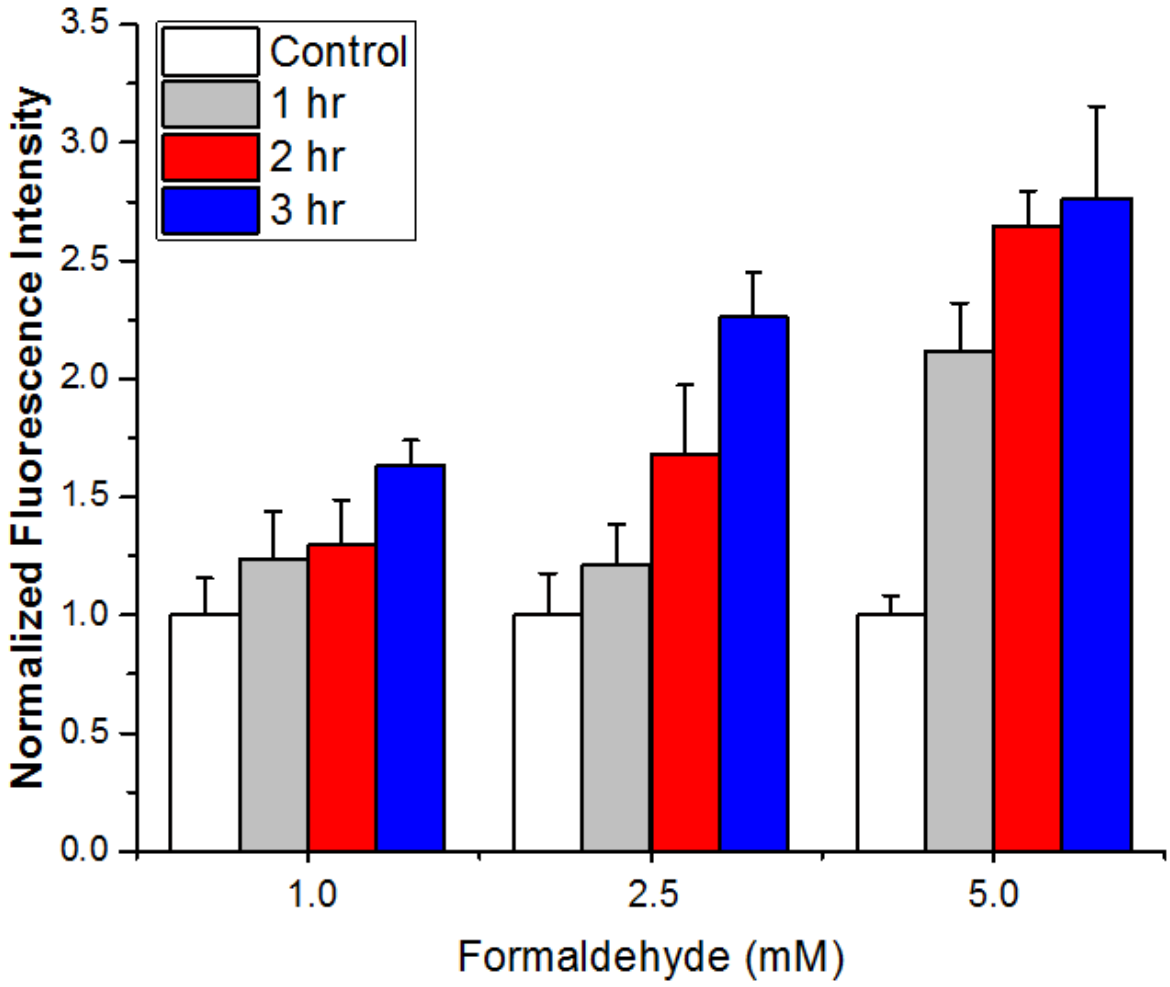

Figure C.4. Quantification of observed fluorescence intensity by confocal imaging in HEK293TN cells after incubation with 1 mM, 2.5 mM or 5 mM FA for 1 (light grey bars), 2 (red bars) and 3 hrs (blue bars). A DMEM vehicle was added to control cells which was normalized to 1 (white bars). Cells incubated with 1 mM FA for 1, 2 and 3 hrs exhibited a 1.2-, 1.3-, and 1.6-fold increase in fluorescence intensity, respectively. Cells incubated with 2.5 mM FA for 1, 2 and 3 hrs resulted in a 1.2-, 1.7-, and 2.2-fold increase in fluorescence intensity, respectively. Cells incubated with 5 mM FA for 1, 2 and 3 hrs resulted in a 2.1-, 2.6-, and 2.8-fold increase in fluorescence intensity, respectively. For each condition, a minimum of 5 images were averaged ($n > 5$). Errors represent standard deviation.

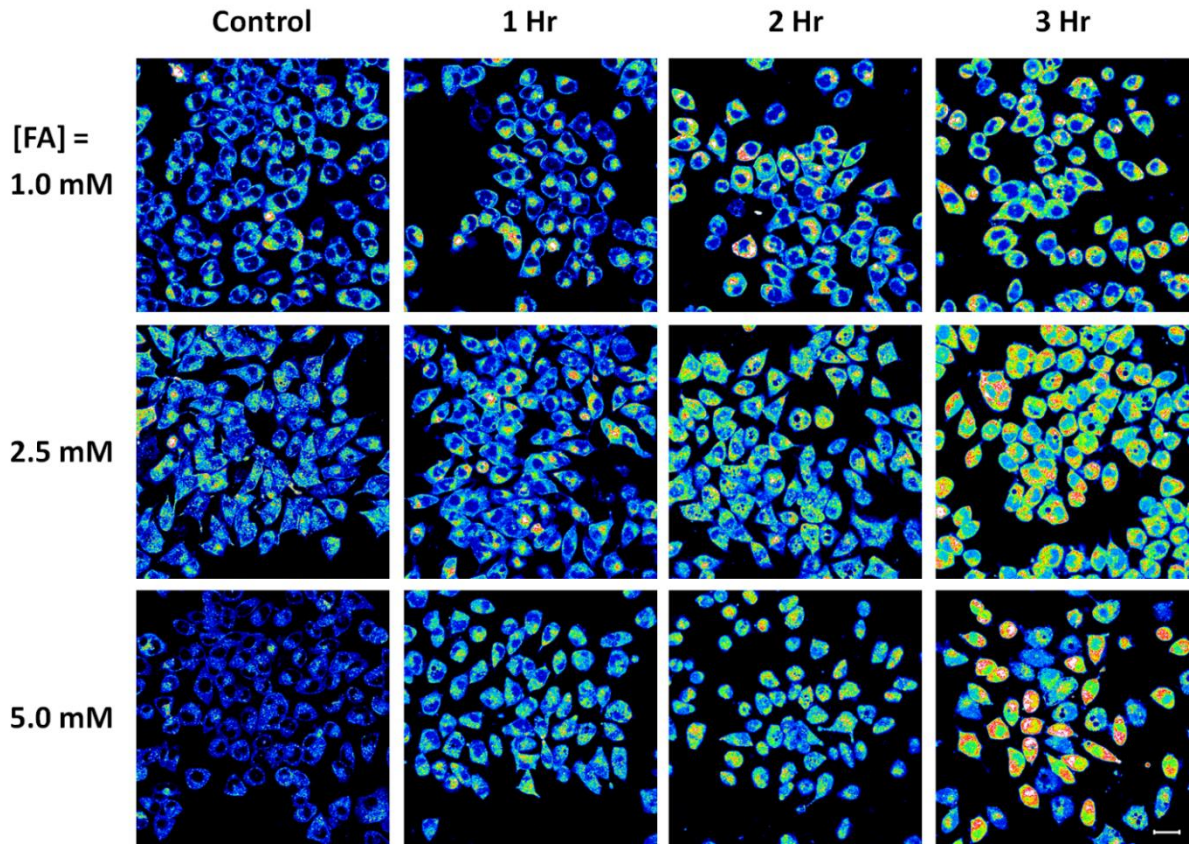

Figure C.5. Live-cell imaging of NC cells. Cells were stained with a solution of 2 µM FP_1 in Ham's F-12K serum-free media for 8 min, washed with fresh media to remove excess dye and then incubated with 1, 2.5, or 5 mM FA at 37 °C for 1, 2, and 3 hrs. Cells were irradiated with the 633 nm HeNe laser set at 3% power with a pinhole size of 1 airy unit. The emission was collected between 645 and 800 nm. Scale bar represents 20 µm.

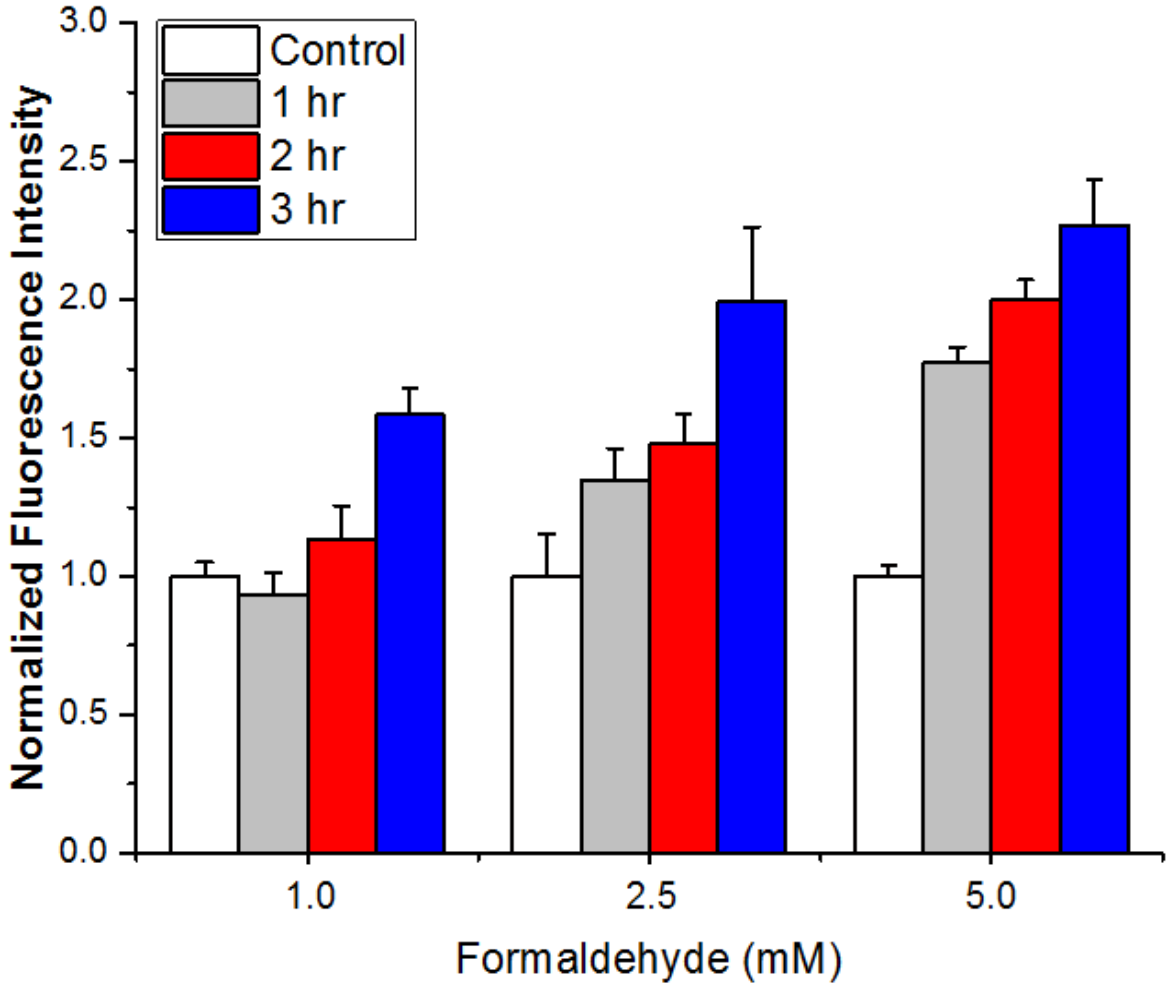

Figure C.6. Quantification of observed fluorescence intensity by confocal imaging in NC cells after incubation with 1 mM, 2.5 mM or 5 mM FA for 1 (light grey bars), 2 (red bars) and 3 h (blue bars). A Ham's F-12K vehicle was added to control cells which was normalized to 1 (white bars). Cells incubated with 1 mM FA for 1, 2 and 3 hrs exhibited a 0-, 1.1-, and 1.6-fold increase in fluorescence intensity, respectively. Cells incubated with 2.5 mM FA for 1, 2 and 3 hrs resulted in a 1.3-, 1.5-, and 2.0-fold increase in fluorescence intensity, respectively. Cells incubated with 5 mM FA for 1, 2 and 3 hrs resulted in a 1.8-, 2.0-, and 2.3-fold increase in fluorescence intensity, respectively. For each condition, a minimum of 5 images were averaged ($n > 5$). Errors represent standard deviation.

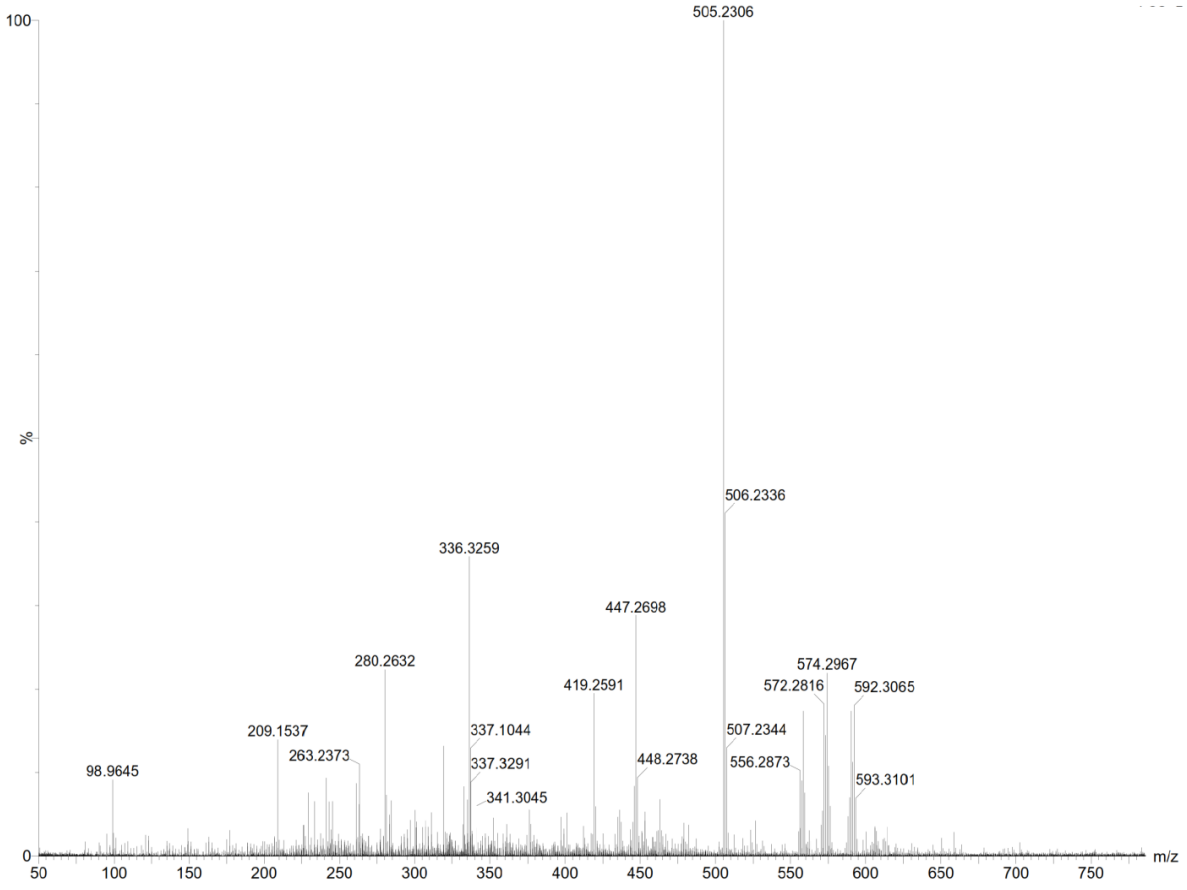

Figure C.7. ESI-HRMS spectrum of a crude reaction mixture after FP_1 (25 µM) was reacted with 5 mM FA at 37 °C for 48 h in the presence of HEK293TN cellular lysates to yield compound **14**. HR-MS calculated for $C_{32}H_{32}N_2O_2Si$ $[M+H]^+$ *m/z* 505.2311, found 505.2306.

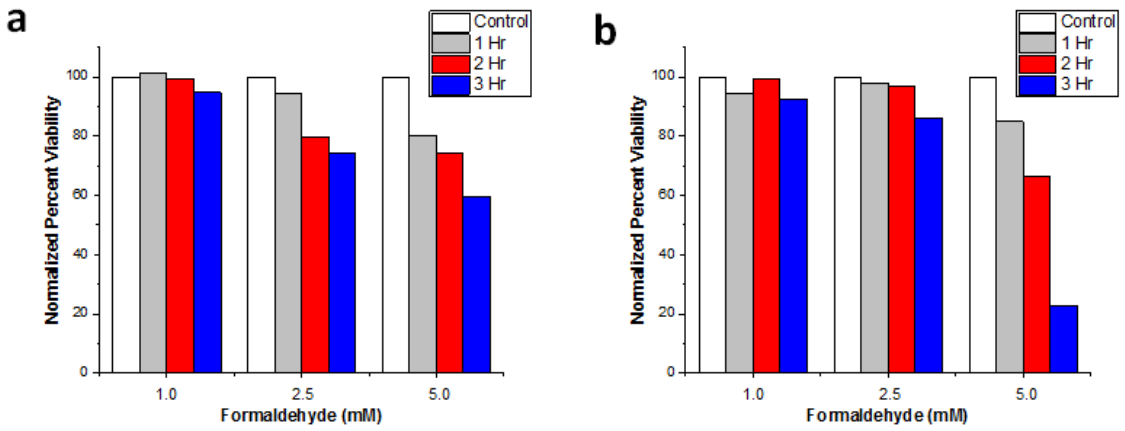

Figure C.8. Trypan blue dye exclusion assay to determine cell viability of a) HEK293TN cells and b) NS-1 cells treated with FA. Both cell lines were treated 1 mM, 2.5 mM and 5 mM FA for 1, 2 and 3 hrs. For each condition, a 10 µL sample of cells was mixed with 10 µL of a 2× trypan blue solution. Live and dead cells were counted at each of the four 4×4 quadrants of a hemocytometer using a light microscope equipped with a 10× objective. Control samples treated with a vehicle control were normalized to 100% viability.

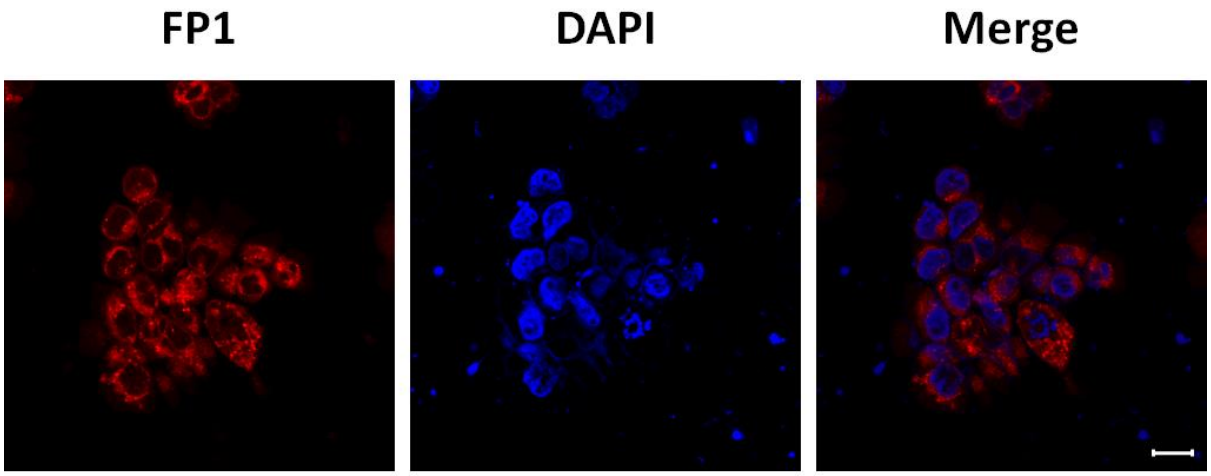

Figure C.9. Nuclear staining of HEK293TN cells with DAPI demonstrates cell viability by showing intact nuclei after FP1 stained cells were treatment with 5 mM FA for 3 hrs. DAPI was applied as a 300 nM solution in serum-free DMEM for 5 min. Left: Fluorescent signal from FP1 obtained by irradiation with the 633 nm HeNe laser. Middle: Fluorescent signal from DAPI obtained by irradiation with the 405 nm laser line. Right: Merged image of both signals. Scale bar represents 20 µm.

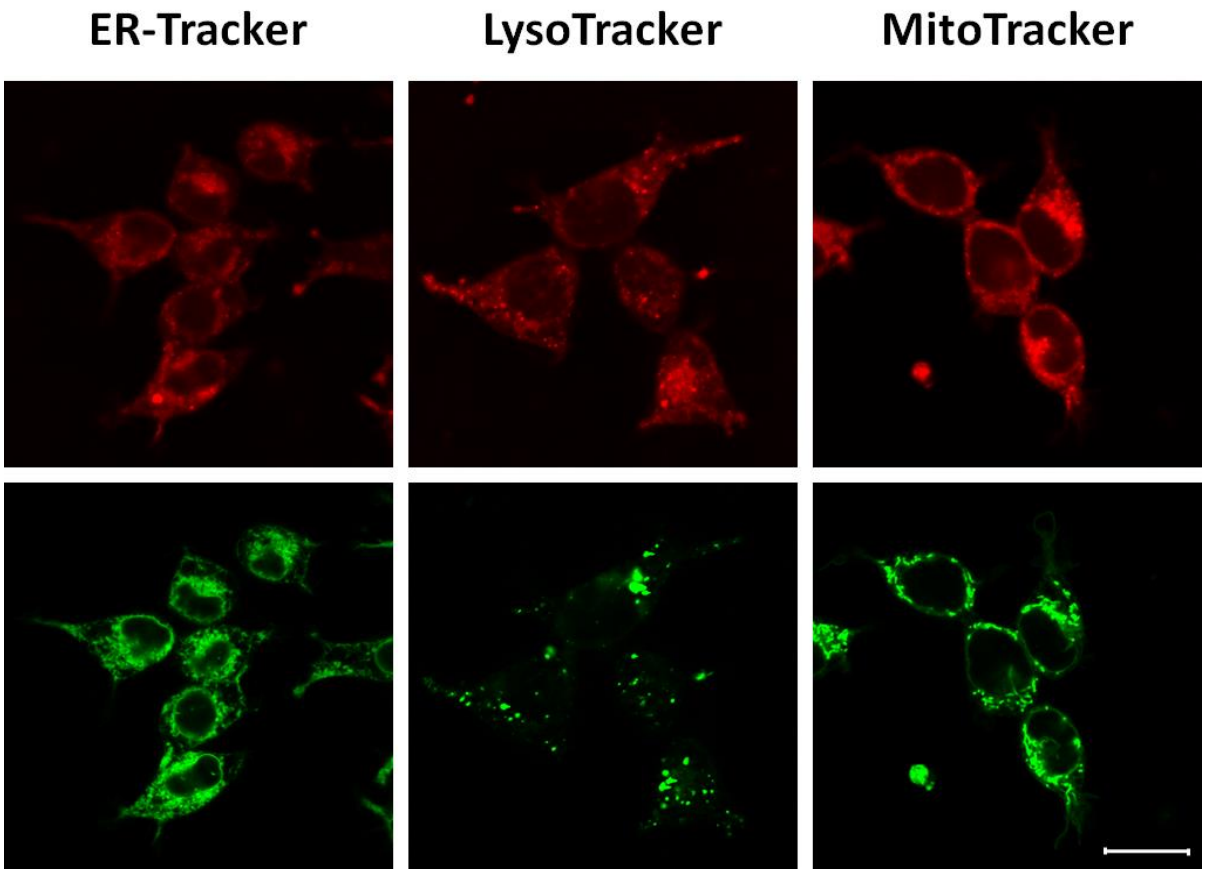

Figure C.10. Confocal microscopy images of co-localization experiments using HEK293TN cells. Cells were co-incubated for 5 min with 2 µM FPI and 1 µM of each tracker in serum-free DMEM, then washed with dye-free DMEM and imaged. Top row of images show fluorescent signal from FP1 obtained by irradiation with the 633 nm HeNe laser. Bottom row of images show fluorescent signal from ER-Tracker Green, LysoTracker, and MitoTracker Green FM obtained by irradiation with the 488 nm laser. Scale bar represents 20 um.

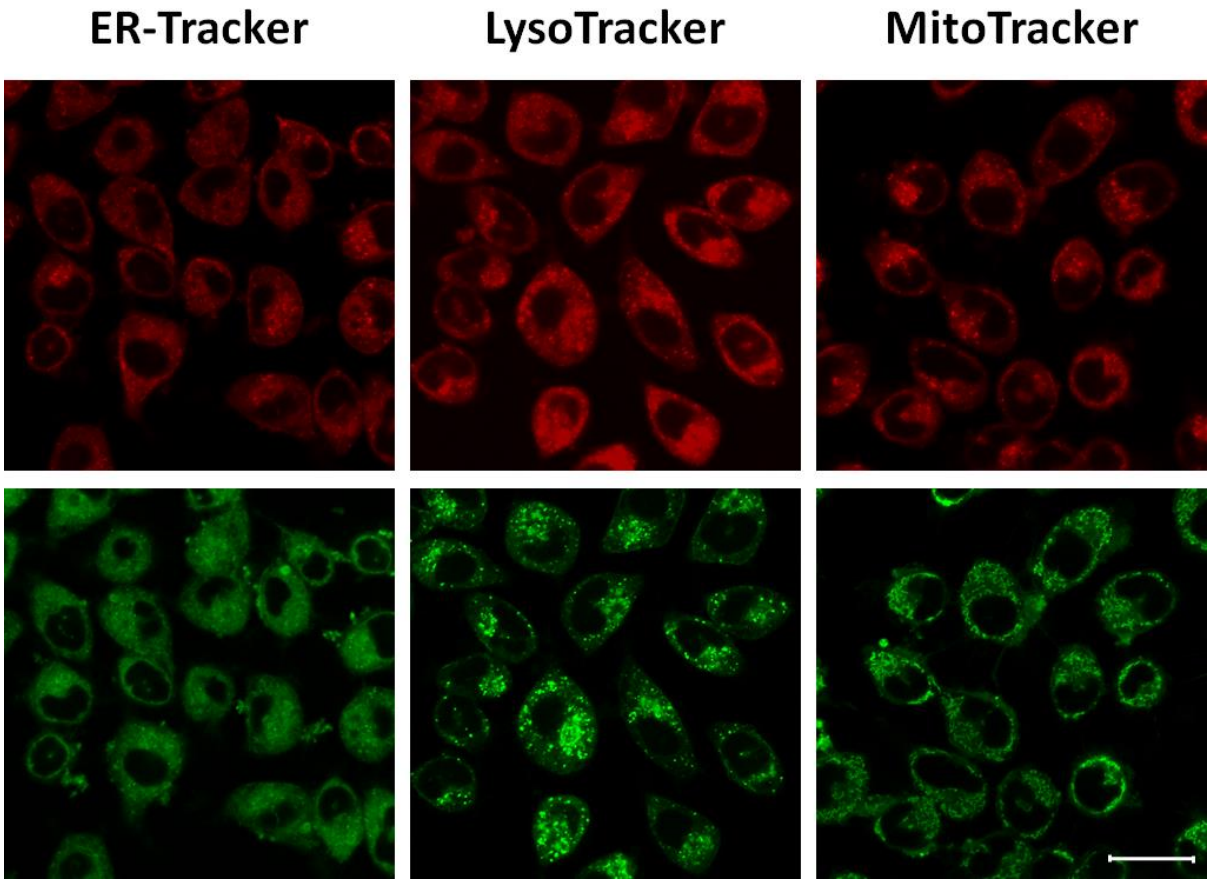

Figure C.11. Confocal microscopy images of co-localization experiments using NC cells. Cells were co-incubated for 5 min with 2 µM FPI and 1 µM of each tracker in serum-free DMEM, then washed with dye-free DMEM and imaged. Top row of images show fluorescent signal from FP1 obtained by irradiation with the 633 nm HeNe laser. Bottom row of images show fluorescent signal from ER-Tracker Green, LysoTracker, and MitoTracker Green FM obtained by irradiation with the 488 nm laser. Scale bar represents 20 um.

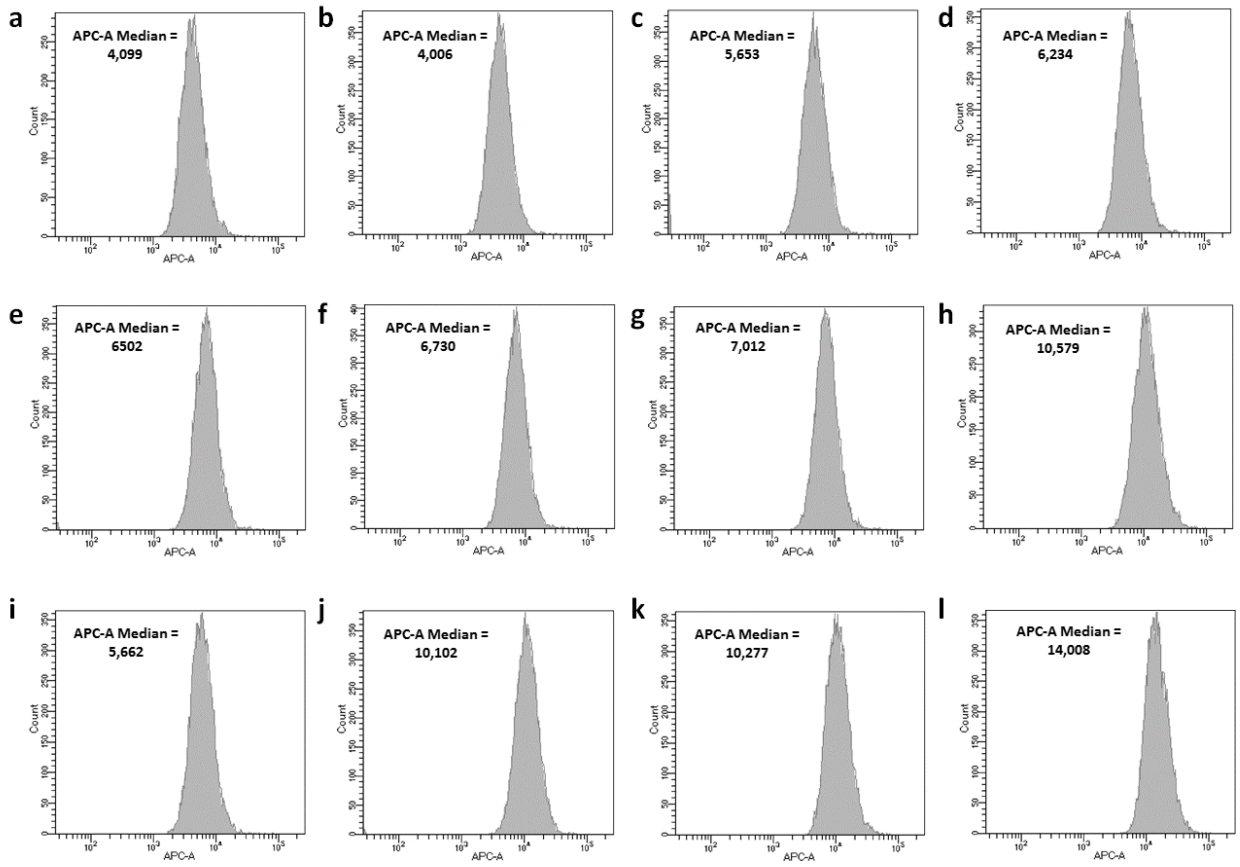

Figure C.12. Flow cytometry analysis of HEK293TN cells. Cells were stained with a solution of 2 µM FP1 in DMEM for 8 min, rinsed with fresh DMEM and then treated with a) a DMEM vehicle control; b) 1 mM FA, 1 hr incubation; c) 1 mM FA, 2 hrs incubation; d) 1 mM FA, 3 hrs incubation; e) a DMEM vehicle control; f) 2.5 mM FA, 1 hr incubation; g) 2.5 mM FA, 2 hrs incubation; h) 2.5 mM FA, 3 hrs incubation; i) a DMEM vehicle control; j) 5 mM FA, 1 hr incubation; k) 5 mM FA, 2 hrs incubation; and l) 5 mM FA, 3 hrs incubation.

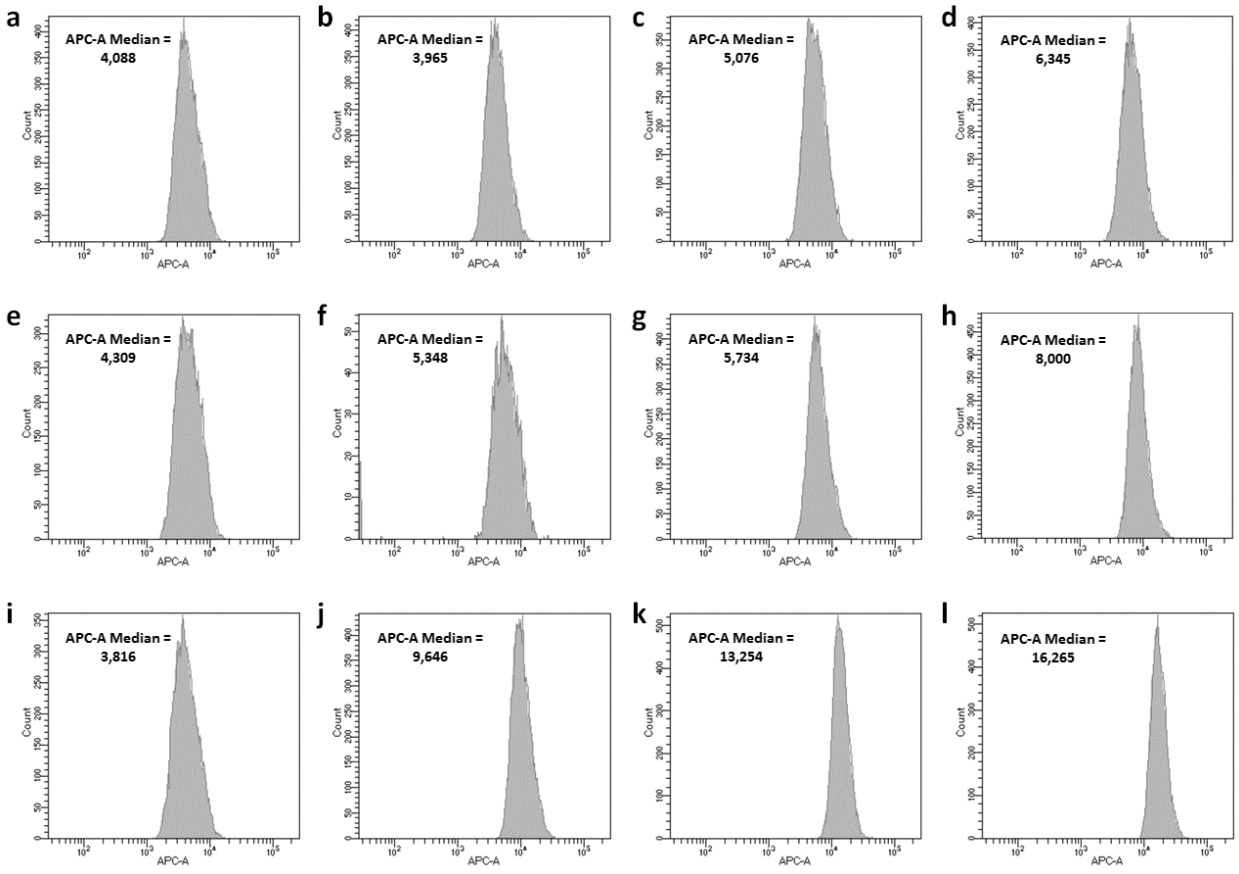

Figure C.13. Flow cytometry analysis of NC cells. Cells were stained with a solution of 2 μM FP1 in Ham's F-12K media for 8 min, rinsed with fresh media and then treated with a) a DMEM vehicle control; b) 1 mM FA, 1 hr incubation; c) 1 mM FA, 2 hrs incubation; d) 1 mM FA, 3 hrs incubation; e) a DMEM vehicle control; f) 2.5 mM FA, 1 hr incubation; g) 2.5 mM FA, 2 hrs incubation; h) 2.5 mM FA, 3 hrs incubation; i) a DMEM vehicle control; j) 5 mM FA, 1 hr incubation; k) 5 mM FA, 2 hrs incubation; and l) 5 mM FA, 3 hrs incubation.

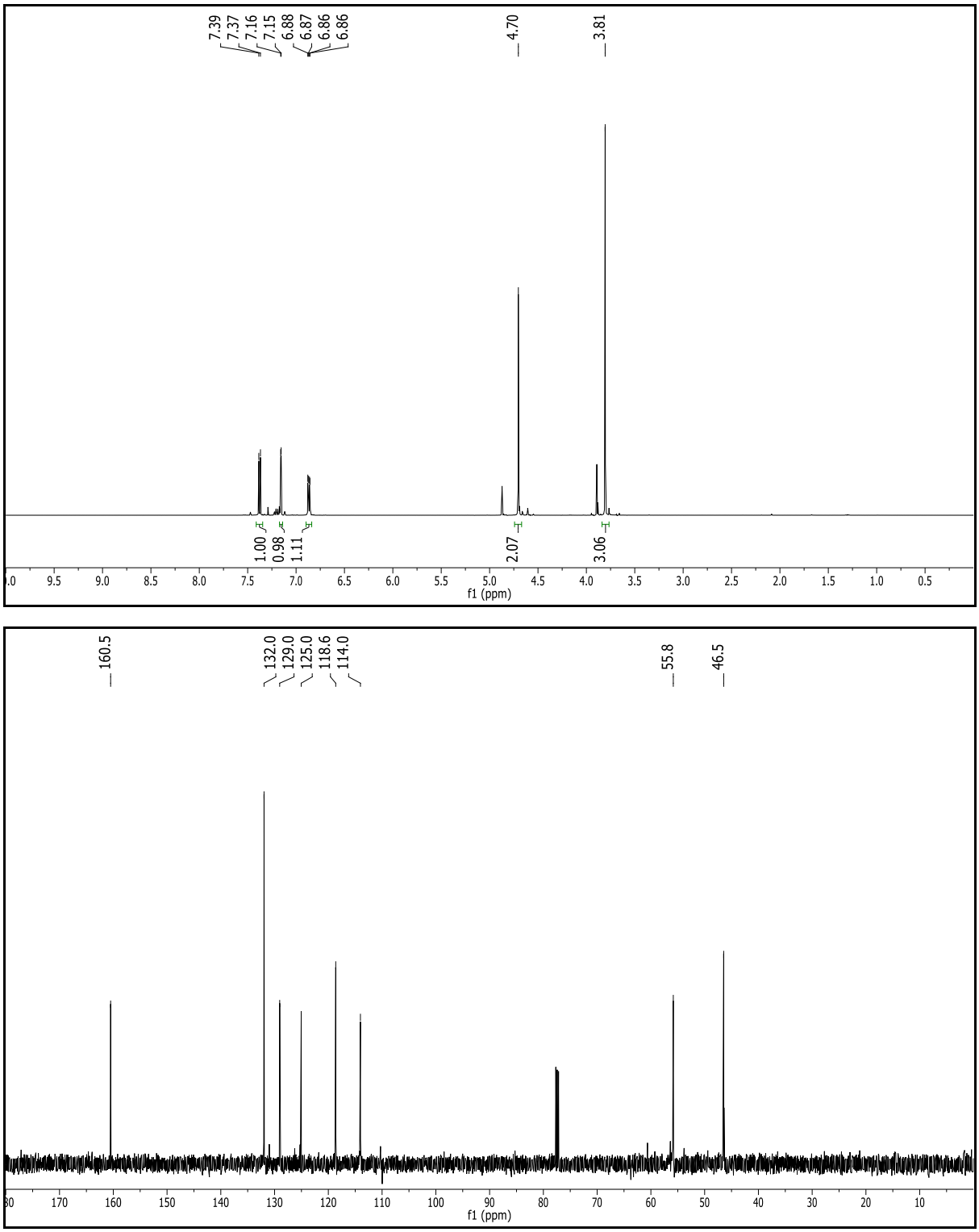

Figure C.14. ^{1}H NMR (500 MHz, $CDCl_3$) and ^{13}C NMR (125 MHz, $CDCl_3$) NMR spectra of **2**.

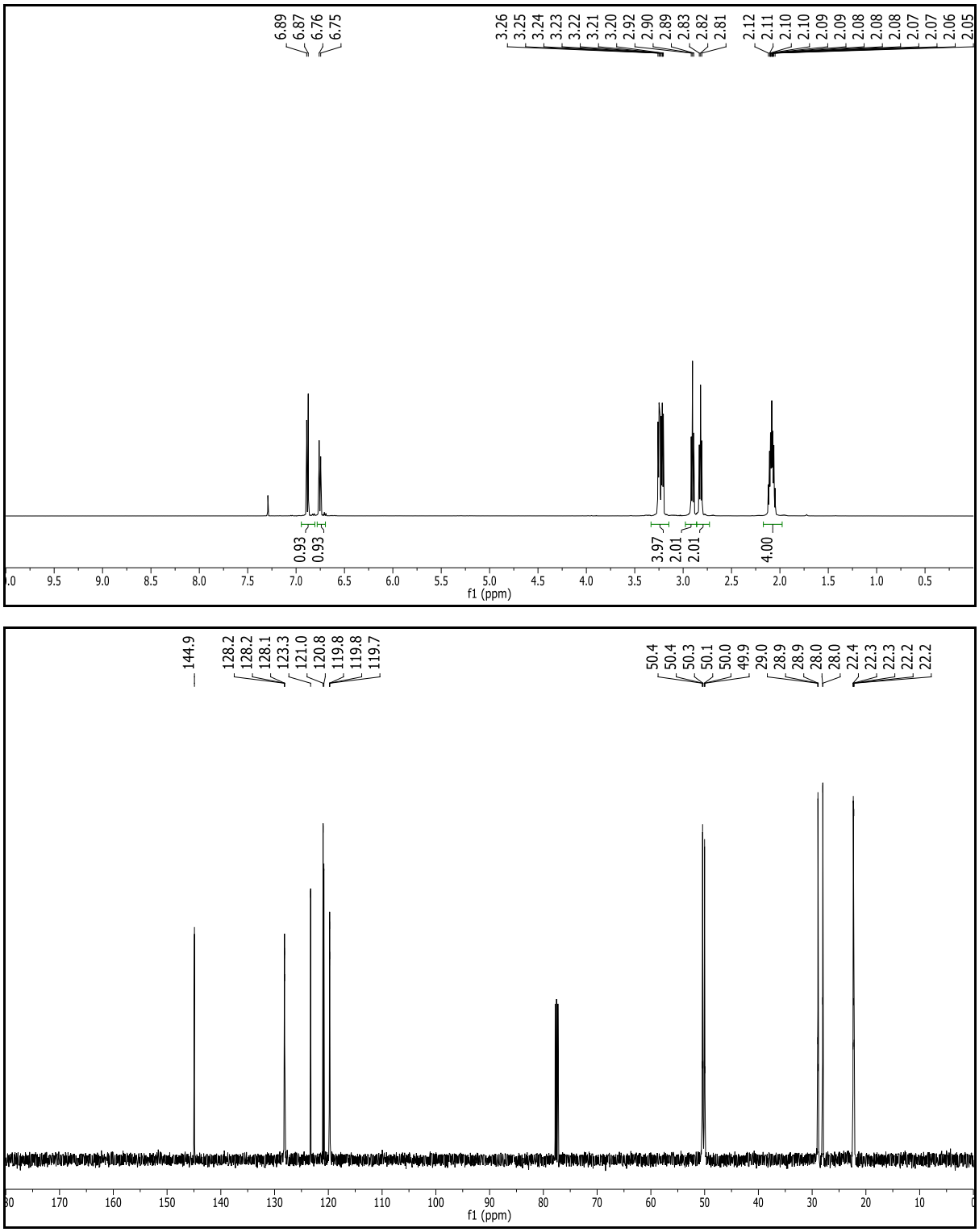

Figure C.15. ^{1}H NMR (500 MHz, $CDCl_3$) and ^{13}C NMR (125 MHz, $CDCl_3$) NMR spectra of **4**.

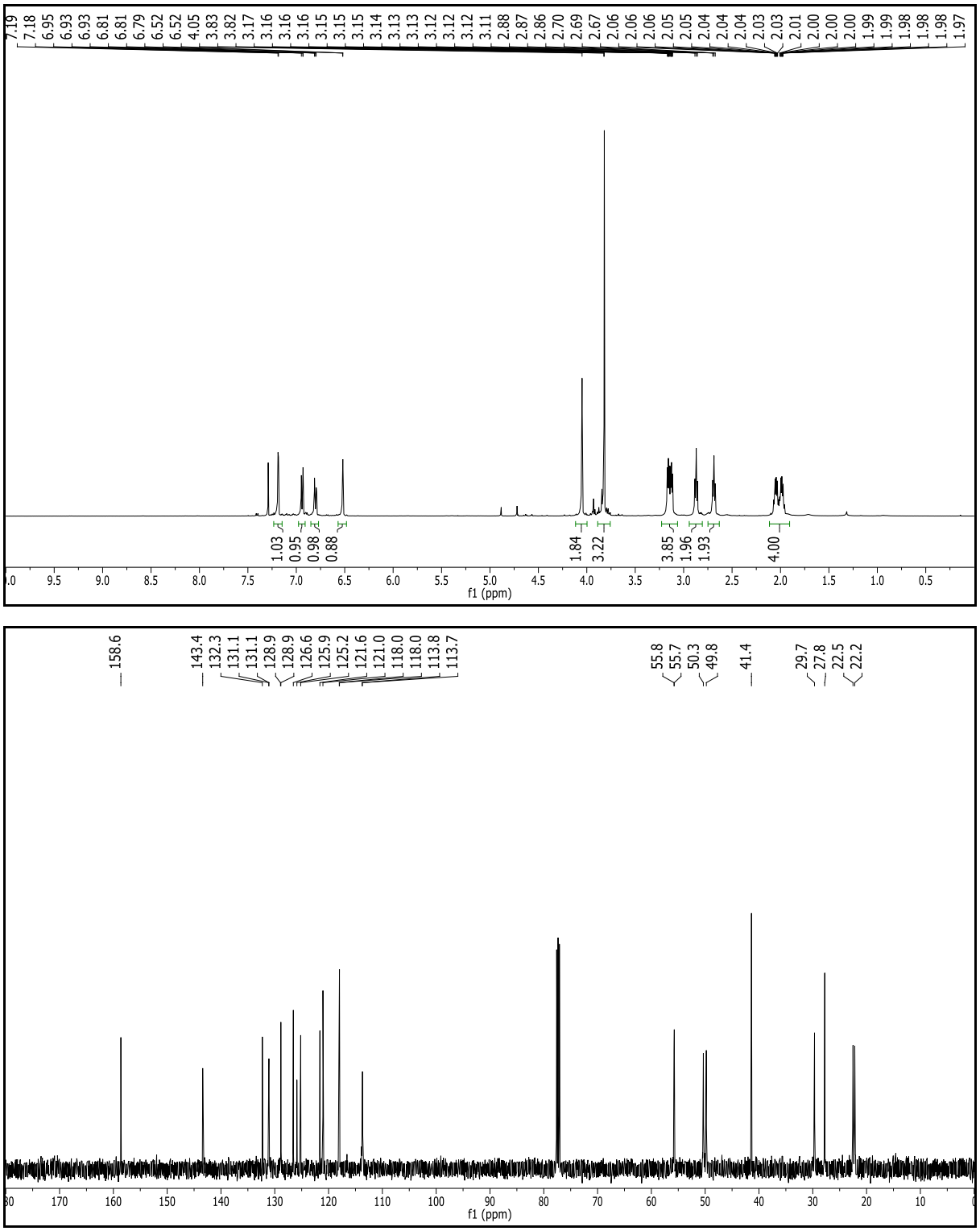

Figure C.16. ^{1}H NMR (500 MHz, $CDCl_3$) and ^{13}C NMR (125 MHz, $CDCl_3$) NMR spectra of **5**.

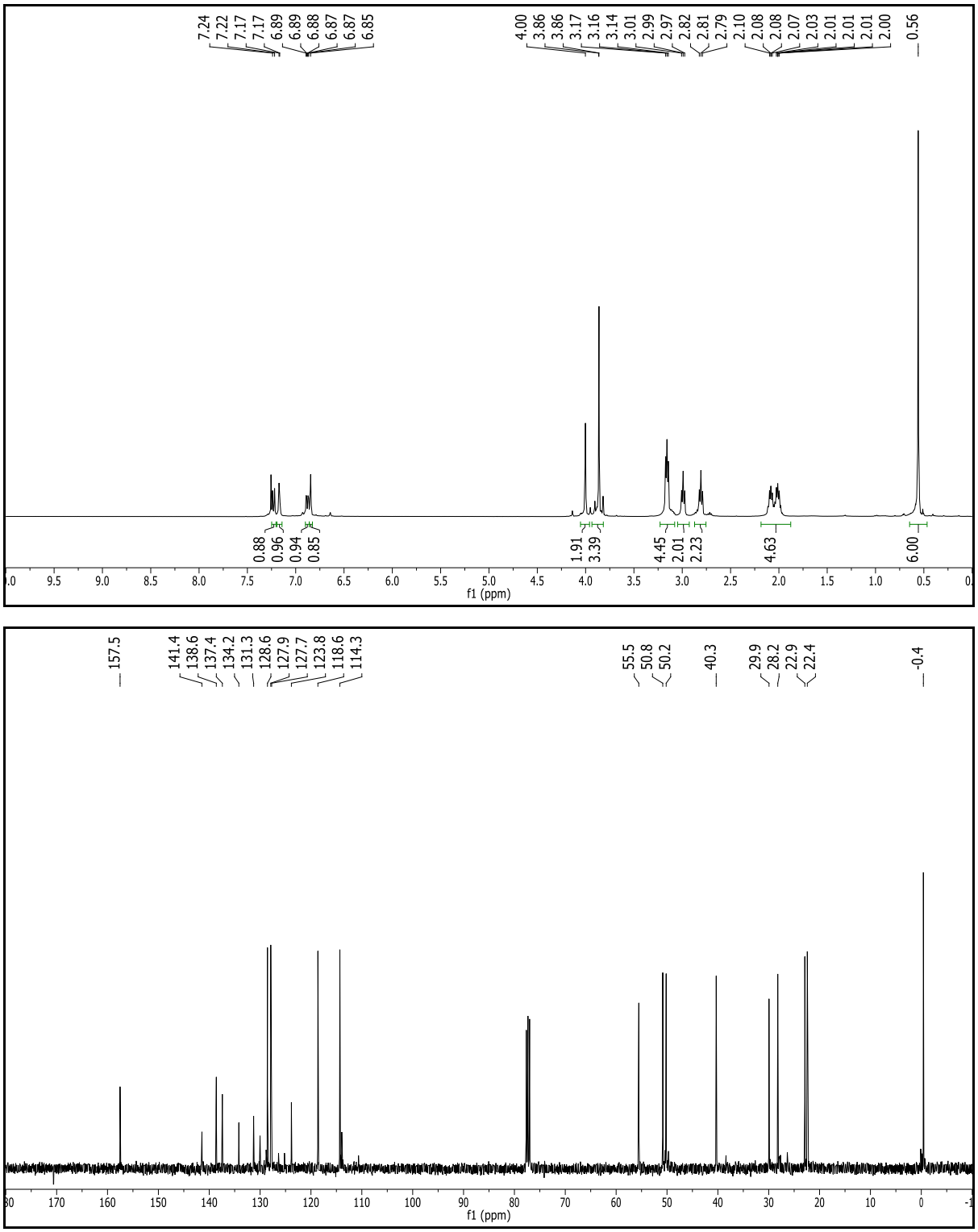

Figure C.17. ^{1}H NMR (500 MHz, $CDCl_3$) and ^{13}C NMR (125 MHz, $CDCl_3$) NMR spectra of **5.5**.

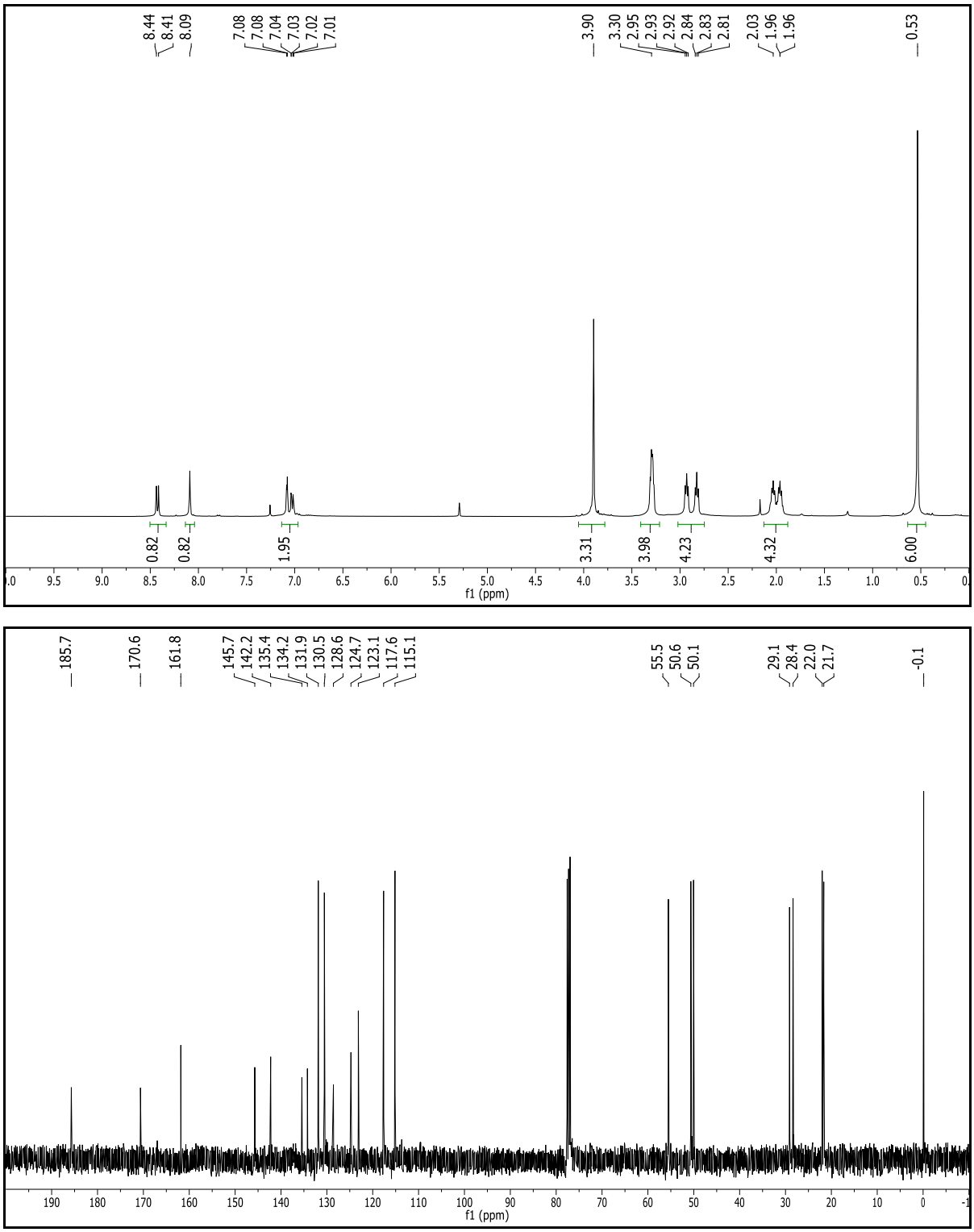

Figure C.18. ^{1}H NMR (500 MHz, $CDCl_3$) and ^{13}C NMR (125 MHz, $CDCl_3$) NMR spectra of **6**.

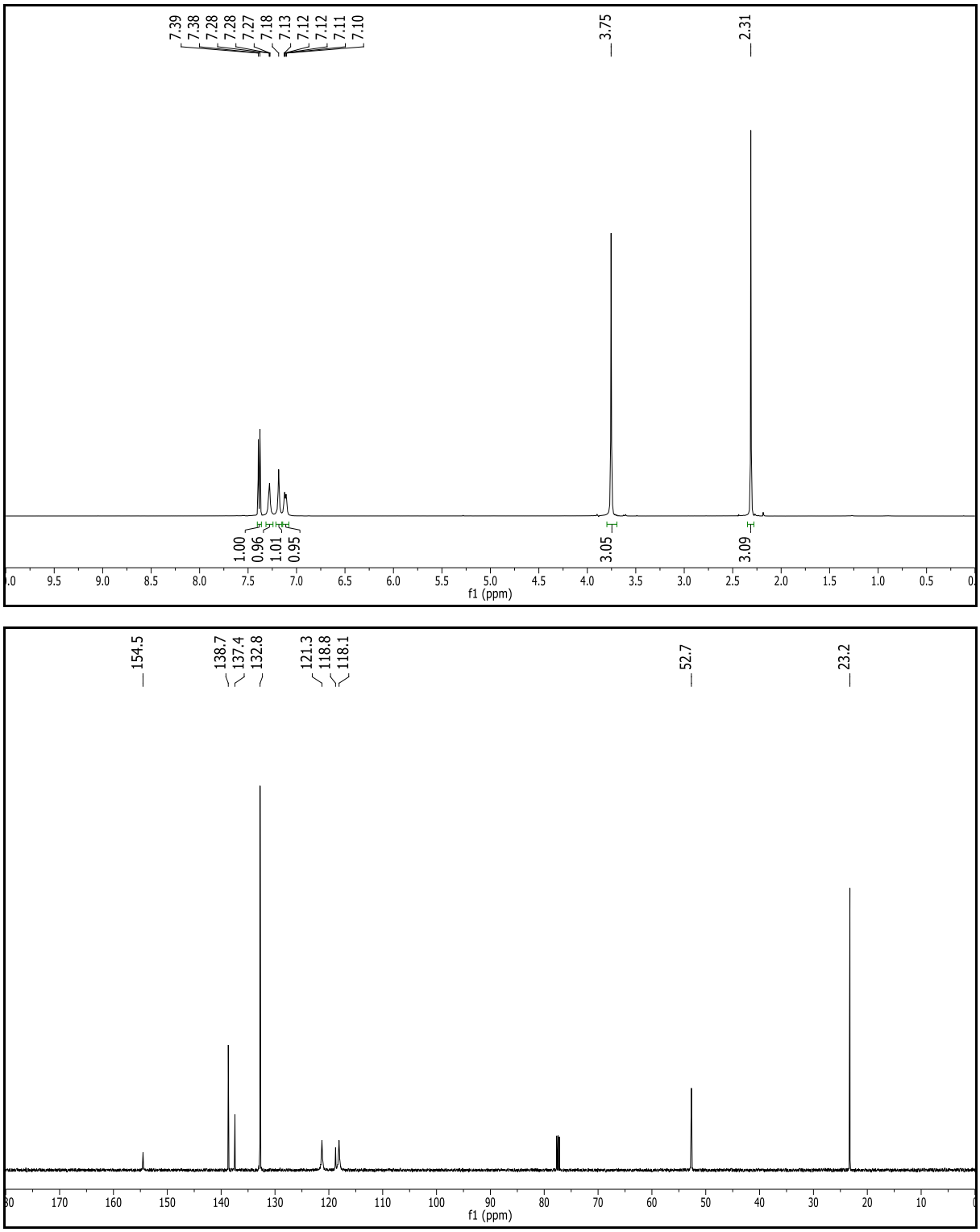

Figure C.19. ^{1}H NMR (500 MHz, $CDCl_3$) and ^{13}C NMR (125 MHz, $CDCl_3$) NMR spectra of **8**.

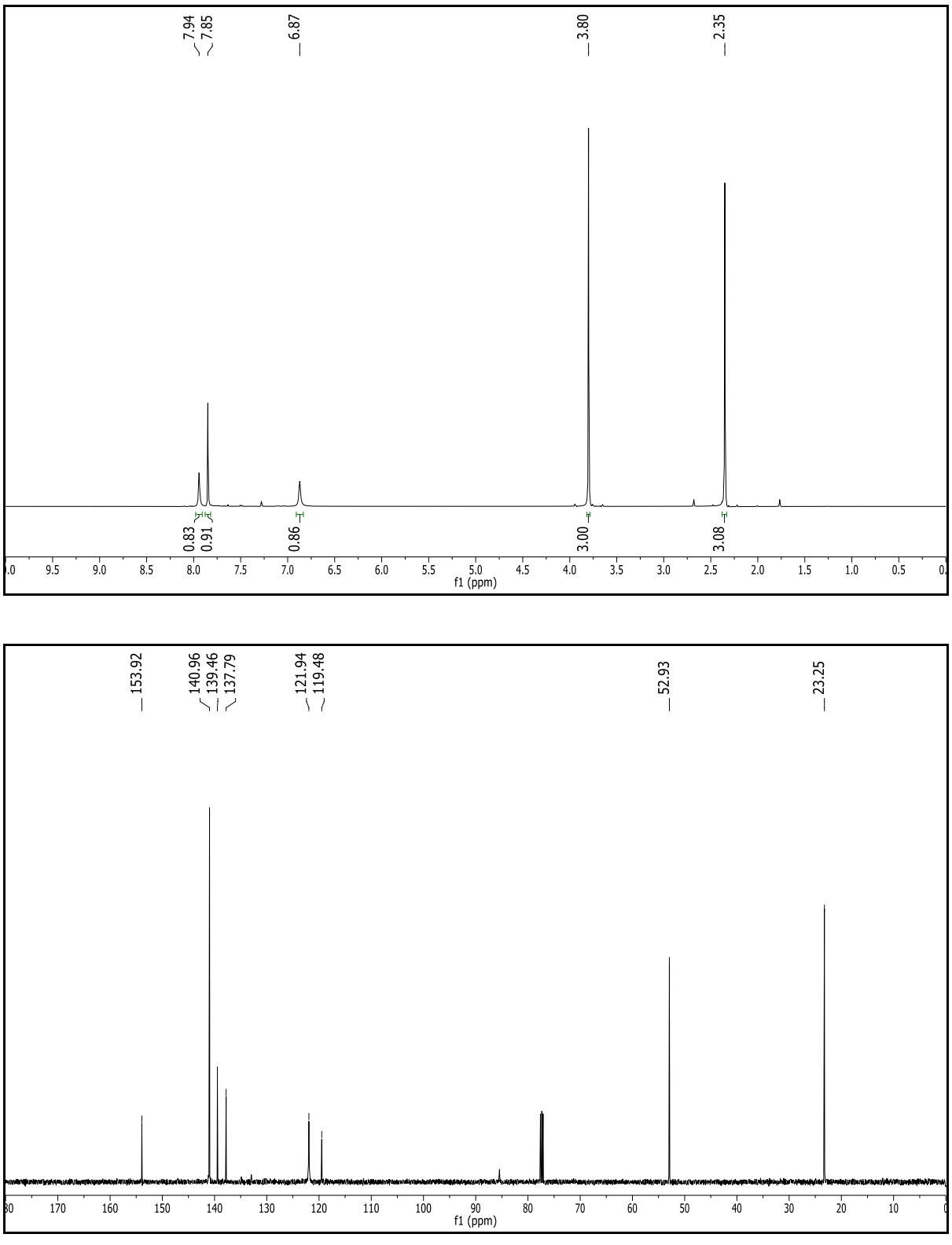

Figure C.20. ^{1}H NMR (500 MHz, $CDCl_3$) and ^{13}C NMR (125 MHz, $CDCl_3$) NMR spectra of **9**.

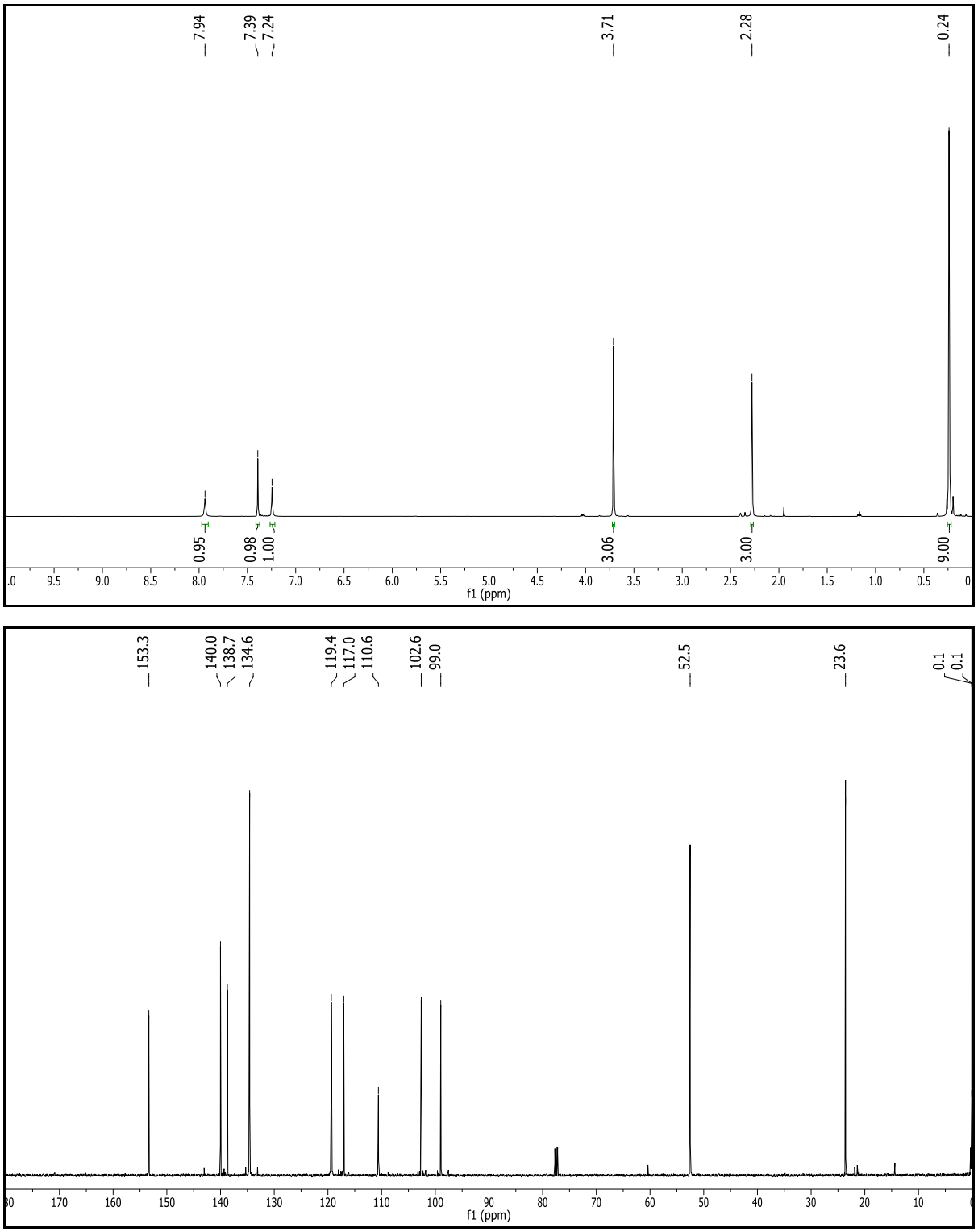

Figure C.21. ^{1}H NMR (500 MHz, $CDCl_3$) and ^{13}C NMR (125 MHz, $CDCl_3$) NMR spectra of **10**.

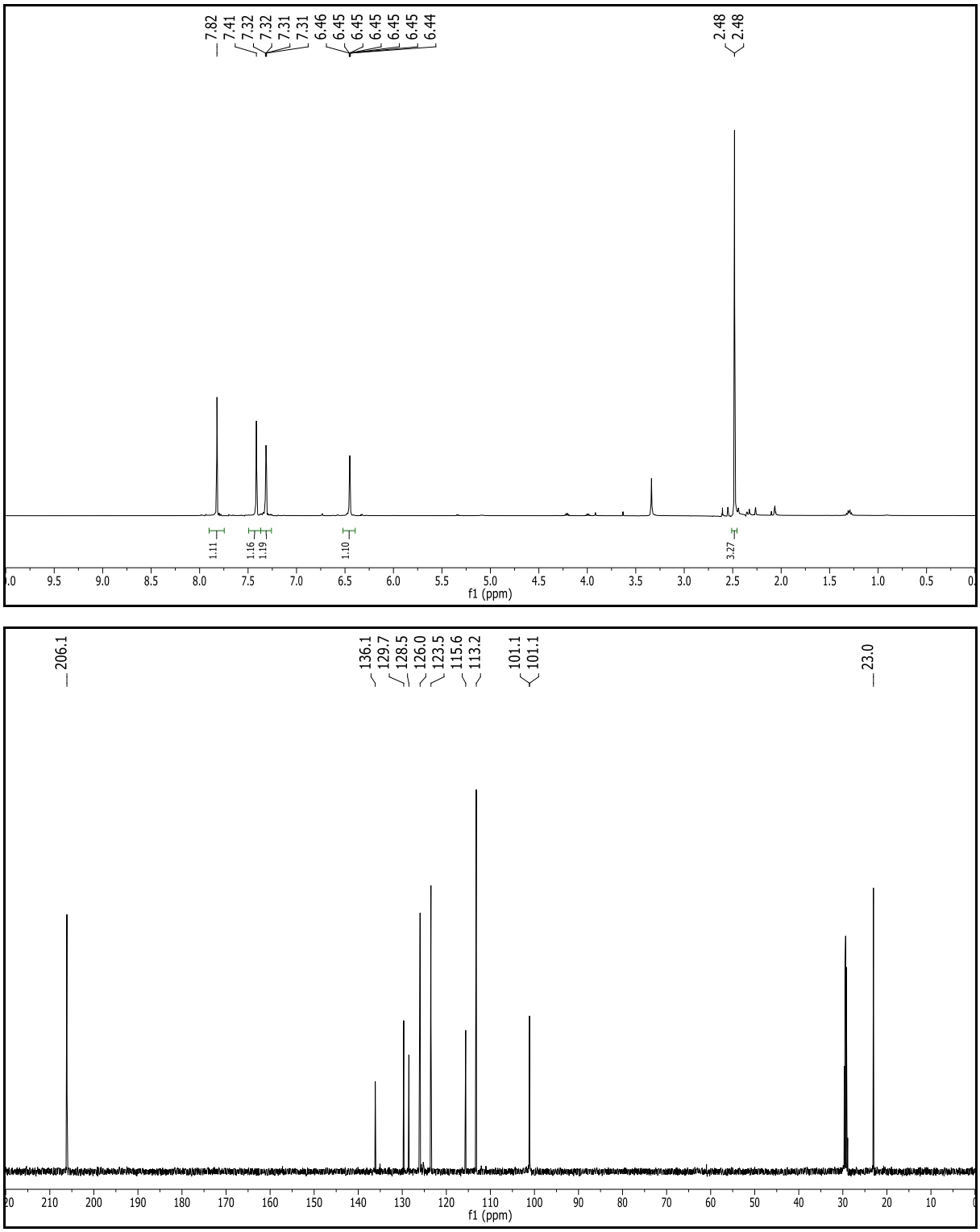

Figure C.22. ^{1}H NMR (500 MHz, $CDCl_3$) and ^{13}C NMR (125 MHz, $CDCl_3$) NMR spectra of **11**.

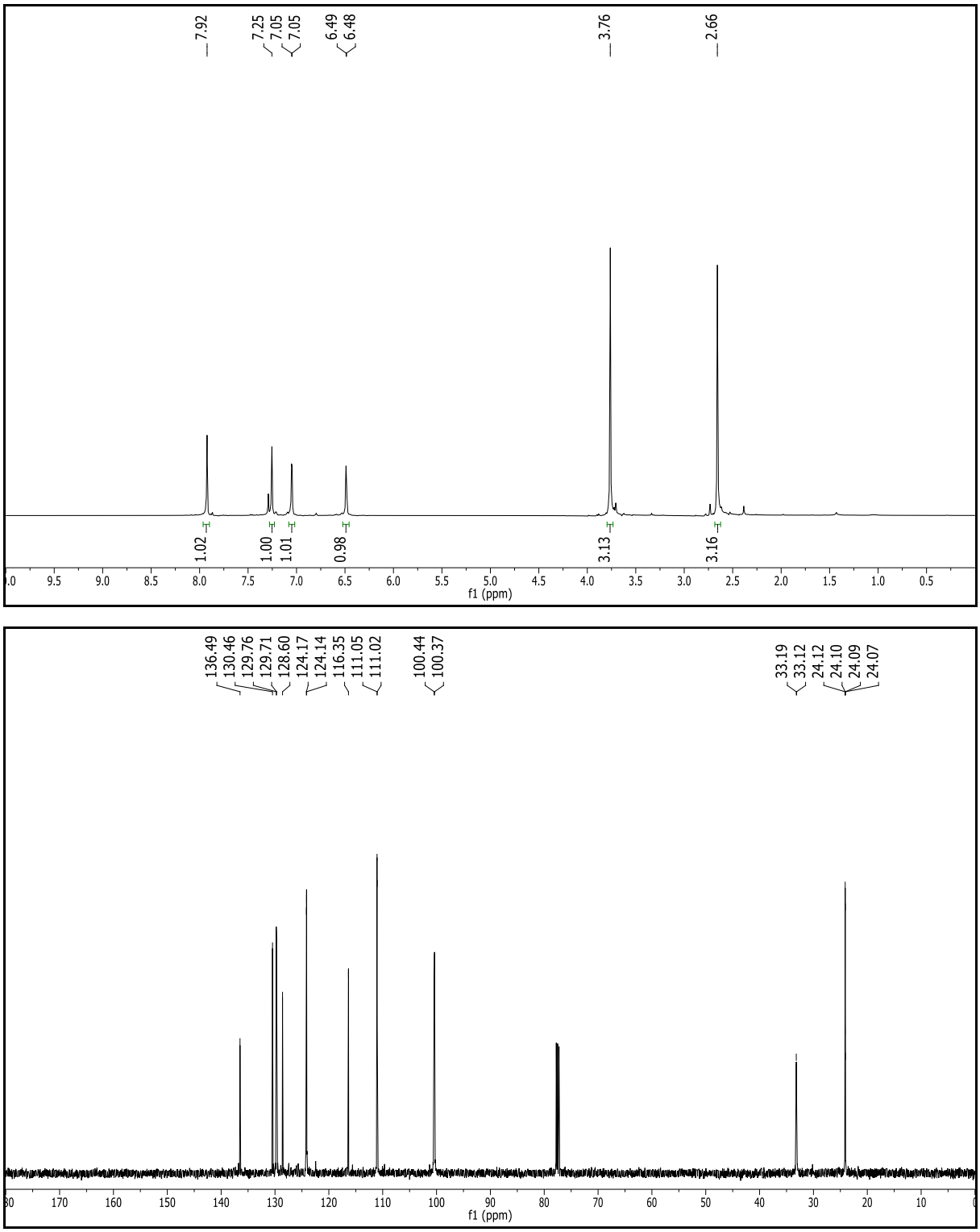

Figure C.23. ^{1}H NMR (500 MHz, Acetone-d_6) and ^{13}C NMR (125 MHz, Acetone-d_6) NMR spectra of **12**.

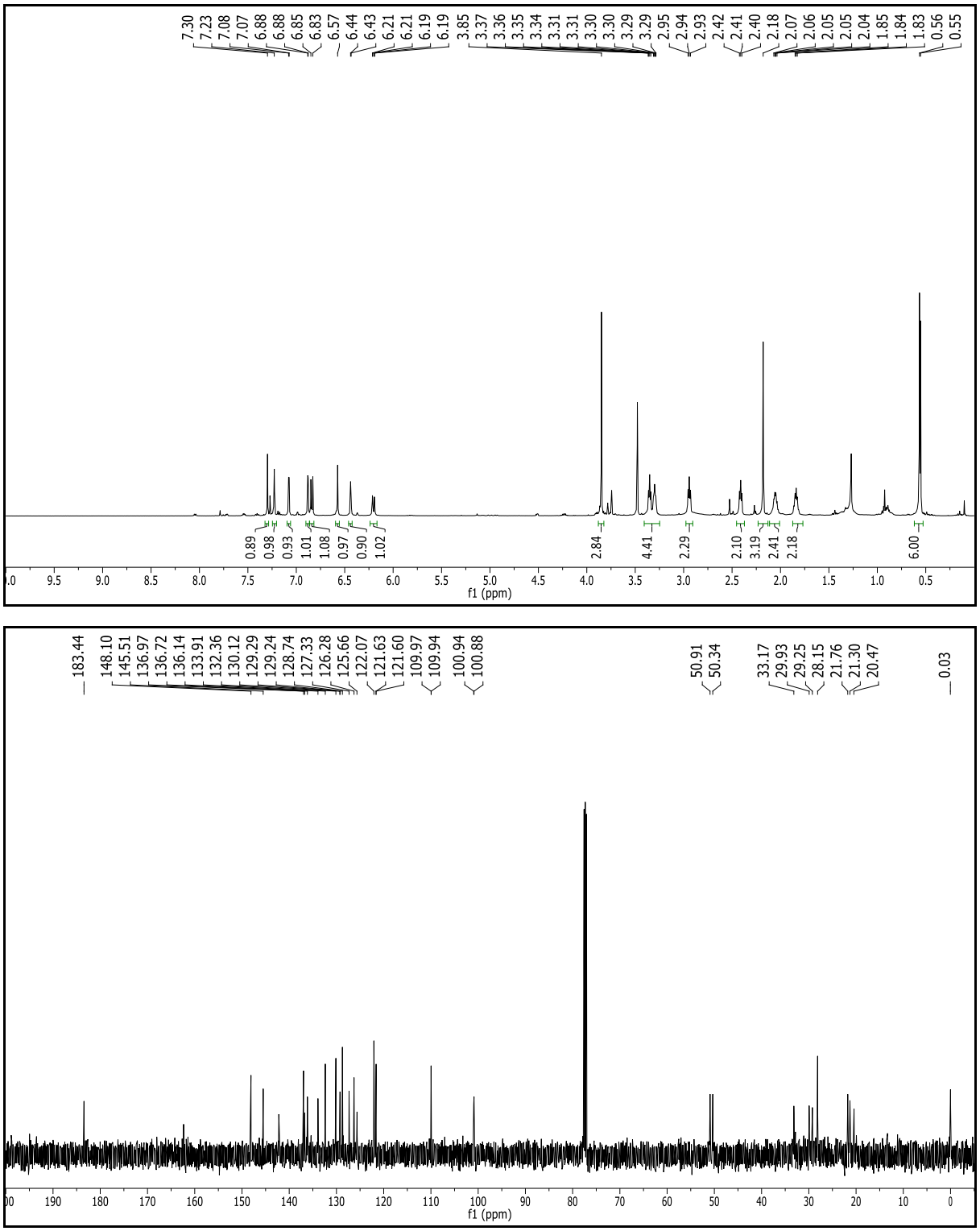

Figure C.24. ^{1}H NMR (500 MHz, $CDCl_3$) and ^{13}C NMR (125 MHz, $CDCl_3$) NMR spectra of **13**.

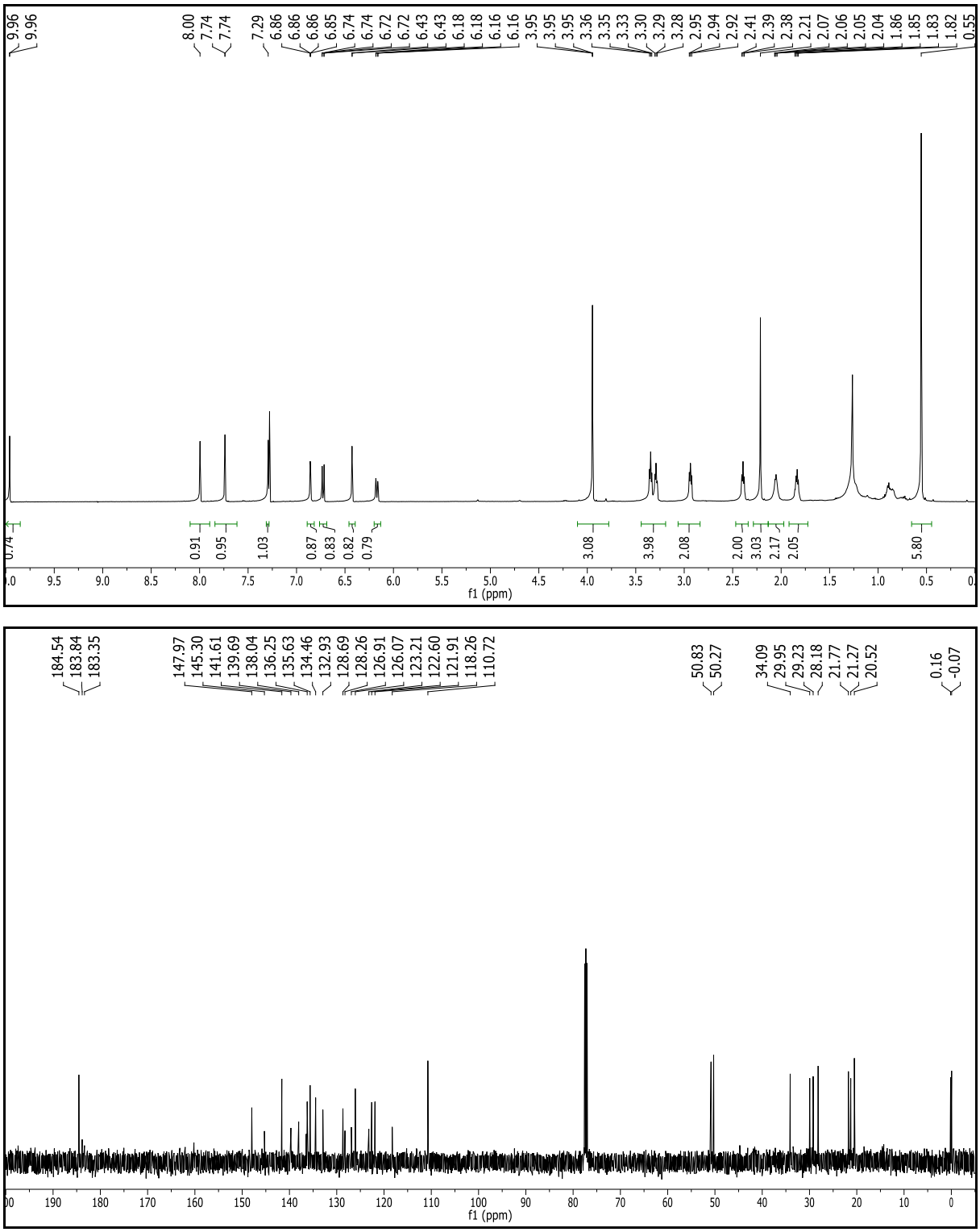

Figure C.25. ^{1}H NMR (500 MHz, $CDCl_3$) and ^{13}C NMR (125 MHz, $CDCl_3$) NMR spectra of **14**.

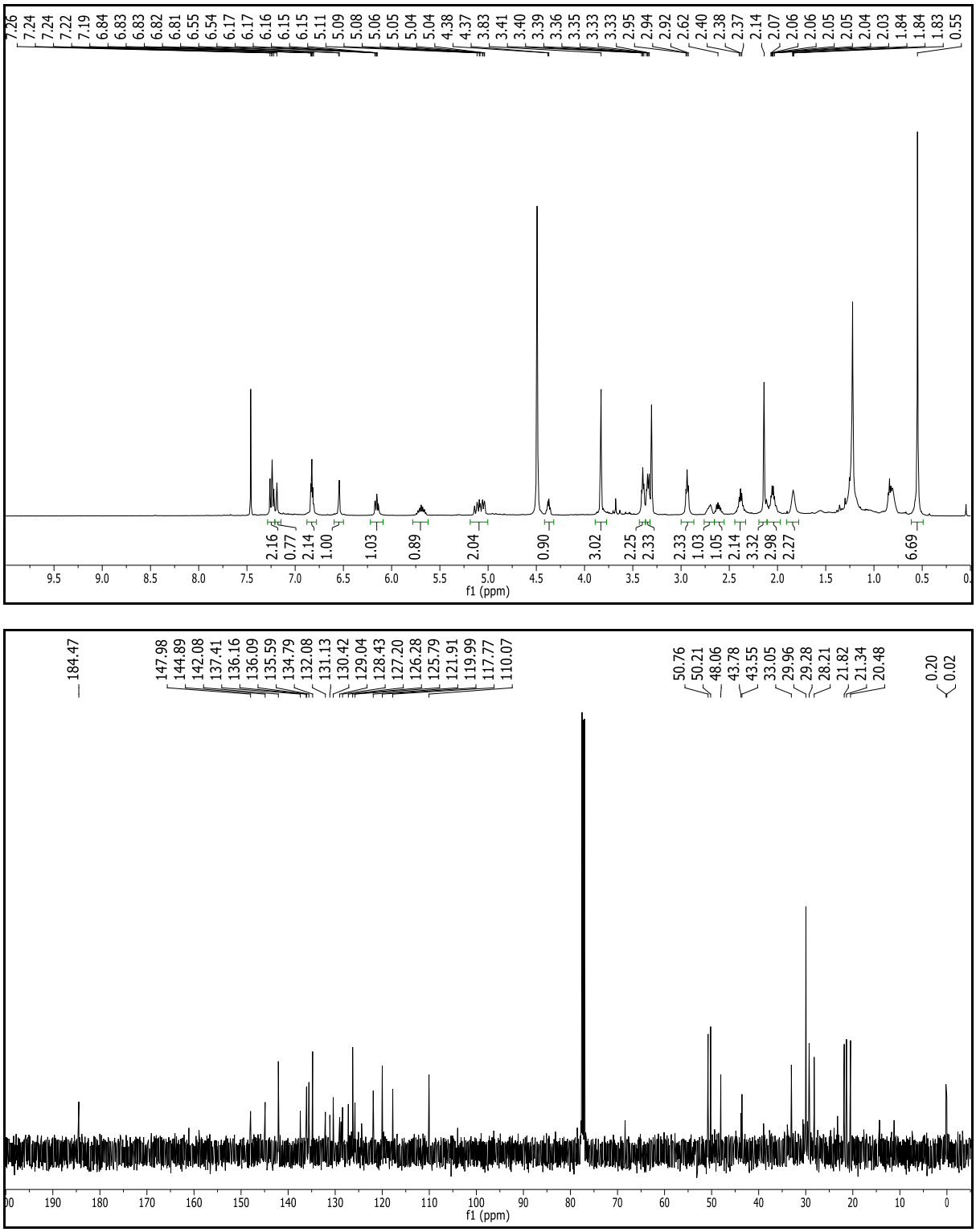

Figure C.26. ^{1}H NMR (500 MHz, $CDCl_3$/MeOD) and ^{13}C NMR (125 MHz, $CDCl_3$) NMR spectra of **15**.

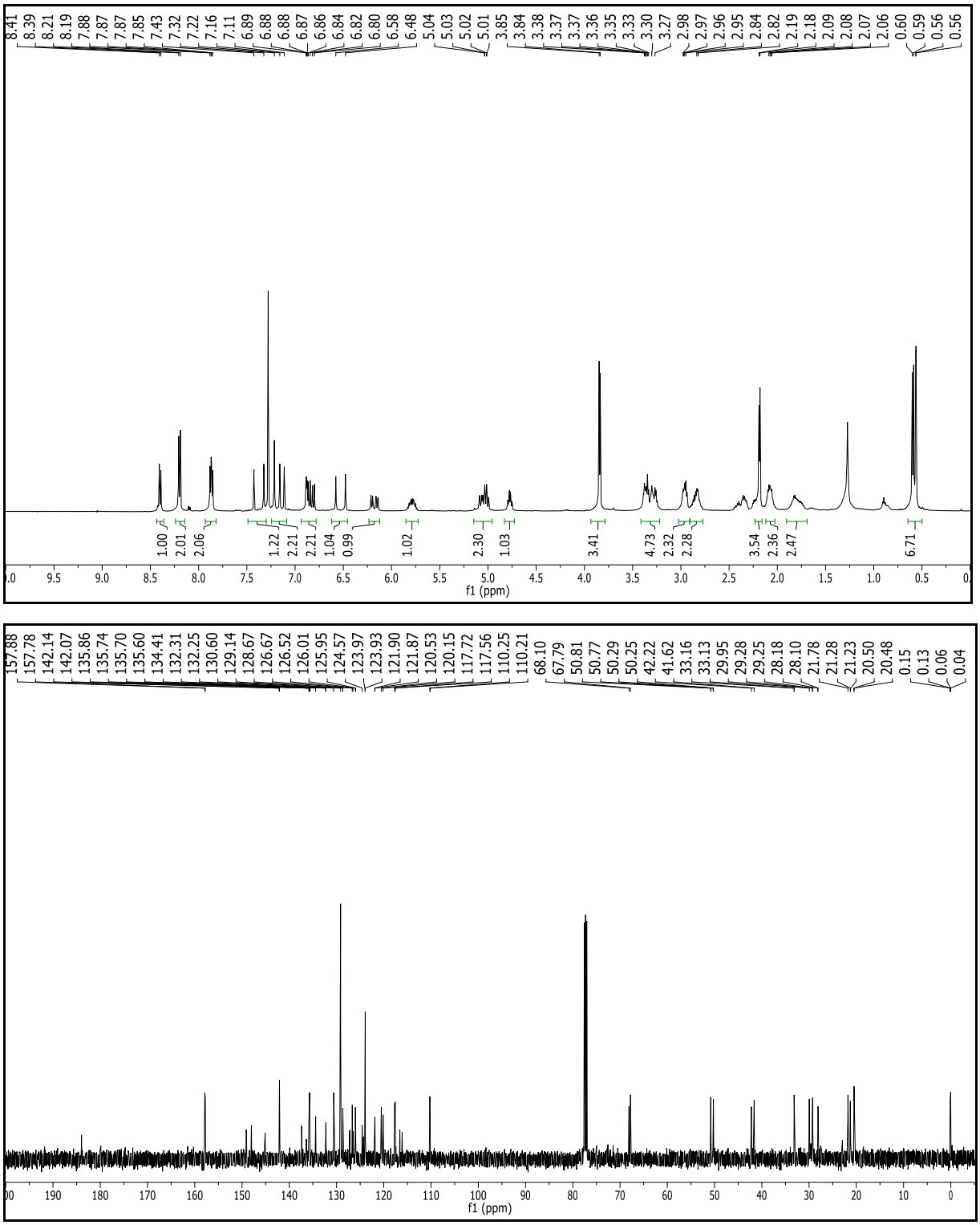

Figure C.27. ^{1}H NMR (500 MHz, $CDCl_3$) and ^{13}C NMR (125 MHz, $CDCl_3$) NMR spectra of **FP1**.

APPENDIX D-MATERIAL AND METHODS FOR CHAPTER 2

This appendix includes information about the source of materials as well as spectroscopic methods used for Chapter 2.

D.1 Materials

Thin-layer chromatography (TLC) was performed on glass-backed TLC plates pre-coated with silica gel containing an UV_{254} fluorescent indicator (Macherey-Nagel). Compounds were visualized with a 254/365nm, handheld UV lamp (UVP). Flash chromatography was performed using 230-400 mesh silica gel P60 (SiliCycle Inc). Preparative TLC purification was performed on 1.00 mm thick TLC plates pre-coated with silica gel containing an UV_{254} fluorescent indicator (Macherey-Nagel). Reversed-phased purification was performed on 20 cc Sep-Pak cartridges preloaded with 5g C18 sorbent ($_{H2O}$s). Solvents used for anhydrous reactions were dried over 3 Å molecular sieves activated via heating under vacuum at 300 °C. All glassware used in anhydrous reactions were flame-dried or heated overnight in an oven at 160 °C and cooled immediately prior to use. Melting point determination was performed on a Büchi B-545 melting point apparatus.

Copper(II) chloride was purchased from Acros. 4-Hydroxyacetophenone, 4-hydroxybenzaldehyde, picolinic acid were purchased from AK Scientific. Magnesium(II) chloride hexahydrate was purchased from Amresco. Kolliphor EL was purchased from Fluka. Nirtomethane was purchased from Macron. Cobalt(II) chloride hexahydrate was purchased from Mallinckrodt. Acetic acid, acetyl chloride, ammonium acetate, calcium chloride, cesium carbonate, citric acid, 2,6-

dichlorophenol, *N*,*N*-diisopropylethylamine, 4-dimethylaminopyridine, 1-ethyl-3-(3-dimethylaminopropyl)carbodiimide, imidazole, potassium carbonate, manganese(II) chloride hexahydrate, potassium hydroxide, sulfur trioxide trimethylamine complex, *tert*-butyldimethylsilyl chloride, tetrakis(triphenylphosphine)palladium(0), and trimethylamine, and triflic acid were purchased from Oakwood Products. Allyl bromide, benzaldehyde, boron trifluoride diethyl etherate, 1,3-dimethylbarbituric acid, iron(II) chloride tetrahydrate, nickel(II) chloride hexahydrate, sodium bicarbonate, sodium phosphate dibasic, tetrabutylammonium fluoride solution, tetrakis(acetonitrile)copper(I) hexafluorophosphate, tosyl chloride, and zinc chloride were purchased from Sigma-Aldrich. Triethylene glycol was purchased from TCI America. Deuterated solvents were purchased from Cambridge Isotope Laboratories. Agarose LE was purchased from Gold Biotechnology. Fluorinated ethylene propylene (FEP) tubing with a wall thickness of 0.01" and inner diameters measuring 0.06" or 0.08" were purchased from McMaster-Carr.

All buffers used for pH titrations were prepared by mixing 0.1 M citric acid in deionized H_2O and 0.2 M dibasic sodium phosphate in deionized H_2O at different ratios. The solutions were diluted by ½ with deionized $_{H2O}$. Fine adjustments to the pH were made by addition of aqueous 0.1 M HCl or 0.1 M NaOH. The pH values were determined using a Mettler Toledo SevenCompact pH meter calibrated using 4.0, 7.0 10.0 standard buffers at 25°C. The pH range of the buffers was 3.0 to 8.2. Kolliphor EL was added to each buffer to make a 0.1% by weight solution.

Tissue phantoms were prepared by dissolving agarose (4.0 g) in a solution of 2% milk (8.0 mL) and deionized H_2O (72.0 mL). The suspension was heated in a microwave oven for 1 min to afford a viscous gel which was poured into a mold made from a 50 mL centrifuge tube. The gel was cooled in a refrigerator for a minimum of 5 hrs. Immediately prior to use, the phantom was removed from the mold and cut with a razor such that there was 1.0 cm of gel above and below where the FEP tubes were inserted.

D.2 SPECTROSCOPIC METHODS

NMR spectra were recorded on Varian 400 or 500 MHz spectrometers at 25 °C. Chemical shifts are reported in ppm (δ) and are referenced to residual protic peaks. The following abbreviations are used to describe coupling constants: singlet (s), doublet (d), triplet (t), quartet (q), doublet doublet (dd), doublet triplet (dt), doublet quartet (dq), doublet doublet triplet (ddt), multiplet (m), and broad singlet (bs). IR spectra were recorded with a PerkinElmer Spectrum Two IR spectrometer. High-resolution mass spectra were acquired with a $_{H2O}$s Q-TOF Ultima ESI mass spectrometer and a $_{H2O}$s Synapt G2-Si ESI/LC-MS mass spectrometer. UV-visible spectra were recorded on a Cary 60 spectrometer. Fluorescence spectra were acquired on a QuantaMaster-400 scanning spectrofluorometer with micro fluorescence quartz cuvettes (Science Outlet). Fluorescence images were acquired on an EVOS FL epifluorescence microscope equipped with a Cy5 light cube. Photoacoustic images were recorded with an Endra Nexus 128 photoacoustic

tomography system (Ann Arbor, MI, USA), and the data were analyzed as described using MicroView v2.5.0-2703 (Parallax Innovations Inc).

APPENDIX E-SYNTHESES FOR CHAPTER 2

This appendix includes the detailed synthetic methods and spectroscopic characterizations for compounds synthesized in Chapter 2.

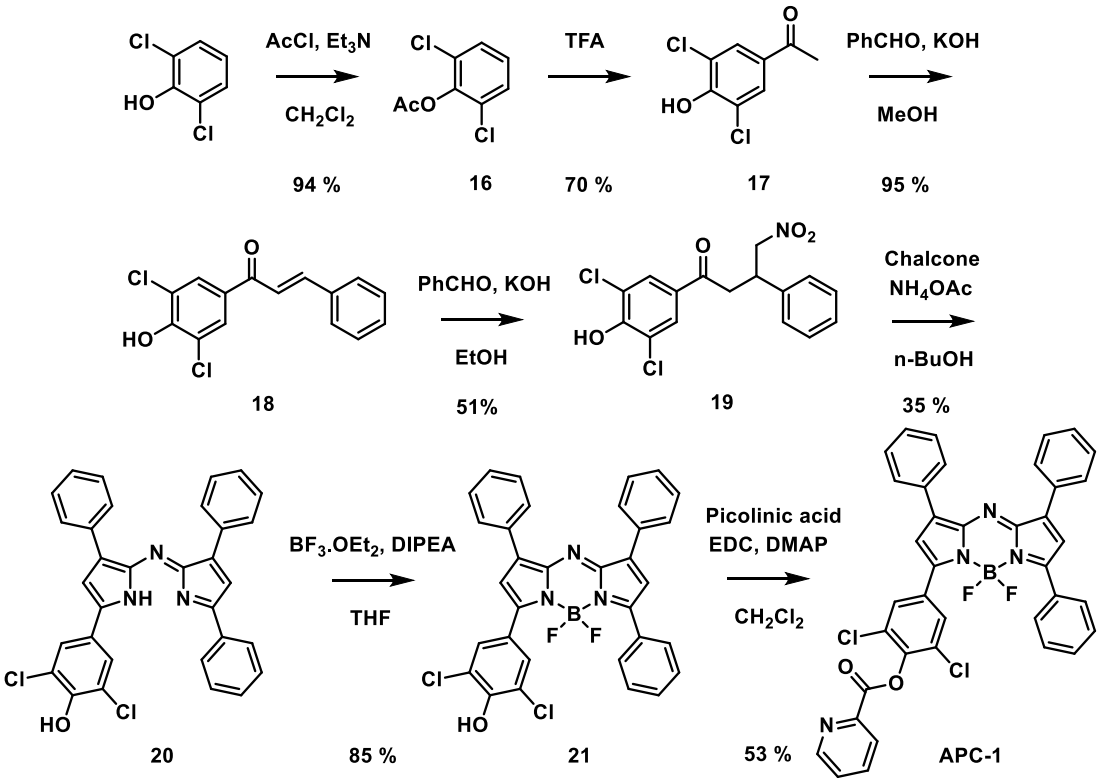

Scheme E.1. Synthesis of APC-1.

2,6-Dichlorophenyl acetate (16). A solution of 2,6-dichlorophenol (9.1 g, 55.8 mmol, 1.0 equiv) and triethylamine (19.4 mL, 139.0 mmol, 2.5 equiv) in CH_2Cl_2 (100 mL) was cooled to 0°C in an ice-bath. After acetyl chloride (4.8 mL, 67.0 mmol, 1.2 equiv) was added dropwise, the solution was warmed to room temperature and stirred for 2.5 hrs. The reaction was treated with sat. Na_2CO_3 (75 mL) and extracted with CH_2Cl_2 (3 × 25 mL). The combined organic fractions were dried (Na_2SO_4), filtered and concentrated

to afford the crude residue which was purified via flash chromatography on a silica column (1:9 v/v EtOAc:Hexanes) to afford the title compound as a colorless oil (10.7 g, 52.5 mmol, 94.1% yield). ^{1}H NMR (500 MHz, $CDCl_3$) δ 7.35 (dd, *J* = 8.1, 1.4 Hz), 7.13 (ddd, *J* = 10.5, 7.3, 1.9 Hz, 1H), 2.39 (s, 3H). ^{13}C NMR (125 MHz, $CDCl_3$) δ 167.5, 144.3, 129.2, 128.9, 127.4, 20.5.

3,5-Dichloro-4-hydroxyacetophenone (17). A solution of **16** (10.7 g, 52.2 mmol, 1.0 equiv) and trifluoromethanesulfonic acid (20 mL) was stirred at 40°C for 16 hrs. The reaction was cooled to 0°C in an ice-bath, treated with sat. Na_2CO_3 until the reaction became neutral, and extracted with EtOAc (4 × 75 mL). The combined organic fractions were dried (Na_2SO_4), filtered and concentrated to afford the crude residue which was purified via flash chromatography on a silica column (1:3 v/v EtOAc:Hexanes) to afford the title compound as a white solid (7.5 g, 36.6 mmol, 70.1% yield). ^{1}H NMR (500 MHz, DMSO-d_6) δ 7.91 (s, 2H), 2.52 (s, 3H). ^{13}C NMR (125 MHz, DMSO-d6) δ 195.5, 154, 130.3, 129.5, 122.8, 27.1. m.p. = 162.5°C. HR-MS calculated for $C_8H_6Cl_2O_2$ $[M-H]^+$ *m/z* 204.9823, found 204.9819.

3',5'-Dichloro-4'-hydroxychalcone (18). A solution of **17** (6.35 g, 31.0 mmol, 1.0 equiv), benzaldehyde (3.8 mL, 37.2 mmol, 1.2 equiv) in MeOH (75 mL) was treated with KOH (20% w/w in H_2O, 17.4 mL) and stirred at room temperature for 24 hrs. MeOH was removed under reduced pressure and the remaining aqueous solution was acidified with AcOH. The reaction was extracted with EtOAc (4 × 25 mL). The combined organic fractions were dried (Na_2SO_4), filtered and concentrated to afford the crude residue which was purified via flash chromatography on a silica column (3:17

v/v EtOAc:Hexanes) to afford the title compound as an off-white solid (8.63 g, 29.4 mmol, 95.0% yield). ^{1}H NMR (500 MHz, Acetone-d_6) δ 8.17 (s, 2H), 7.93 (d, *J* = 15.6 Hz, 1H), 7.88–7.83 (m, 2H), 7.81 (d, *J* = 15.6 Hz, 1H), 7.49–7.43 (m, 3H). ^{13}C NMR (125 MHz, Acetone-d_6) δ 205.6, 185.7, 153.2, 144.8, 135.2, 131.4, 130.8, 129.3, 129.1, 129.1, 129.1, 122.3, 121.2. m.p. = 163°C. HR-MS calculated for $C_{15}H_{10}Cl_2O_2$ $[M-H]^+$ *m/z* 293.0136, found 293.0142.

1-(3,5-Dichloro-4-hydroxyphenyl)-4-nitro-3-phenylbutan-1-one (19). A solution of **18** (8.6 g, 29.4 mmol, 1.0 equiv) in EtOH (50 mL) was treated with $MeNO_2$ (16.0 mL, 298.8 mmol, 10.2 equiv) and KOH (20% w/w in H_2O, 10.0 mL). The reaction was refluxed for 12 hrs. EtOH was removed with reduced pressure and the resultant aqueous solution was diluted with brine (100 mL) and extracted with EtOAc (4 × 25 mL). The combined organic fractions were dried (Na_2SO_4), filtered and concentrated to afford the crude residue which was purified via flash chromatography on a silica column (3:17 v/v EtOAc:Hexanes) to afford the title compound as a tan oil (5.1 g, 14.2 mmol, 50.5% yield). ^{1}H NMR (500 MHz, $CDCl_3$) δ 7.84 (s, 2H), 7.36–7.28 (m, 5H), 4.82 (dd, *J* = 12.6, 6.8Hz, 1 H), 4.70 (dd, *J* = 12.5, 7.8 Hz, 1H) 4.21 (p, *J* = 7.1 Hz, 1H), 3.44-3.34 (m, 2H). ^{13}C NMR (125 MHz, $CDCl_3$) δ 193.9, 152.5, 139.0, 130.1, 129.4, 128.8, 128.3, 127.7, 121.9, 79.7, 41.4, 39.5. HR-MS calculated for $C_{16}H_{13}Cl_2NO_4$ $[M-H]^+$ *m/z* 354.0300, found 354.0302.

(Z)-2,6-dichloro-4-(5-((3,5-diphenyl-2H-pyrrol-2-ylidene)amino)-4-phenyl-1H-pyrrol-2-yl)phenol (20). A solution of **19** (600 mg, 1.7 mmol, 1.0 equiv) and chalcone (1.4 g, 5.1 mmol, 3.0 equiv) was dissolved in n-butanol (15 mL). Ammonium acetate

(2.0 g, 25.4 mmol, 15.0 equiv) was added and the reaction was stirred at 115°C for 3 hrs. Volatiles were removed under reduced pressure. The crude residue suspended in brine (100 mL) and extracted with EtOAc (3 × 15 mL). The combined organic fractions were dried (Na_2SO_4), filtered and concentrated to afford the crude residue which was purified via flash chromatography on a silica column (3:7 v/v CH_2Cl_2:Hexanes to 100% CH_2Cl_2) to afford the title compound as a dark blue film (320 mg, 0.6 mmol, 35.3% yield). ^{1}H NMR (500 MHz, DMSO-d_6) δ 8.18 (s, 2H), 8.06–8.05 (m, 4H), 7.96 (d, *J* = 7.7 Hz, 1H), 7.54 (t, *J* = 7.6 Hz, 1H), 7.50-7.33 (m, 6H). ^{13}C NMR (125 MHz, DMSO-d_6) δ 133.4, 130.2, 129.0, 128.9, 128.9, 128.8, 128.8, 128.6, 128.5, 128.4, 128.2, 128.0, 127.8, 127.8, 127.7, 126.7, 125.1, 110.0.

3,5-Dichloro-4-hydroxy-aza-BODIPY (21). A solution of **20** (128 mg, 0.24 mmol, 1.0 equiv) in anhydrous CH_2Cl_2 (15 mL) was treated with anhydrous DIPEA (0.6 mL, 2.4 mmol, 10.0 equiv) and boron trifluoride etherate (0.45 mL, 3.6 mmol, 15 equiv). The solution was stirred at room temperature for 3 hrs and concentrated under reduced pressure. The crude residue was purified via flash chromatography on a silica column (1:1 v/v CH_2Cl_2:Hexanes) to afford the title compound as a dark green film (118.6 mg, 0.2 mmol, 85.1%). ^{1}H NMR (500 MHz, DMSO-d_6) δ 8.19 (s, 2H), 8.13–8.07 (m, 6H), 7.68 (s, 1H), 7.55–7.42 (m, 10H). ^{13}C NMR (125 MHz, acetone-d6) δ 158.8, 156.6, 153.2, 145.8, 145.3, 143.8, 143.3, 132.4, 132.2, 131.8, 131.7, 130.8, 130.5, 130.4, 130.2, 129.9, 129.9, 129.4, 123.3, 123.2, 121.1, 120.7. HR-MS calculated for $C_{32}H_{20}BCl_2F_2N_3O$ $[M\text{-}H]^+$ *m/z* 582.1123, found 582.1129.

APC-1. A solution of **21** (31.9 mg, 0.06 mmol, 1.0 equiv) in anhydrous CH_2Cl_2 (3 mL) was treated with 2-picolinic acid (27 mg, 0.22 mmol, 4.0 equiv), DMAP (0.7 mg, 0.01 mmol, 0.1 equiv), and EDC (15.8 mg, 0.08 mmol, 1.5 equiv). The resultant solution was stirred at room temperature for 1 hr. The reaction was diluted with H_2O, the organic layer was separated and washed with a 1% aqueous HCl solution. The combined organic fractions were dried (Na_2SO_4), filtered and concentrated to afford the crude residue which was purified via flash chromatography on a silica column (1:3 v/v EtOAc:Hexanes) to afford the title compound as a teal film (19.9 mg, 0.3 mmol, 53.0% yield). ^{1}H NMR (500 MHz, $CDCl_3$) δ 8.93 (d, *J* = 4.0 Hz, 1H), 8.37 (d, *J* = 7.6 Hz, 1H), 8.13–8.11, 8.09–8.05 (m, 6H), 7.98 (dt, *J* = 7.6, 1.8 Hz, 1H), 7.63 (ddd, *J* = 7.7, 4.7, 1.2 Hz, 1H), 7.56–7.55 (m, 3H), 7.50–7.46 (m, 6H), 7.14 (s, 1H), 6.99 (s, 1H). ^{13}C NMR (125 MHz, $CDCl_3$) δ 162.7, 161.6, 153.7, 150.7, 146.4, 146.2, 145.6, 143.6, 137.6, 132.5, 132.1, 132.0, 131.9, 131.1, 130.3, 130.1, 129.8, 129.6, 129.3, 129.1, 129.0, 128.9, 128.1, 126.6, 120.5, 118.5. HR-MS calculated for $C_{38}H_{23}BCl_2F_2N_4O_2$ [M-H]$^+$ *m/z* 687.1337, found 687.1345.

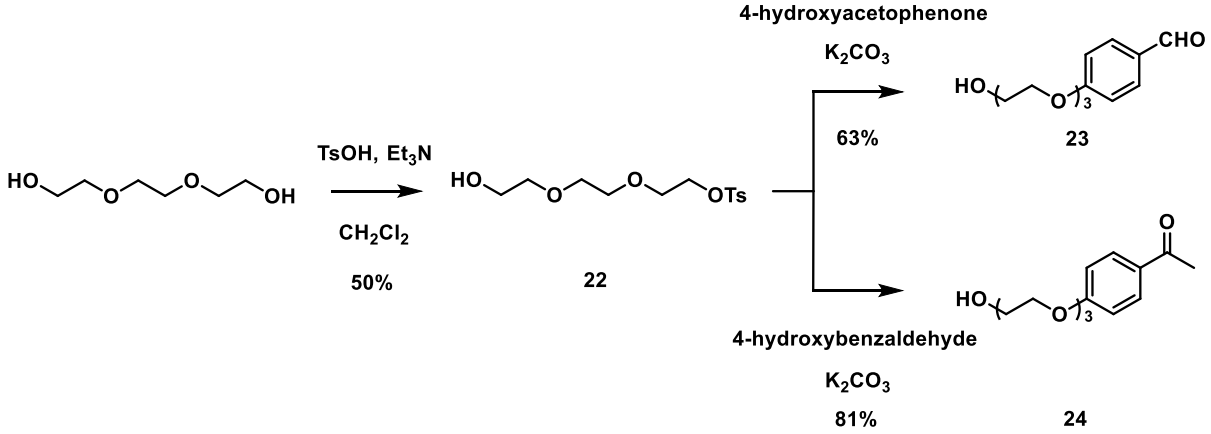

Scheme E.2. Synthesis of PEGylated intermediates **23** and **24**.

2-(2-(2-Hydroxyethoxy)ethoxy)ethyl 4-methylbenzenesulfonate (22). A solution of triethylene glycol (11 g, 73.3 mmol, 4.1 equiv), triethylamine (2.6 mL, 19.1 mmol, 1.1 equiv), DMAP (45 mg, 0.37 mmol, 0.02 equiv), and CH_2Cl_2 (95 mL) was cooled to 0°C in an ice-bath and treated with tosyl chloride (3.5 g, 18.1 mmol, 1.0 equiv). After 4.5 hrs, 1 N HCl aqueous solution (100 mL) was added, the organic layer was separated and washed sequentially with H_2O (100 mL) and brine (100 mL). The combined organic fractions were dried (Na_2SO_4), filtered and concentrated to afford the crude residue which was purified via flash chromatography on a silica column (3:1 v/v EtOAc:Hexanes) to afford the title compound as a colorless oil (2.74 g, 9.0 mmol, 49.7% yield). ^{1}H NMR (500 MHz, $CDCl_3$) δ 7.82 (d, *J* = 8.2 Hz, 2H), 7.36 (d, *J* = 8.4 Hz, 2H), 4.20–4.18 (m, 2 H), 3.83–3.73 (m, 4H), 3.63 (s, 4H), 3.60–3.58 (m, 2H), 2.47 (s, 3H). ^{13}C NMR (125 MHz, $CDCl_3$) δ 145.1, 133.2, 130.1, 128.2, 72.7, 71.0, 70.6, 69.4, 69.0, 62.0, 21.9.

4-(2-(2-(2-Hydroxyethoxy)ethoxy)ethoxy)benzaldehyde (23). A round-bottom flask was charged with **22** (24.4 g, 80.0 mmol, 1.0 equiv), 4-hydroxybenzaldehyde (12.7 g, 104.0 mmol, 1.3 equiv), K_2CO_3 (22.1 g, 160.0 mmol, 2.0 equiv) and anhydrous DMF (50.0 mL). After stirring at 80°C overnight, the reaction was cooled to room temperature and the volatiles were removed under reduced pressure. The resulting mixture was washed with brine (100 mL), H_2O (100 mL) and extracted with 1:2 v/v isopropanol:CH_2Cl_2 (3 × 100 mL). The combined organic fractions were dried (Na_2SO_4), filtered, and concentrated under reduced pressure to afford the crude compound as a red oil which was purified via flash chromatography on a silica column

(3:1 v/v EtOAc:Hexanes) to afford the title compound as a colorless oil (13.3 g, 52.2 mmol, 65.3% yield). ^{1}H NMR (400 MHz, $CDCl_3$) δ 9.83 (s, 1H), 7.80–7.76 (m, 2H), 7.00–6.96 (m, 2H), 4.21–4.15 (m, 2H), 3.89–3.81 (m, 2H), 3.74–3.63 (m, 6H), 3.60–3.54 (m, 2H). ^{13}C NMR (100 MHz, $CDCl_3$) δ 191.1, 163.9, 132.2, 130.2, 115.1, 72.7, 71.0, 70.5, 69.6, 67.9, 61.9.

1-(4-(2-(2-(2-hydroxyethoxy)ethoxy)ethoxy)phenyl)ethan-1-one (24). A round-bottom flask was charged with **22** (12.2 g, 40.0 mmol, 1.0 equiv), 4-hydroxyacetophenone (7.08 g, 52.0 mmol, 1.3 equiv), K_2CO_3 (11.1 g, 80.0 mmol, 2.0 equiv) and anhydrous DMF (50.0 mL). After stirring at 80°C overnight, the reaction cooled to room temperature and the volatiles were removed under reduced pressure. The resulting mixture was washed with brine (100 mL), H_2O (100 mL) and extracted with 1:2 v/v isopropanol:CH_2Cl_2 (3 × 100 mL). The combined organic fractions were dried (Na_2SO_4), filtered, and concentrated under reduced pressure to afford the crude compound which was purified via flash chromatography on a silica column (3:1 v/v EtOAc:Hexanes) to afford the title compound as a colorless oil (8.7 g, 32.2 mmol, 80.5% yield). ^{1}H NMR (400 MHz, $CDCl_3$) δ 9.83 (s, 1H), 7.80–7.76 (m, 2H), 7.00–6.96 (m, 2H), 4.21–4.15 (m, 2H), 3.89–3.81 (m, 2H), 3.74–3.63 (m, 6H), 3.60–3.54 (m, 2H). ^{13}C NMR (100 MHz, $CDCl_3$) δ 191.1, 163.9, 132.2, 130.2, 115.1, 72.7, 71.0, 70.5, 69.6, 67.9, 61.9. HR-MS calculated for $C_{14}H_{20}NaO_5$ $[M+Na]^+$ *m/z* 291.1130, found 291.1221.

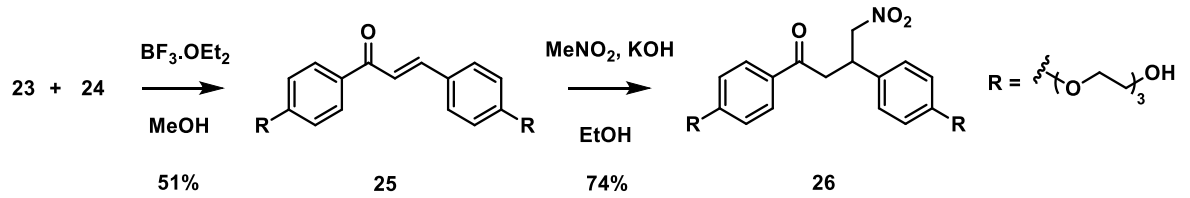

Scheme E.3. Synthesis of compound **26**.

(E)-1,3-Bis(4-(2-(2-(2-hydroxyethoxy)ethoxy)ethoxy)phenyl)prop-2-en-1-one (25): A pressure tube was charged with **23** (6.4 g, 25.0 mmol, 1.0 equiv), **24** (6.7 g, 25.0 mmol, 1.0 equiv), boron trifluoride etherate (3.7 mL, 25.0 mmol, 1.2 equiv) and MeOH (50 mL). The pressure tube was sealed and heated at 100°C for 48 hrs. The volatiles were removed under reduced pressure and the crude residue was purified via flash chromatography on a silica column (100% EtOAc to 7:93 v/v MeOH/CH_2Cl_2) to afford the title compound as a light yellow oil (6.4 g, 12.7 mmol, 50.6% yield). ^{1}H NMR (400 MHz, CD_3OD) δ 8.06 (d, *J* = 8.8 Hz, 2H), 7.72 (d, *J* = 15.6 Hz, 1H), 7.68 (d, *J* = 8.8 Hz, 2H), 7.62 (d, *J* = 15.5 Hz, 1H), 7.05 (d, *J* = 8.9 Hz, 2H), 6.99 (d, *J* = 8.7 Hz, 2H), 4.25–4.11 (m, 5H), 3.90–3.82 (m, 5H), 3.73–3.67 (m, 4H), 3.67–3.60 (m, 10H), 3.57–3.50 (m, 5H). ^{13}C NMR (100 MHz, CD_3OD) δ 189.6, 163.2, 161.3, 144.3, 131.2, 130.8, 130.4, 128.0, 119.2, 114.9, 114.4, 72.5, 70.6, 70.2, 69.5, 67.7, 67.5, 61.0. HR-MS calculated for $C_{27}H_{37}O_9$ $[M+H]^+$ *m/z* 505.2438, found 505.2450.

1,3-Bis(4-(2-(2-(2-hydroxyethoxy)ethoxy)ethoxy)phenyl)-4-nitrobutan-1-one (26): A round-bottom flask was charged with **25** (6.4 g, 12.7 mmol, 1.0 equiv), $MeNO_2$ (10.2 mL, 190.5 mmol, 15.0 equiv), KOH (20% w/w in H_2O, 7.2 mL, 25.4 mmol, 2.0 equiv), and EtOH (15 mL). The reaction mixture was heated to reflux for 3 hrs and

then concentrated under reduced pressure. The crude residue was purified via flash chromatography on a silica column (7:93 v/v MeOH/CH_2Cl_2) to afford the title compound as a brown oil (5.3 g, 9.4 mmol, 74.3% yield). ^{1}H NMR (400 MHz, CD_3OD) δ 7.85 (d, *J* = 8.9 Hz, 2H), 7.18 (d, *J* = 8.7 Hz, 2H), 6.92 (d, *J* = 8.9 Hz, 2H), 6.80 (d, *J* = 8.7 Hz, 2H), 4.79 (dd, *J* = 12.5, 9.2 Hz, 1H), 4.66 (dd, *J* = 12.5, 9.2 Hz, 1H), 4.14–4.10 (m, 2H), 4.08–4.02 (m, 1H), 4.02–3.99 (m, 2H), 3.87–3.47 (m, 22H), 3.38 (dd, *J* = 17.4, 7.2 Hz, 1H), 3.32–3.24 (dd, *J* = 17.4, 7.2 Hz, 1H). ^{13}C NMR (100 MHz, CD_3OD) δ 196.7, 163.3, 158.3, 132.1, 130.4, 129.9, 128.8, 114.6, 114.3, 79.8, 72.5, 70.6, 70.5, 70.2, 69.6, 69.4, 67.7, 67.3, 41.1, 39.3. HR-MS calculated for $C_{28}H_{40}NO_{11}$ $[M+H]^+$ *m/z* 566.2601, found 566.2611.

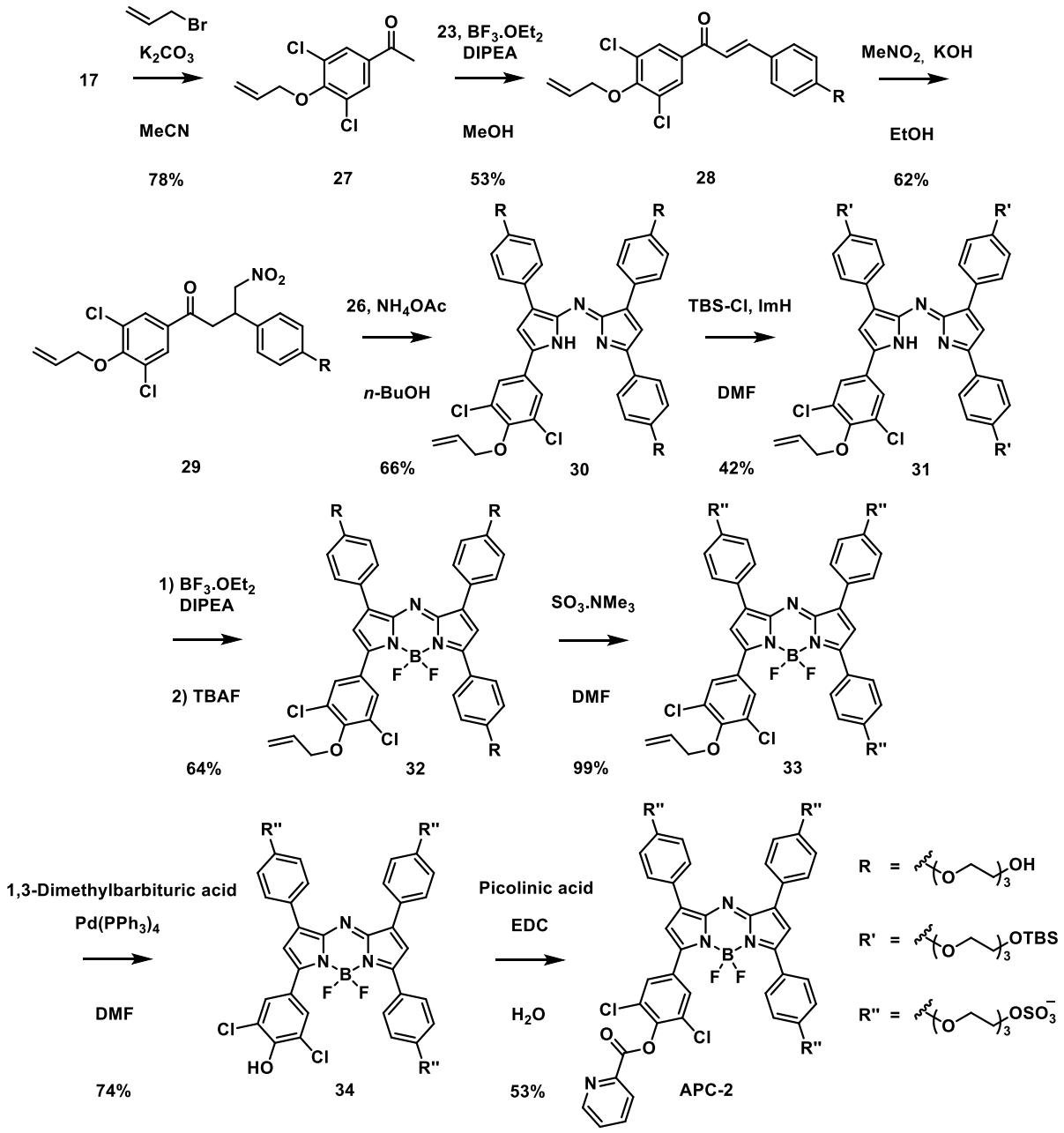

Scheme E.4. Synthesis of APC-2.

1-(4-(Allyloxy)-3,5-dichlorophenyl)ethan-1-one (27). A round-bottom flask was charged with **17** (47.7 g, 233.0 mmol, 1.0 equiv), allyl bromide (32.1 mL, 373.0 mmol, 1.6 equiv), K_2CO_3 (64.4 g, 466.0 mmol, 2.0 equiv) and CH_3CN (200 mL). The reaction was refluxed for 2 hrs, cooled to room temperature, filtered through a bed of celite and

washed with MeCN (100 mL). The filtrate was concentrated under reduced pressure and the crude residue was purified via flash chromatography on a silica column (1:19 v/v EtOAc:Hexanes) to afford the title compound as a light yellow oil. (37.3 g, 182.0 mmol, 78.1% yield). ^{1}H NMR (500 MHz, $CDCl_3$) δ 7.90 (s, 2H), 6.31–5.98 (m, 1H), 5.45 (dq, *J* = 17.2, 1.4 Hz, 1H), 5.32 (dp, *J* = 10.3, 1.0 Hz, 1H), 4.65 (dt, *J* = 6.0, 1.3 Hz, 2H), 2.58 (s, 3H). ^{13}C NMR (125 MHz, $CDCl_3$) δ 195.0, 155.3, 134.2, 132.7, 130.4, 129.3, 119.7, 109.9, 74.9, 26.7. HR-MS calculated for $C_{11}H_{11}Cl_2O_2$ $[M+H]^+$ *m/z* 245.0136, found 245.0140.

(E)-1-(4-(Allyloxy)-3,5-dichlorophenyl)-3-(4-(2-(2-(2-hydroxyethoxy)ethoxy)ethoxy)phenyl) prop-2-en-1-one (28): A pressure tube was charged with **23** (3.8 g, 15.0 mmol, 1.0 equiv), **27** (4.4 g, 18.0 mmol, 1.2 equiv), boron trifluoride etherate (1.9 mL, 15.0 mmol, 1.0 equiv) and MeOH (30 mL). The pressure tube was sealed and heated at 100 °C for 48 hrs. The volatiles were removed under reduced pressure and the crude residue was purified via flash chromatography on a silica column (4:1 v/v EtOAc:Hexanes to 100% EtOAc) to afford the title compound as a light yellow solid (3.8 g, 8.0 mmol, 53.2% yield). ^{1}H NMR (400 MHz, CD_3OD) δ 8.04 (s, 2H), 7.74 (d, *J* = 15.4 Hz, 1H), 7.68 (d, *J* = 8.8 Hz, 2H), 7.53 (d, *J* = 15.5 Hz, 1H), 6.96 (d, *J* = 8.8 Hz, 2H), 6.12 (ddt, *J* = 17.3, 10.4, 5.9 Hz, 1H), 5.40 (dd, *J* = 17.2, 1.6 Hz, 1H), 5.26 (dd, *J* = 10.4, 1.4 Hz, 1H), 4.61 (dt, *J* = 5.9, 1.3 Hz, 2H), 4.27–4.05 (m, 2H), 3.94–3.77 (m, 2H), 3.76–3.48 (m, 8H). ^{13}C NMR (100 MHz, CD_3OD) δ 187.1, 161.6, 154.7, 146.0, 135.5, 132.9, 130.8, 130.0, 129.1, 127.6, 118.1, 114.9, 74.5, 72.5,

70.6, 70.2, 69.5, 67.5, 61.0. m.p. = 70°C. HR-MS calculated for $C_{24}H_{27}O_6Cl_2$ $[M+H]^+$ *m/z* 481.1185, found 481.1194.

1-(4-(Allyloxy)-3,5-dichlorophenyl)-3-(4-(2-(2-(2-hydroxyethoxy)ethoxy)ethoxy)phenyl)-4-nitrobutan-1-one (29): A round-bottom flask was charged with **28** (3.84 g, 8.0 mmol, 1.0 equiv), $MeNO_2$ (6.4 mL, 120.0 mmol, 15.0 equiv), KOH (20% w/w in H_2O, 4.5 mL, 16.0 mmol, 2.0 eq.), and EtOH (10 mL). The reaction mixture was refluxed for 3 hrs, cooled to room temperature, and concentrated under reduced pressure. The crude residue was purified via flash chromatography on a silica column (4:1 v/v EtOAc:Hexanes) to afford the title compound as a brown oil (2.7 g, 5.0 mmol, 61.5% yield). ^{1}H NMR (400 MHz, CD_3OD) δ 7.85 (s, 1H), 7.19 (d, *J* = 8.7 Hz, 1H), 6.81 (d, *J* = 8.7 Hz, 1H), 6.08 (ddt, *J* = 17.3, 10.4, 6.0 Hz, 1H), 5.37 (dq, *J* = 17.2, 1.5 Hz, 1H), 5.23 (dq, *J* = 10.5, 1.3 Hz, 1H), 4.81 (dd, *J* = 12.7, 6.1 Hz, 1H), 4.66 (dd, *J* = 12.6, 9.2 Hz, 1H), 4.56 (dt, *J* = 6.0, 1.3 Hz, 2H), 4.08–3.93 (m, 3H), 3.83–3.73 (m, 2H), 3.71–3.48 (m, 9H), 3.42 (dd, *J* = 17.8, 7.1 Hz, 1H), 3.34 (dd, *J* = 17.8, 6.8 Hz, 1H). ^{13}C NMR (100 MHz, CD_3OD) δ 195.0, 158.4, 155.0, 133.9, 132.8, 131.8, 129.9, 128.8, 128.8, 118.2, 114.6, 79.6, 74.5, 72.5, 70.5, 70.2, 69.6, 67.3, 61.0, 41.4, 39.0. HR-MS calculated for $C_{27}H_{28}NO_8Cl_2$ $[M+H]^+$ *m/z* 564.1192, found 564.1187.

(Z)-2,2'-(((((((2-((5-(4-(Allyloxy)-3,5-dichlorophenyl)-3-(4-(2-(2-(2-hydroxyethoxy)ethoxy) ethoxy)phenyl)-1H-pyrrol-2-yl)imino)-2H-pyrrole-3,5-diyl)bis(4,1-phenylene))bis(oxy))bis (ethane-2,1-diyl))bis(oxy))bis(ethane-2,1-diyl))bis(oxy))bis(ethan-1-ol) (30). A solution of **26** (5.3 g, 9.4 mmol, 1.9 equiv), **29**

(2.7 g, 5.0 mmol, 1.0 equiv), in n-butanol (30 mL) was treated with NH_4OAc (11.4g, 148.0 mmol, 30.0 equiv). The reaction mixture was refluxed for 5 hrs, cooled to room temperature, diluted with brine (200 mL), and extracted with CH_2Cl_2 (3 × 200 mL). The combined organic fractions were dried (Na_2SO_4), filtered and concentrated under reduced pressure. The crude residue was purified by flash chromatography on a silica column (3:47 v/v MeOH/CH_2Cl_2) to afford the title compound as a dark blue solid (1.66 g, 1.6 mmol, 66.3 % yield). ^{1}H NMR (500 MHz, $CDCl_3$) δ 7.91 (d, *J* = 8.7 Hz, 2H), 7.88 (d, *J* = 8.6 Hz 1H), 7.79 (d, *J* = 8.6 Hz, 2H), 7.62 (s, 2H), 7.29 (s, 1H), 7.01–6.92 (m, 3H), 6.89 (m, 3H), 6.80 (s, 1H), 6.20 (ddt, *J* = 16.5, 10.3, 6.0 Hz, 1H), 5.50 (dd, *J* = 17.2, 1.5 Hz, 1H), 5.36 (dd, *J* = 10.3, 1.5 Hz, 1H), 4.61 (d, *J* = 6.0 Hz, 2H), 4.20 (m, 6H), 3.98–3.65 (m, 30H). ^{13}C NMR (125 MHz, $CDCl_3$) δ 161.2, 159.3, 159.2, 158.7, 153.1, 151.4, 146.9, 146.2, 144.5, 139.4, 133.2, 130.6, 130.3, 130.3, 129.8, 128.9, 127.2, 126.7, 126.1, 125.0, 119.2, 115.3, 114.5, 74.9, 72.9, 71.2, 70.7, 70.0, 69.9, 67.7, 67.7, 62.0. m.p. = 158°C. HR-MS calculated for $C_{53}H_{62}N_3O_{13}Cl_2$ $[M+H]^+$ *m/z* 1018.3660, found 1018.3654.

(Z)-N-(5-(4-(allyloxy)-3,5-dichlorophenyl)-3-(4-((2,2,3,3-tetramethyl-4,7,10-trioxa-3-siladodecan-12-yl)oxy)phenyl)-1H-pyrrol-2-yl)-3,5-bis(4-((2,2,3,3-tetramethyl-4,7,10-trioxa-3-siladodecan-12-yl)oxy)phenyl)-2H-pyrrol-2-imine (31). To a solution of compound **30** (1.7 g, 1.6 mmol, 1.0 equiv) in anhydrous CH_2Cl_2 (30 mL) was added imidazole (1.1g, 16.3 mmol, 10 eq.) and TBS-Cl (1.8 g, 12.2 mmol, 7.5 equiv). The reaction mixture was stirred overnight room temperature, poured in brine (150 mL) and extracted with CH_2Cl_2 (3 × 60 mL). The combined organic fractions were

dried (Na_2SO_4), filtered and concentrated under reduced pressure. The crude residue was purified by flash chromatography on a silica column (3:7 v/v EtOAc:Hexanes) to afford the title compound as a dark blue film (929 mg, 0.7 mmol, 41.8 % yield) ^{1}H NMR (500 MHz, $CDCl_3$) δ 7.99 (d, *J* = 8.7 Hz, 2H), 7.95 (d, *J* = 8.7 Hz, 2H), 7.89 (d, *J* = 8.7 Hz, 2H), 7.71 (s, 2H), 7.05 (s, 1H), 7.02 (d, *J* = 8.7 Hz, 2H), 6.96 (d, *J* = 3.7 Hz, 2H), 6.94 (d, *J* = 3.7 Hz, 2H), 6.87 (s, 1H), 6.20 (ddt, *J* = 16.3, 10.3, 5.9 Hz, 1H), 5.49 (dd, *J* = 16.3, 1.5 Hz, 1H), 5.35 (dd, *J* = 10.4, 1.3 Hz, 1H), 4.63 (dt, *J* = 6.1, 1.3 Hz, 2H), 4.22 (m, 6H), 3.98–3.58 (m, 30H), 0.92 (s, 27H), 0.09 (s, 18H). ^{13}C NMR (125 MHz, $CDCl_3$) δ 161.4, 159.7, 159.4, 158.9, 153.3, 151.5, 146.8, 146.1, 144.8, 139.5, 133.1, 130.6, 130.4, 130.2, 129.9, 129.0, 127.1, 126.6, 126.1, 125.0, 119.3, 115.4, 115.3, 114.6, 111.2, 74.9, 73.0, 72.9, 71.2, 71.2, 71.1, 70.1, 70.0, 69.9, 67.8, 67.7, 63.0, 26.2, 18.6, -5.0. m.p. = 153°C. HR-MS calculated for $C_{71}H_{104}N_3O_{13}Si_3Cl_2$ $[M+H]^+$ *m/z* 1360.6254, found 1360.6211.

2,2',2''-(((((((7-(4-(Allyloxy)-3,5-dichlorophenyl)-5,5-difluoro-5H-4l4,5l4-dipyrrolo[1,2-c:2',1'-f][1,3,5,2]triazaborinine-1,3,9-triyl)tris(benzene-4,1-diyl))tris(oxy))tris(ethane-2,1-diyl))tris(oxy))tris(ethane-2,1-diyl))tris(oxy))tris(ethan-1-ol) (32). To a solution of **31** (929 mg, 0.7 mmol, 1.0 equiv) in anhydrous CH_2Cl_2 (30 mL) was treated with DIPEA (1.2 mL, 6.8 mmol, 10.0 equiv) and boron trifluoride etherate (1.7 mL, 13.7 mmol, 20.0 equiv). The reaction mixture was stirred at room temperature for 2 hrs, poured into H_2O (100 mL) and extracted with CH_2Cl_2 (3 × 50 mL). The combined organic fractions were dried (Na_2SO_4), filtered, concentrated under reduced pressure and transferred to a flame-dried round-bottom

flask. The intermediate was dissolved in THF (40 mL) and treated with TBAF (1M in THF, 6.1 mL, 6.1 mmol, 9.0 equiv) dropwise under a nitrogen atmosphere. After 10 min, the reaction was diluted with sat. $NaHCO_3$ (100 mL) and extracted with CH_2Cl_2 (3 × 50 mL). The combined organic fractions were dried (Na_2SO_4), filtered and concentrated to afford the crude residue which was purified via flash chromatography on a silica column (7:93 v/v MeOH/CH_2Cl_2) to afford the title compound as a dark blue solid (464 mg, 0.4 mmol, 63.6% yield over two-steps). ^{1}H NMR (500 MHz, $CDCl_3$) δ 8.06 (d, *J* = 8.5 Hz, 2H), 7.97 (d, *J* = 9.3 Hz, 2H), 7.94 (d, *J* = 9.3 Hz, 2H), 7.93 (s, 2fH), 6.99–6.89 (m, 8H), 6.76 (s, 1H), 6.17 (ddt, *J* = 16.4, 10.8, 5.8 Hz, 1H), 5.47 (d, *J* = 16.9 Hz, 1H), 5.32 (d, *J* = 10.3 Hz, 1H), 4.60 (d, *J* = 6.0 Hz, 2H), 4.15 (dq, *J* = 5.6, 3.2 Hz, 6H), 3.92–3.55 (m, 30H), 3.09–2.99 (b, 2H), 2.85 (b, 1H). ^{13}C NMR (125 MHz, $CDCl_3$) δ 162.0, 161.4, 160.6, 159.9, 152.4, 151.8, 146.9, 144.9, 144.1, 141.2, 133.2, 132.4, 132.4, 132.3, 131.2, 130.8, 130.0, 129.9, 129.8, 129.8, 129.7, 125.9, 125.1, 123.7, 119.1, 118.5, 116.5, 115.1, 114.9, 77.6, 77.6, 74.8, 72.8, 72.8, 71.1, 71.1, 70.6, 69.9, 69.8, 69.8, 69.7, 67.7, 67.7, 67.7, 67.6, 61.9, 61.9. m.p. = 168°C. HR-MS calculated for $C_{53}H_{60}BCl_2F_2N_3O_{13}$ $[M+Na]^+$ *m/z* 1088.3384, found 1088.3448.

Sodium 2-(2-(2-(4-(7-(4-(allyloxy)-3,5-dichlorophenyl)-5,5-difluoro-3,9-bis(4-(2-(2-(2-(sulfonatooxy)ethoxy)ethoxy)ethoxy)phenyl)-5H-4l4,5l4-dipyrrolo[1,2-c:2',1'-f][1,3,5,2] triazaborinin-1-yl)phenoxy)ethoxy)ethoxy)ethyl sulfate (33). A flame-dried round-bottom flask was charged with **32** (386 mg, 0.36 mmol, 1.0 equiv), SO_3-NMe_3 (454 mg, 3.3 mmol, 9.0 equiv) and anhydrous DMF (20 mL). The reaction was stirred at room temperature overnight. Volatiles were removed under reduced

pressure, the crude residue was dissolved in H_2O (10 ml), and loaded onto a 20 cc Sep-Pak cartridge preloaded with 5g C18 sorbent for reversed-phased purification (0-50% v/v MeCN/H_2O gradient) to afford the title compound as a blue solid (490 mg, 0.36 mmol, 99.0%). ^{1}H NMR (500 MHz, CD_3OD) δ 8.05 (d, *J* = 8.6 Hz, 2H), 7.92 (s, 2H), 7.87 (d, *J* = 8.6 Hz, 2H), 7.83 (d, *J* = 8.6 Hz, 2H), 7.02–6.97 (s, 1H), 6.94 (d, *J* = 8.5 Hz, 2H), 6.77 (m, 4H), 6.15 (ddt, *J* = 16.3, 10.8, 5.6 Hz, 1H), 5.46 (dd, *J* = 17.2, 1.6 Hz, 1H), 5.30 (dd, *J* = 10.6, 1.5 Hz, 1H), 4.54 (d, *J* = 5.8 Hz, 2H), 4.22–4.12 (m, 8H), 4.04 (m, 4H), 3.89–3.83 (m, 6H), 3.78–3.71 (m, 18H). ^{13}C NMR (125 MHz, DMSO-d6) δ 162.8, 161.7, 161.3, 160.5, 160.5, 157.1, 156.1, 152.2, 151.4, 150.8, 146.9, 143.7, 140.8, 133.7, 133.7, 133.1, 131.7, 131.2, 130.2, 130.1, 129.4, 126.8, 125.5, 124.6, 123.3, 119.7, 115.8, 115.6, 115.3, 115.2, 115.2, 115.2, 75.1, 70.6, 70.4, 70.0, 69.6, 68.4, 60.9, 52.4, 44.8. HR-MS calculated for $C_{53}H_{57}BCl_2F_2N_3Na_4O_{22}S_3$ $[M+Na]^+$ *m/z* 1394.1625, found 1394.1606.

Sodium 2-(2-(2-(4-(7-(3,5-dichloro-4-hydroxyphenyl)-5,5-difluoro-3,9-bis(4-(2-(2-(2-(sulfonatooxy)ethoxy)ethoxy)ethoxy)phenyl)-5H-4l4,5l4-dipyrrolo[1,2-c:2',1'-f][1,3,5,2] triazaborinin-1-yl)phenoxy)ethoxy)ethoxy)ethyl sulfate (34). A flame-dried round-bottom flask was charged with **33** (490 mg, 0.36 mmol, 1.0 equiv), 1,3-dimethylbarbituric acid (70.8 mg, 0.45 mmol, 1.25 equiv), $Pd(PPh_3)_4$ (84.0 mg, 0.73 mmol, 0.2 equiv) and anhydrous DMF (40 mL). The reaction was stirred at room temperature overnight. All volatiles were removed under reduced pressure. The crude residue was treated with EtOAc and extracted with H_2O (3 × 50 mL). The combined aqueous fractions were washed with Et_2O (3 × 100 mL), concentrated to 5 mL, and

loaded onto a 20 cc Sep-Pak cartridge preloaded with 5g C18 sorbent for reversed-phased purification (0-35% v/v MeCN/H_2O gradient) to yield the title compound as a dark pink solid (360 mg, 0.27 mmol, 74.4%. ^{1}H NMR (500 MHz, DMSO-d_6) δ 8.44 (s, 2H), 8.25 (d, *J* = 8.3 Hz, 2H), 8.04–7.93 (m, 3H), 7.87 (d, *J* = 8.3 Hz, 2H), 7.10 (d, *J* = 8.4 Hz, 2H), 7.04 (d, *J* = 8.5 Hz, 2H), 6.99 (d, *J* = 8.5 Hz, 2H), 6.90 (s, 1H), 3.77 (dt, *J* = 24.1, 4.8 Hz, 18H), 3.58–3.51 (m, 18H). ^{13}C NMR (125 MHz, DMSO-d6) δ 168.2, 164.3, 164.3, 160.4, 160.4, 159.1, 159.1, 158.6, 158.6, 158.0, 153.8, 153.8, 148.4, 148.4, 144.6, 141.6, 140.3, 140.2, 133.0, 131.1, 130.6, 129.8, 127.4, 127.1, 126.9, 124.9, 122.1, 115.3, 114.9, 113.9, 113.9, 110.0, 72.9, 70.6, 70.4, 70.0, 69.6, 68.1, 67.9, 65.7. m.p. = 237°C. HR-MS calculated for $C_{50}H_{53}BCl_2F_2N_3Na_4O_{22}S_3$ $[M+H]^+$ *m/z* 1354.1312, found 1354.1329.

APC-2. A round-bottom flask was charged with **34** (100 mg, 0.075 mmol, 1.0 equiv) in H_2O (3 mL). EDC (21.6 mg, 0.113 mmol, 1.5 equiv), picolinic acid (27.7 mg, 0.225 mmol, 3.0 equiv), and 4-dimethylaminopyridine (1.38 mg, 0.011 mmol, 0.15 equiv) were added. The reaction was stirred at room temperature for 2 hrs and then washed with 1:2 v/v CH_2Cl_2:EtOAc (6 × 200 mL). The reaction was loaded onto a 1.0 mm thick preparative TLC plate for purification (9:11 v/v MeOH/$CH_2Cl_{2)}$ to yield APC-2 (57.5 mg, 0.40 mmol, 53.0 %) as a blue solid. ^{1}H NMR (500 MHz, DMSO-d_6) δ 8.89 (d, *J* = 4.7 Hz, 1H), 8.45 (s, 2H), 8.36 (d, *J* = 7.9 Hz, 1H), 8.25 (d, *J* = 8.5 Hz, 2H), 8.15 (t, *J* = 8.1Hz, 1H), 8.06 – 7.97 (m, 3H), 7.88 (d, *J* = 8.4 Hz, 2H), 7.83 (dd, *J* = 7.8, 4.7 Hz, 1H), 7.12 (d, *J* = 8.8 Hz, 2H), 7.05 (d, *J* = 8.5 Hz, 2H), 7.01 (d, *J* = 8.4 Hz, 2H), 6.89

(s, 1H), 3.84–3.75 (m, 30H), 3.60 (s, 17H), 3.54 (s, 35H). HR-MS calculated for $C_{56}H_{56}BCl_2F_2N_4Na_4O_{23}S_3$ $[M+H]^+$ *m/z* 1459.1526, found 1459.1532.

APPENDIX F-SUPPLEMENTARY FIGURES FOR CHAPTER 2

This appendix includes supplementary figures including ^{1}H NMR and ^{13}C NMR spectrum for the compounds used in Chapter 2.

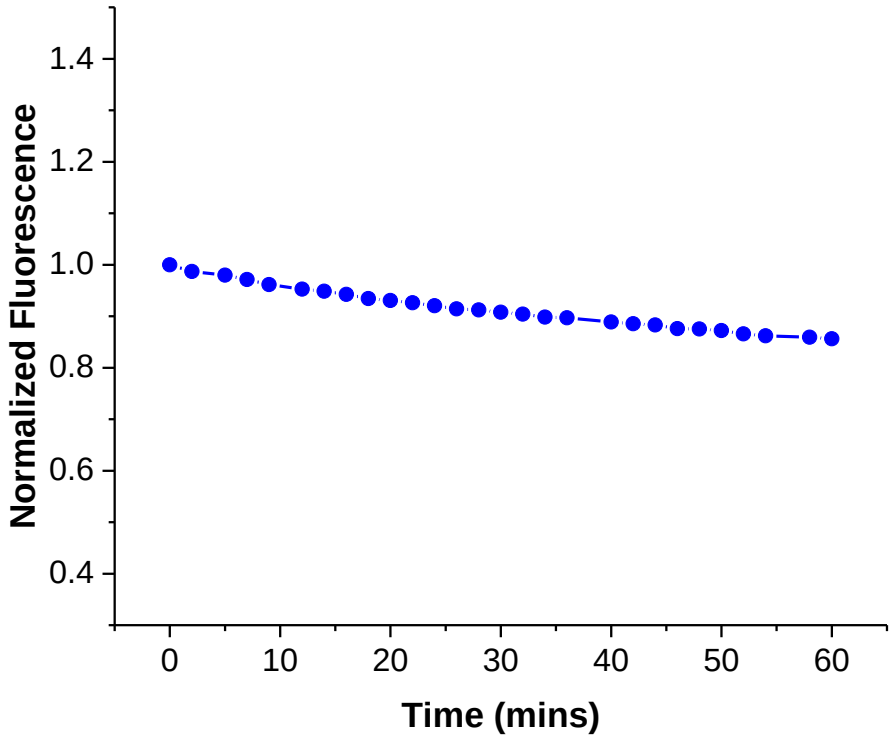

Figure F.1. Normalized fluorescence emission of 2 µM APC-2 in EtOH:citrate-phosphate buffer (pH 7.4) + 0.1% CrEL. The sample was irradiated continuously for 1 hr with 90% light intensity. Time points recorded are 0, 2, 5, 7, 9, 12, 14, 16, 18, 20, 22, 24, 26, 28, 30, 32, 34, 36, 40, 42, 44, 46, 48, 50, 52, 54, 58, and 60 mins.

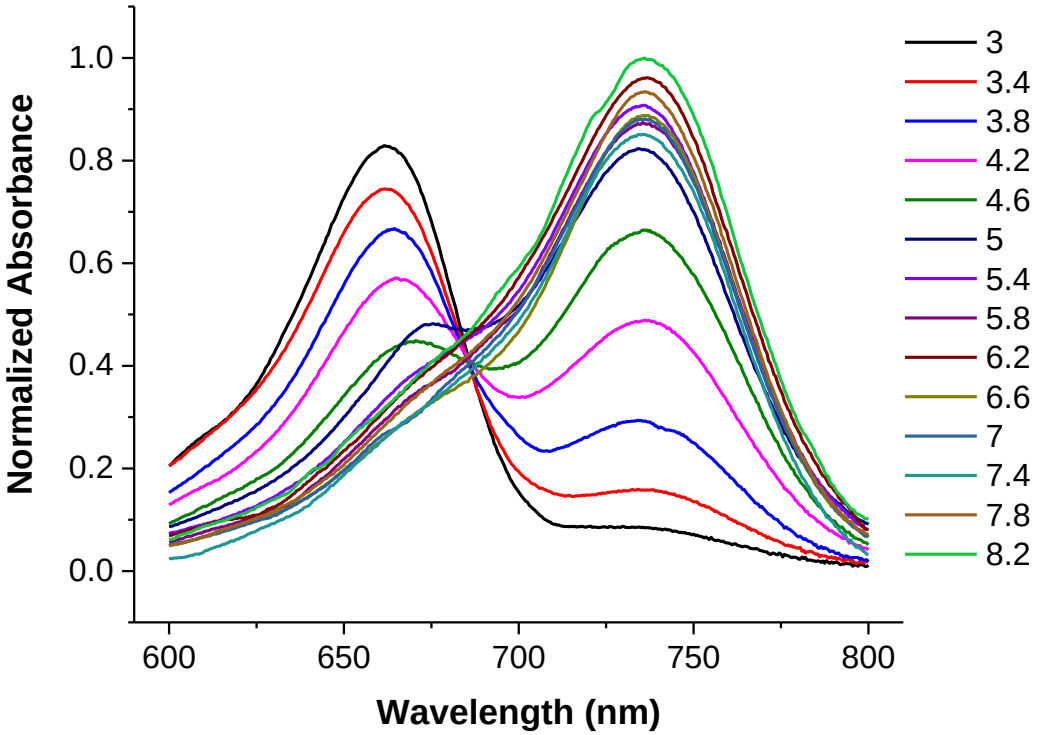

Figure F.2. Normalized absorbance spectra of 2 µM **21** in 2:3 v/v EtOH:citrate-phosphate buffer at various pHs. pH values examined were 3.0, 3.4, 3.8, 4.2, 4.6, 5.0, 5.4, 5.8, 6.2, 6.6, 7.0, 7.4, 7.8, and 8.2.

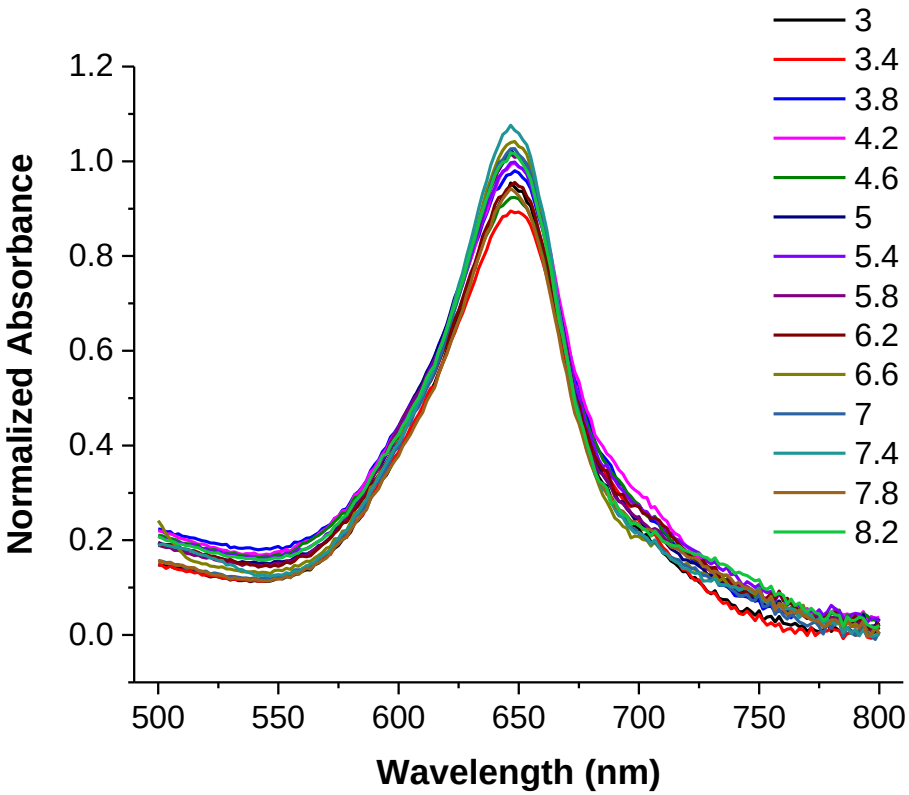

Figure F.3. Normalized absorbance spectra of 2 µM APC-1 in 2:3 v/v EtOH:citrate-phosphate buffer at various pHs. pH values examined were 3.0, 3.4, 3.8, 4.2, 4.6, 5.0, 5.4, 5.8, 6.2, 6.6, 7.0, 7.4, 7.8, and 8.2.

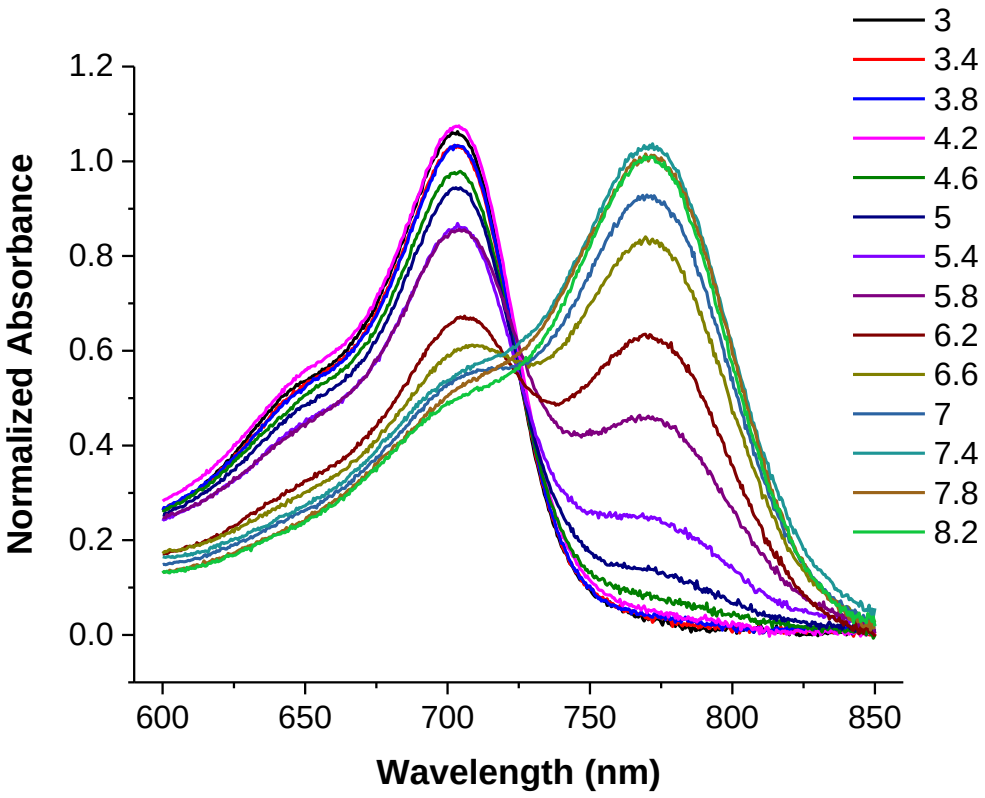

Figure F.4. Normalized absorbance spectra of 2 µM **34** in citrate-phosphate buffer + 0.1% CrEL at various pHs. pH values examined were 3.0, 3.4, 3.8, 4.2, 4.6, 5.0, 5.4, 5.8, 6.2, 6.6, 7.0, 7.4, 7.8, and 8.2.

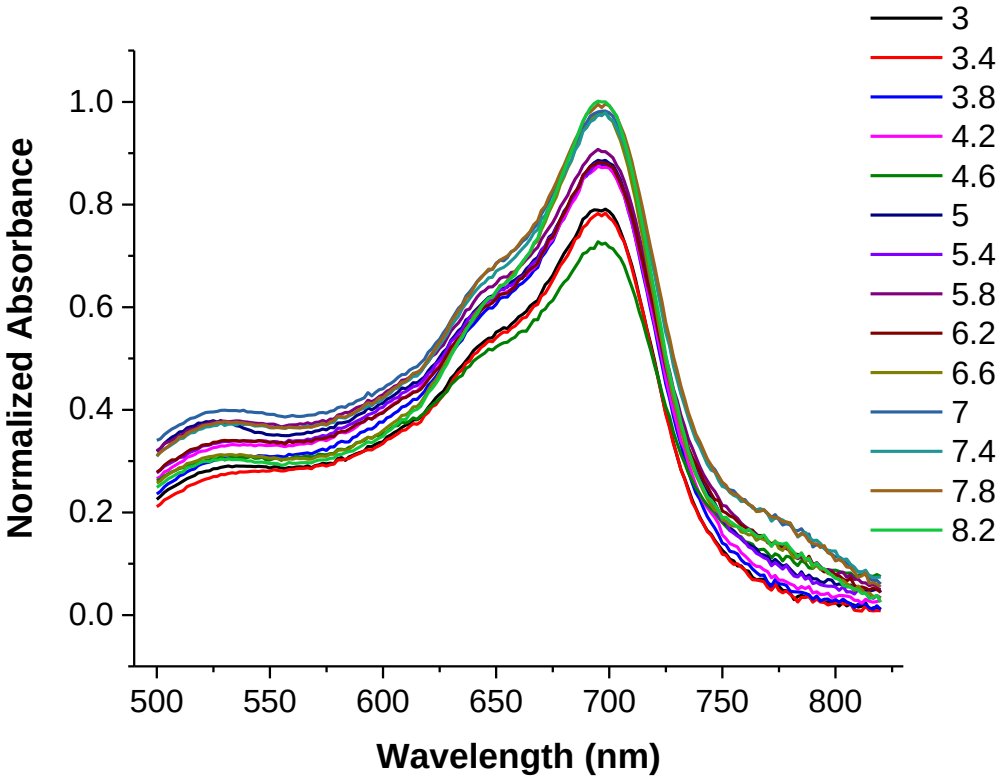

Figure F.5. Normalized absorbance spectra of 2 µM APC-2 in citrate-phosphate buffer + 0.1% CrEL at various pHs. pH values examined were 3.0, 3.4, 3.8, 4.2, 4.6, 5.0, 5.4, 5.8, 6.2, 6.6, 7.0, 7.4, 7.8, and 8.2.

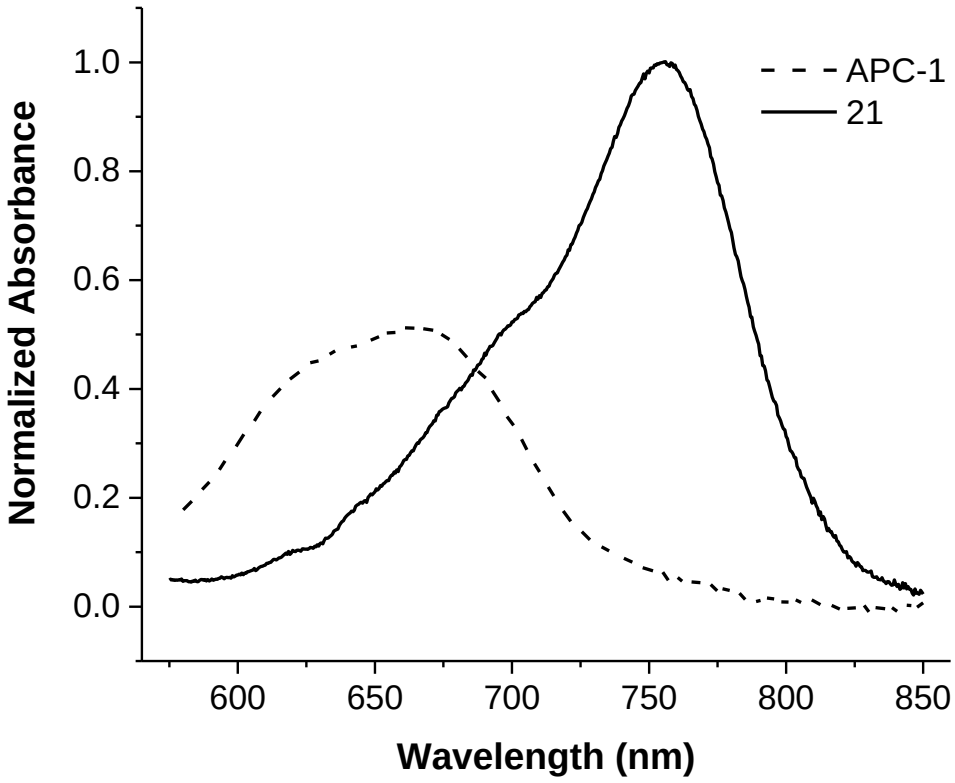

Figure F.6. Normalized absorbance spectra of 2 µM APC-1 (dashed line) and 2 µM **21** (solid line) in PBS + 0.1% CrEL (pH 7.4).

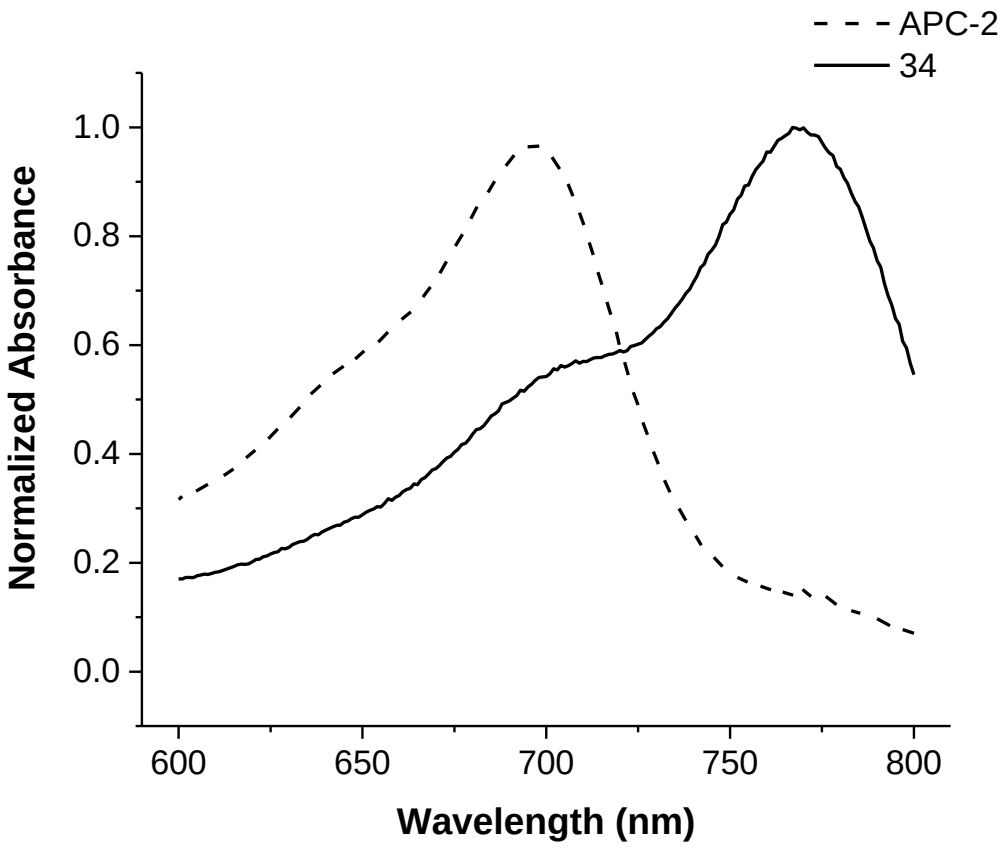

Figure F.7. Normalized absorbance spectra of 2 µM APC-2 (dashed line) and 2 µM **34** (solid line) in PBS + 0.1% CrEL (pH 7.4).

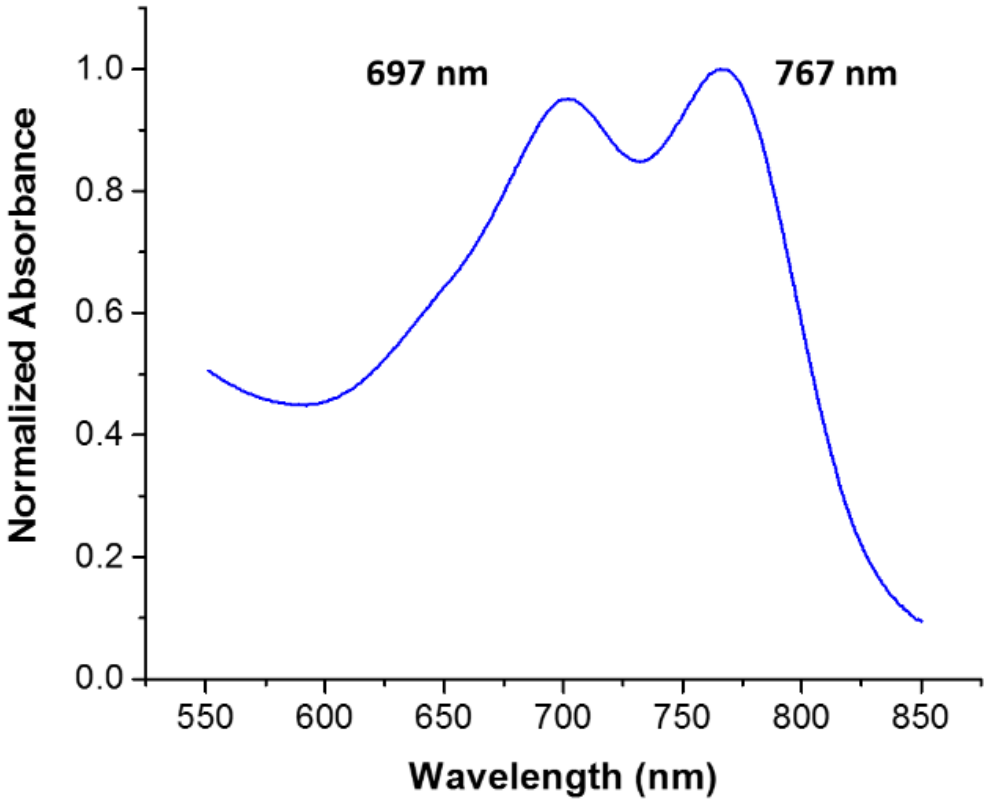

Figure F.8. Normalized absorbance spectrum of 2 µM APC-2 being partly converted to **34** with the addition of 10 µM Cu(II) in PBS + 0.1% CrEL.

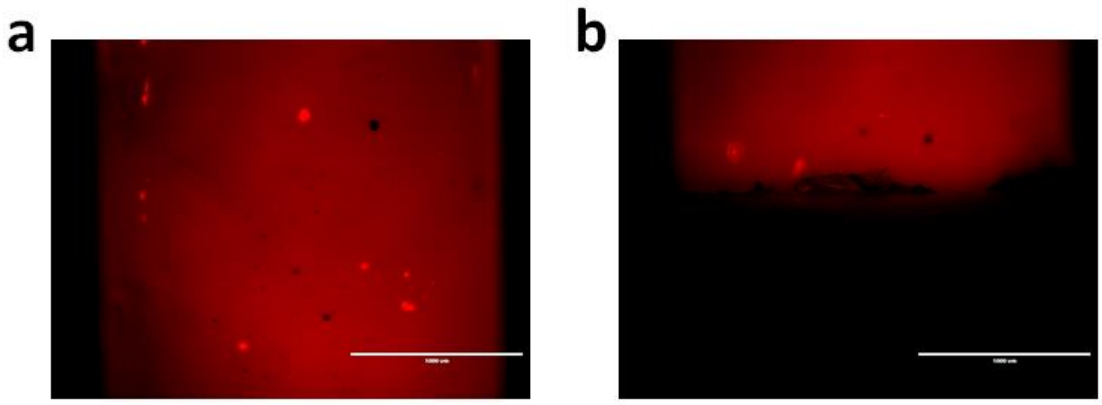

Figure F.9. Fluorescence imaging of APC-1. a) A 10 µM solution of APC-1 in 2:3 v/v EtOH:PBS buffer at pH 7.4 was loaded into a 0.08" FEP tube and imaged using an EVOS FL microscope equipped with a 4× objective and a Cy5 light cube filter. b) The lower region of the FEP tube was overlaid with a 1 cm thick agarose tissue phantom. Scale bar represents 1000 µm.

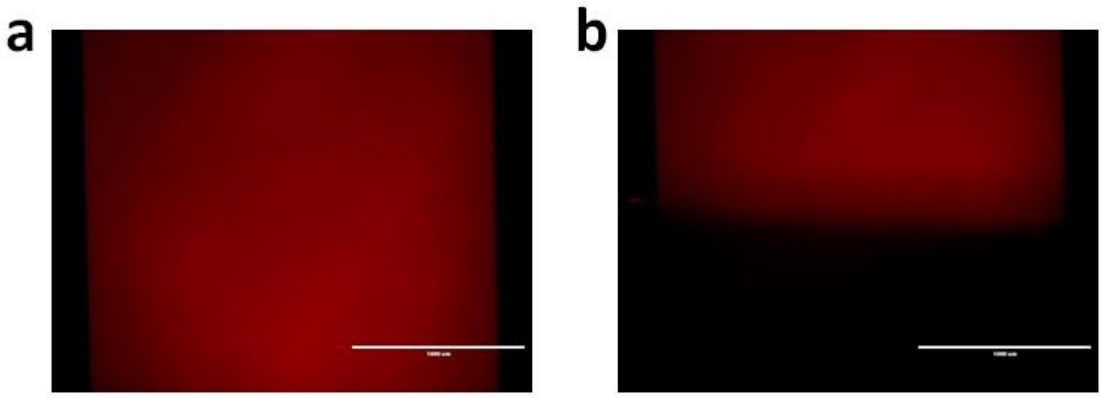

Figure F.10. Fluorescence imaging of APC-2. a) A 10 µM solution of APC-2 in 2:3 v/v EtOH:PBS buffer at pH 7.4 was loaded into a 0.08" FEP tube and imaged using an EVOS FL microscope equipped with a 4× objective and a Cy5 light cube filter. b) The lower region of the FEP tube was overlaid with a 1 cm thick agarose tissue phantom. Scale bar represents 1000 µm.

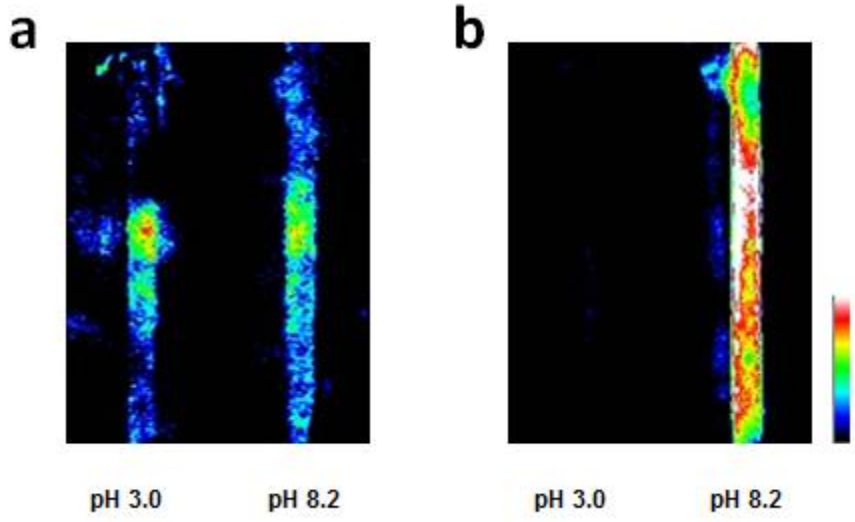

Figure F.11. Photoacoustic imaging of compound **21** at pH 3.0 and 8.2 with excitation provided at a) 680 nm and b) 755 nm. Pseudo-coloring represents intensity distribution from highest intensity indicated by white to the lowest intensity designated by black.

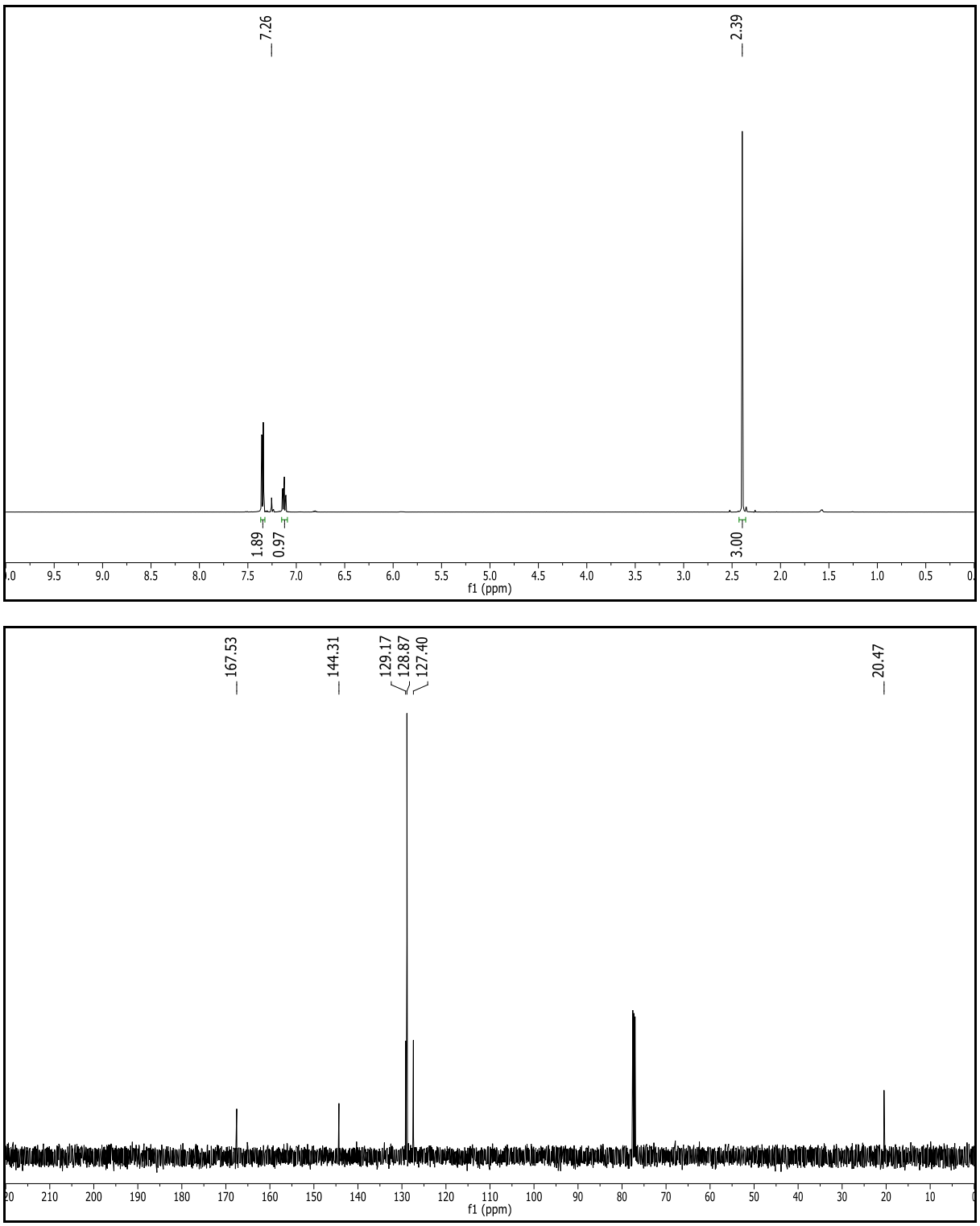

Figure F.12. ^{1}H NMR (500 MHz, $CDCl_3$) and ^{13}C NMR (125 MHz, $CDCl_3$) spectra of **16**.

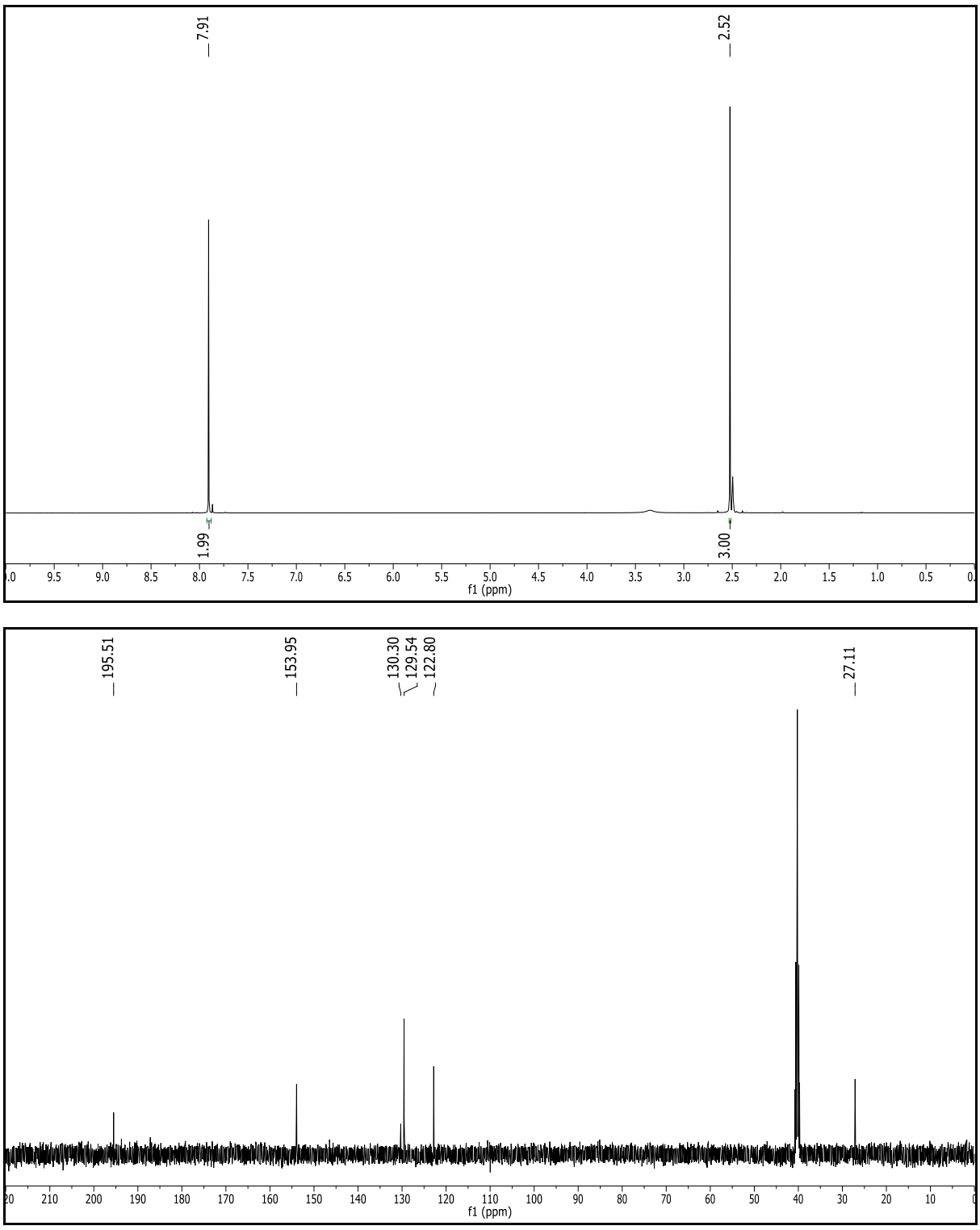

Figure F.13. ^{1}H NMR (500 MHz, DMSO-d6) and ^{13}C NMR (125 MHz, DMSO-d6) spectra of **17**.

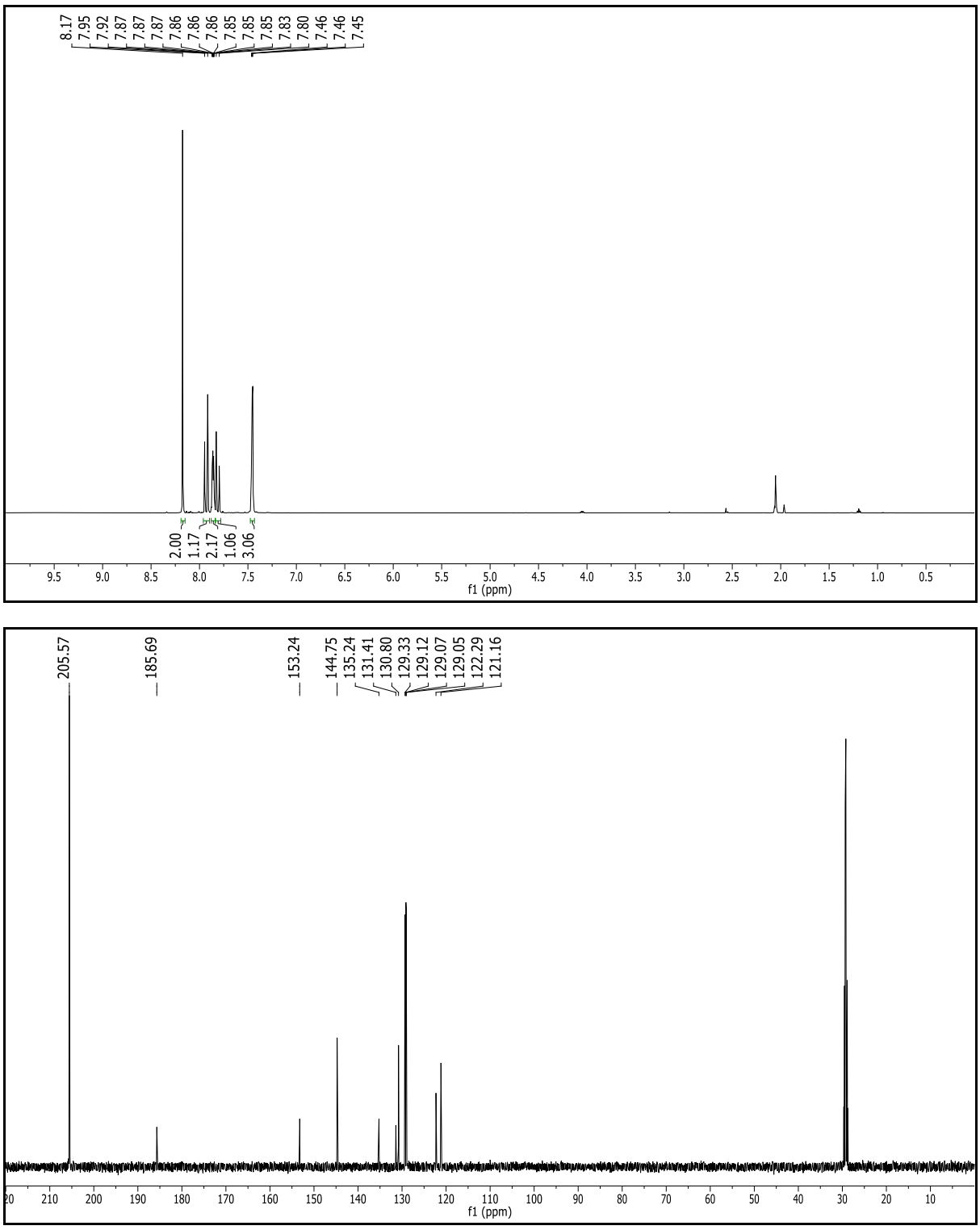

Figure F.14. ^{1}H NMR (500 MHz, Acetone-d6) and ^{13}C NMR (125 MHz, Acetone-d6) spectra of **18**.

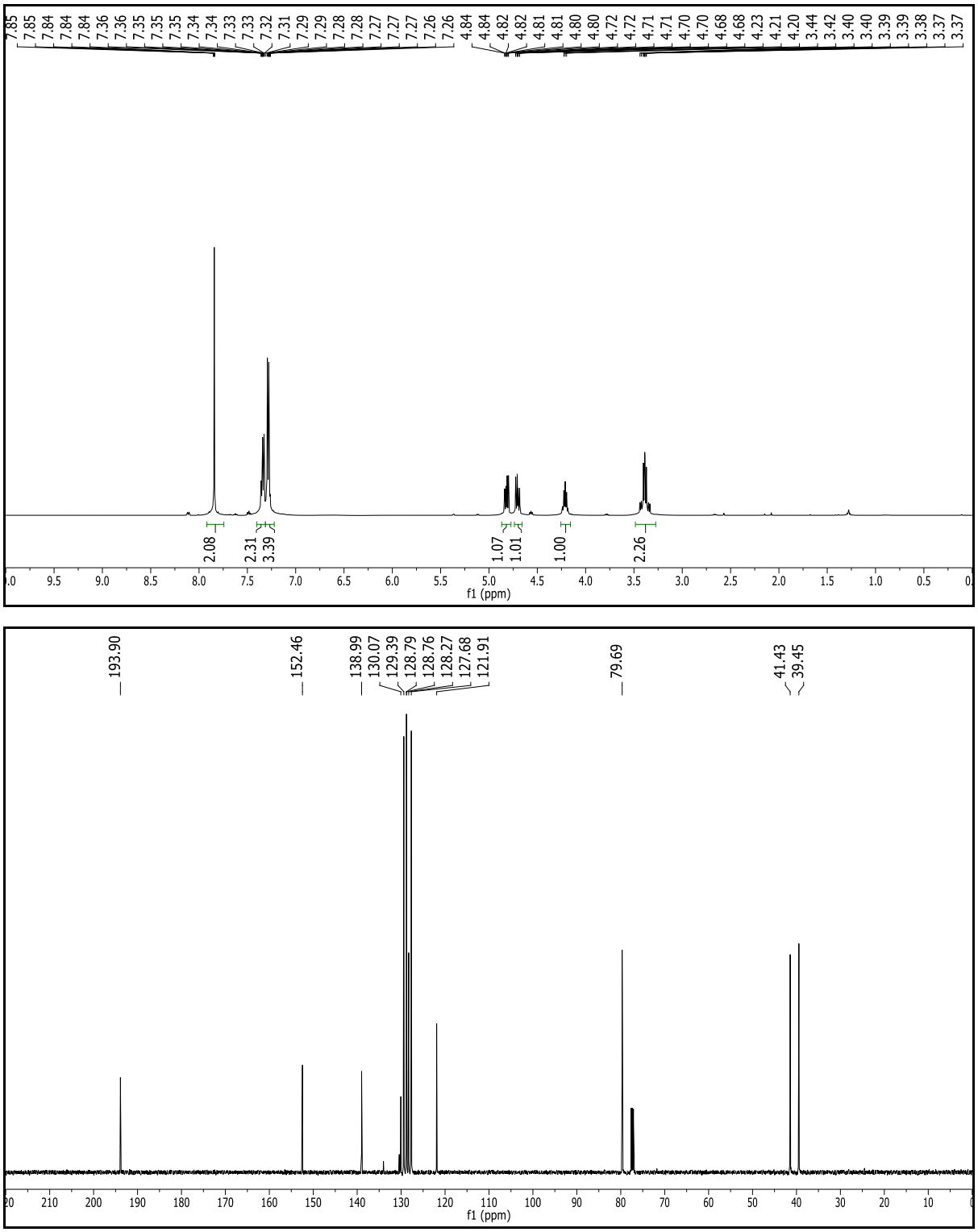

Figure F.15. ^{1}H NMR (500 MHz, $CDCl_3$) and ^{13}C NMR (125 MHz, $CDCl_3$) spectra of **19**.

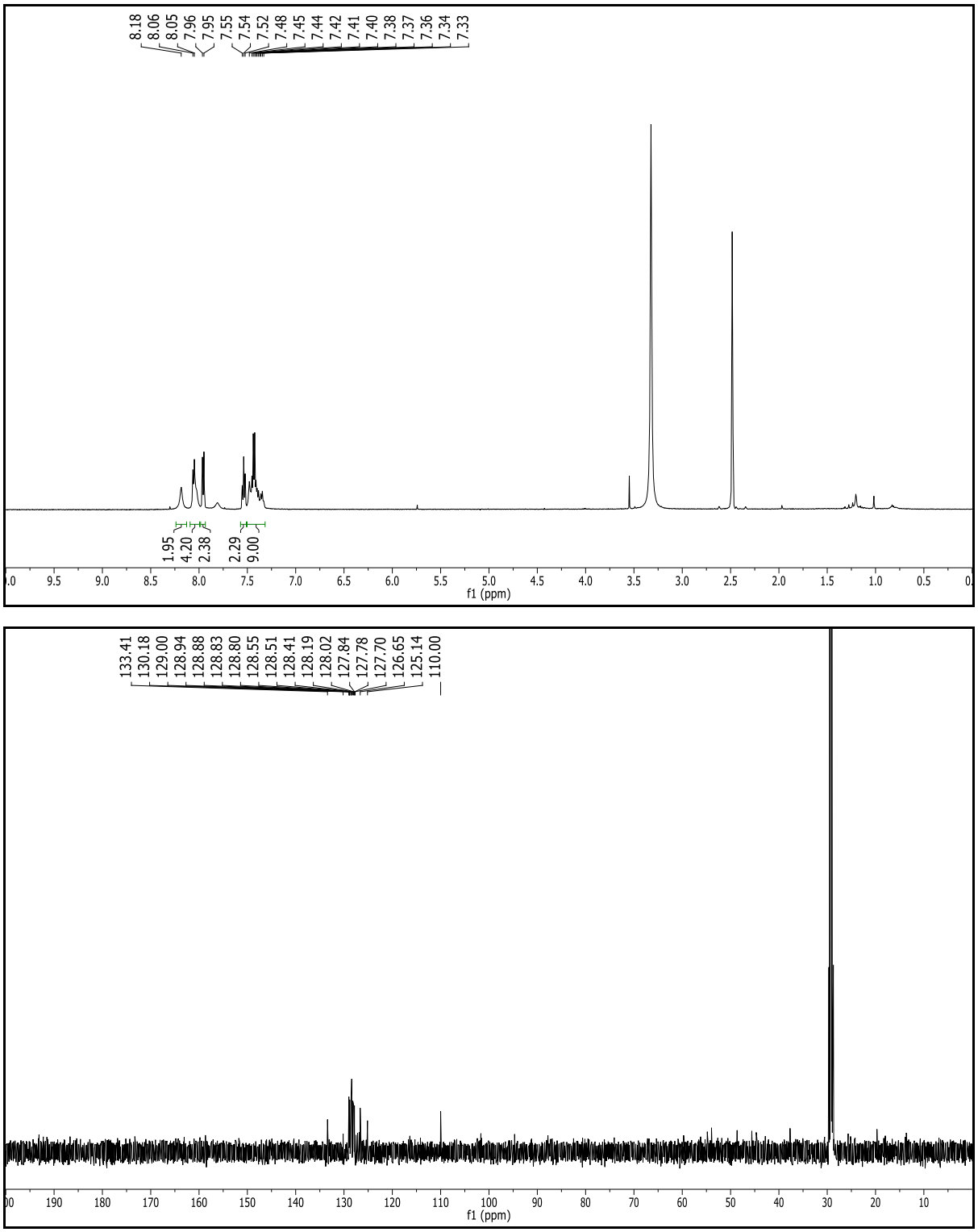

Figure F.16. ^{1}H NMR (500 MHz, DMSO-d6) and ^{13}C NMR (125 MHz, DMSO-d6) spectra of **20**.

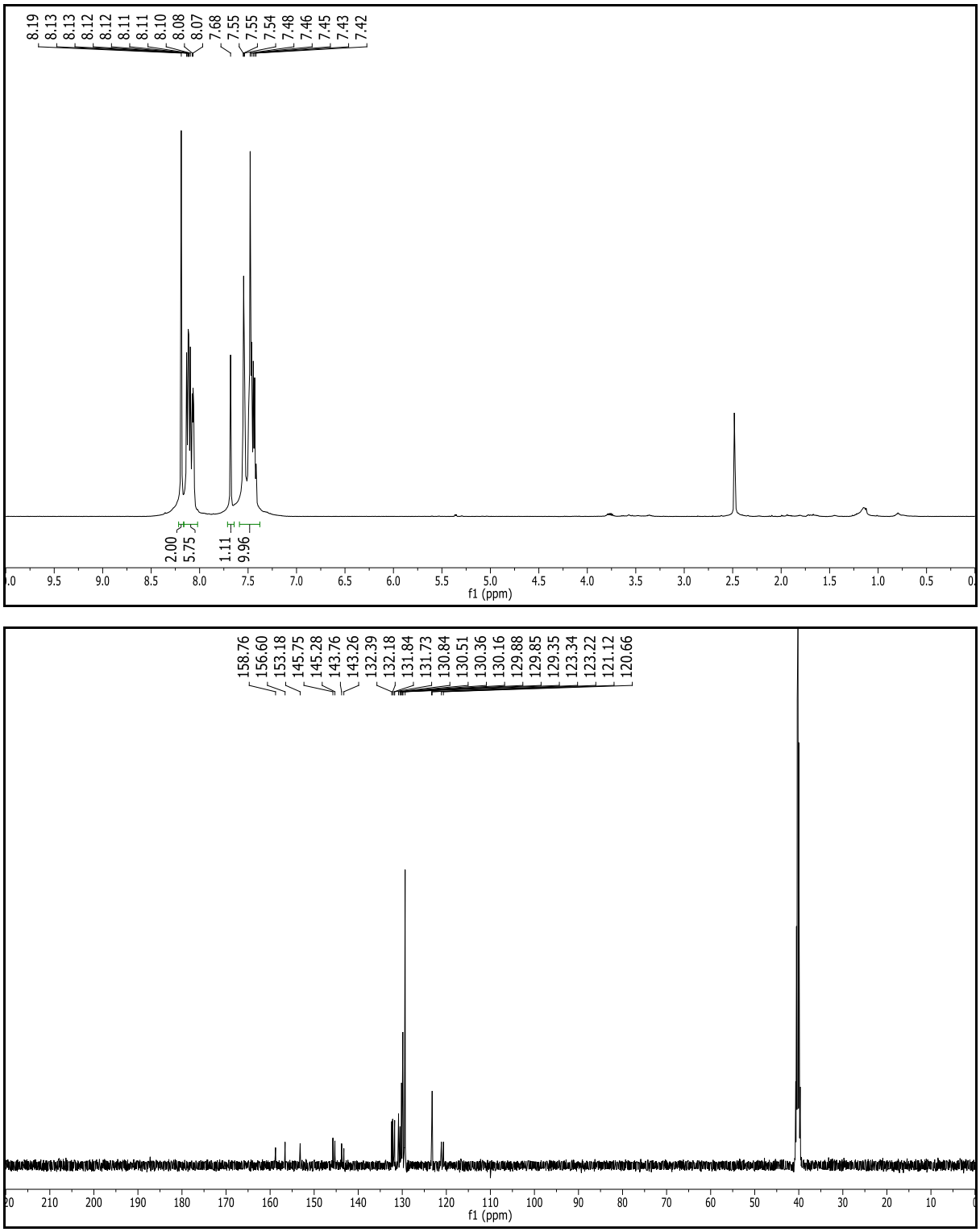

Figure F.17. ^{1}H NMR (500 MHz, DMSO-d6) and ^{13}C NMR (125 MHz, Acetone-d6) spectra of **21**.

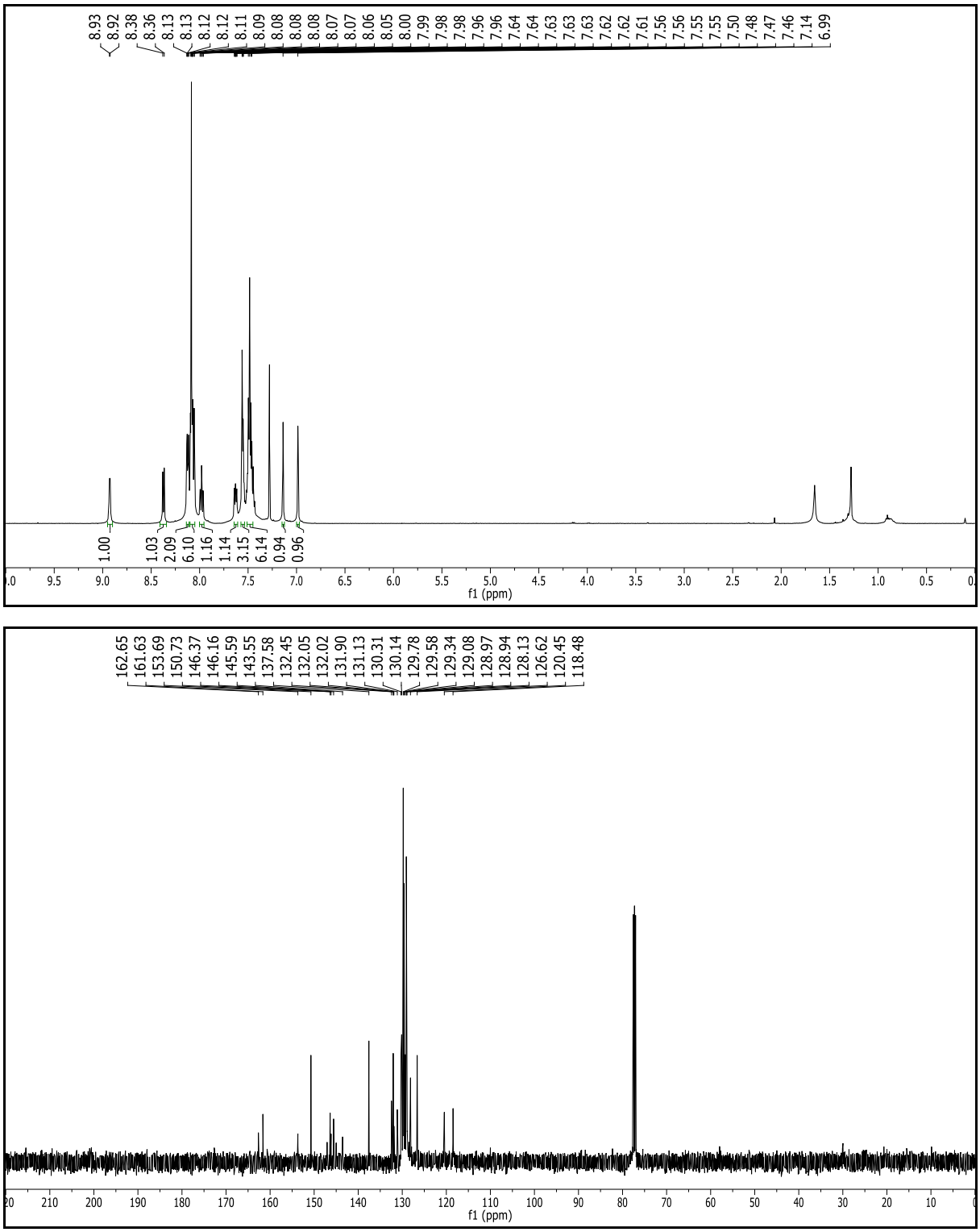

Figure F.18. ^{1}H NMR (500 MHz, $CDCl_3$) and ^{13}C NMR (125 MHz, $CDCl_3$) spectra of APC-1.

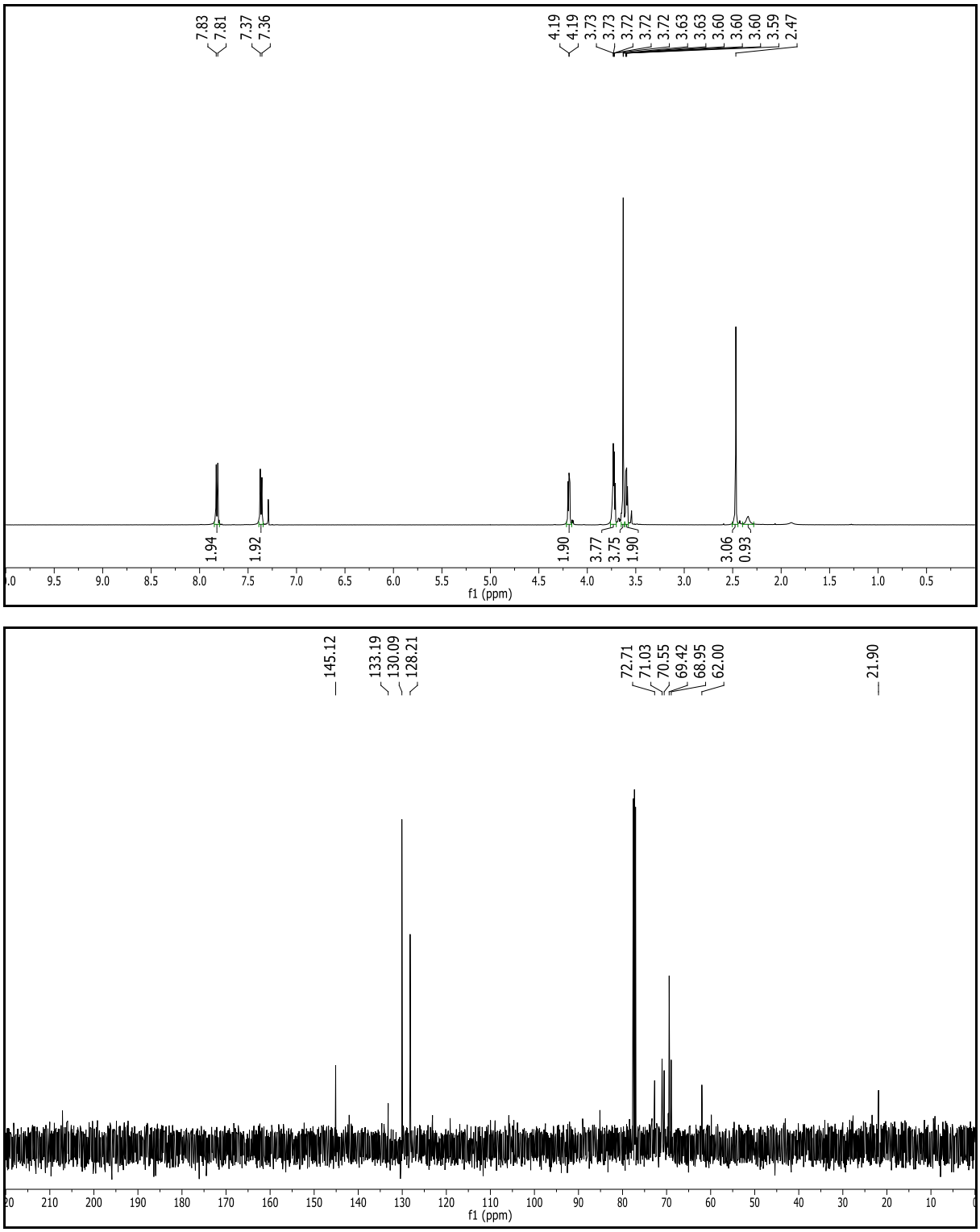

Figure F.19. ^{1}H NMR (500 MHz, $CDCl_3$) and ^{13}C NMR (125 MHz, $CDCl_3$) spectra of **22**.

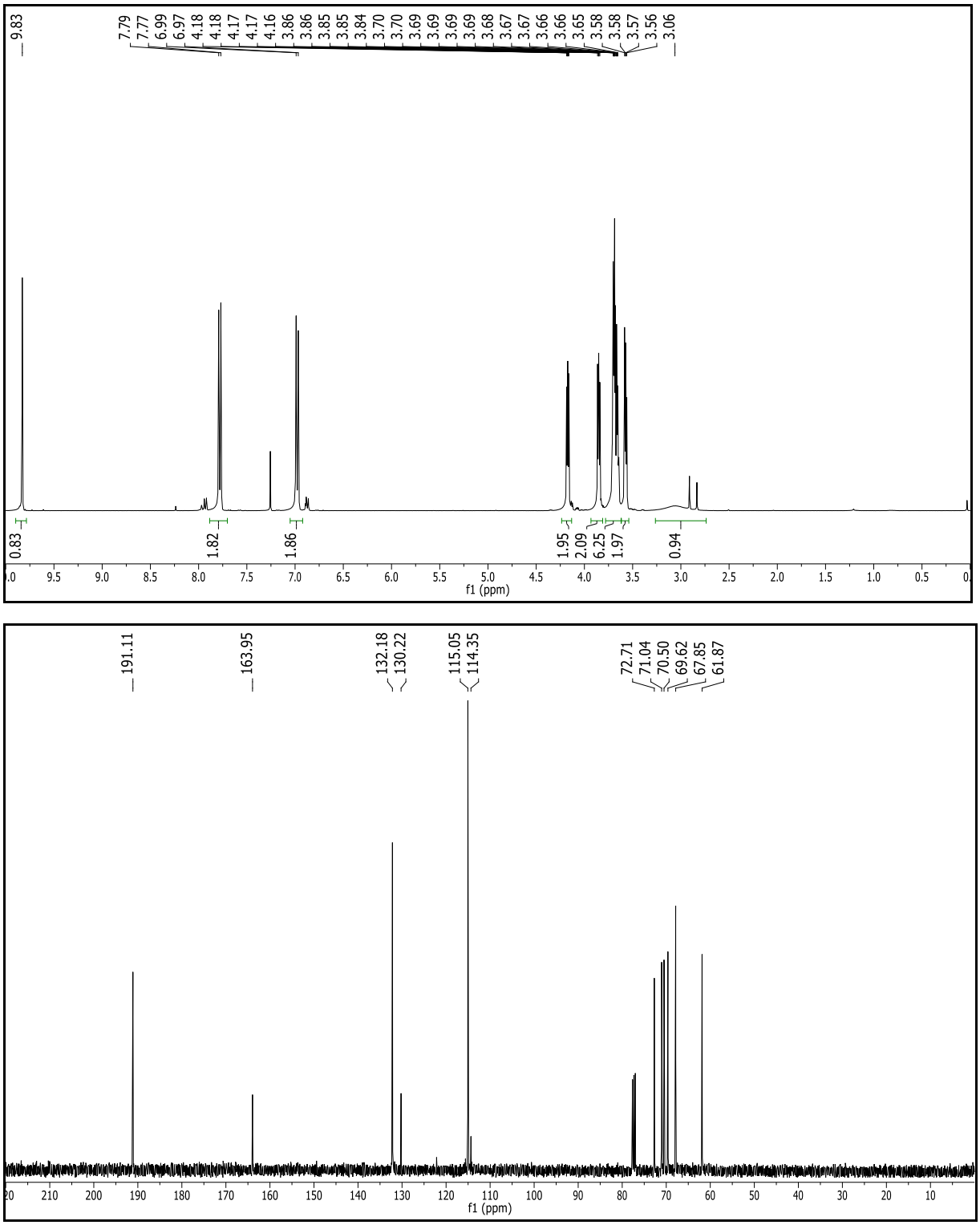

Figure F.20. ^{1}H NMR (400 MHz, $CDCl_3$) and ^{13}C NMR (100 MHz, $CDCl_3$) spectra of **23**.

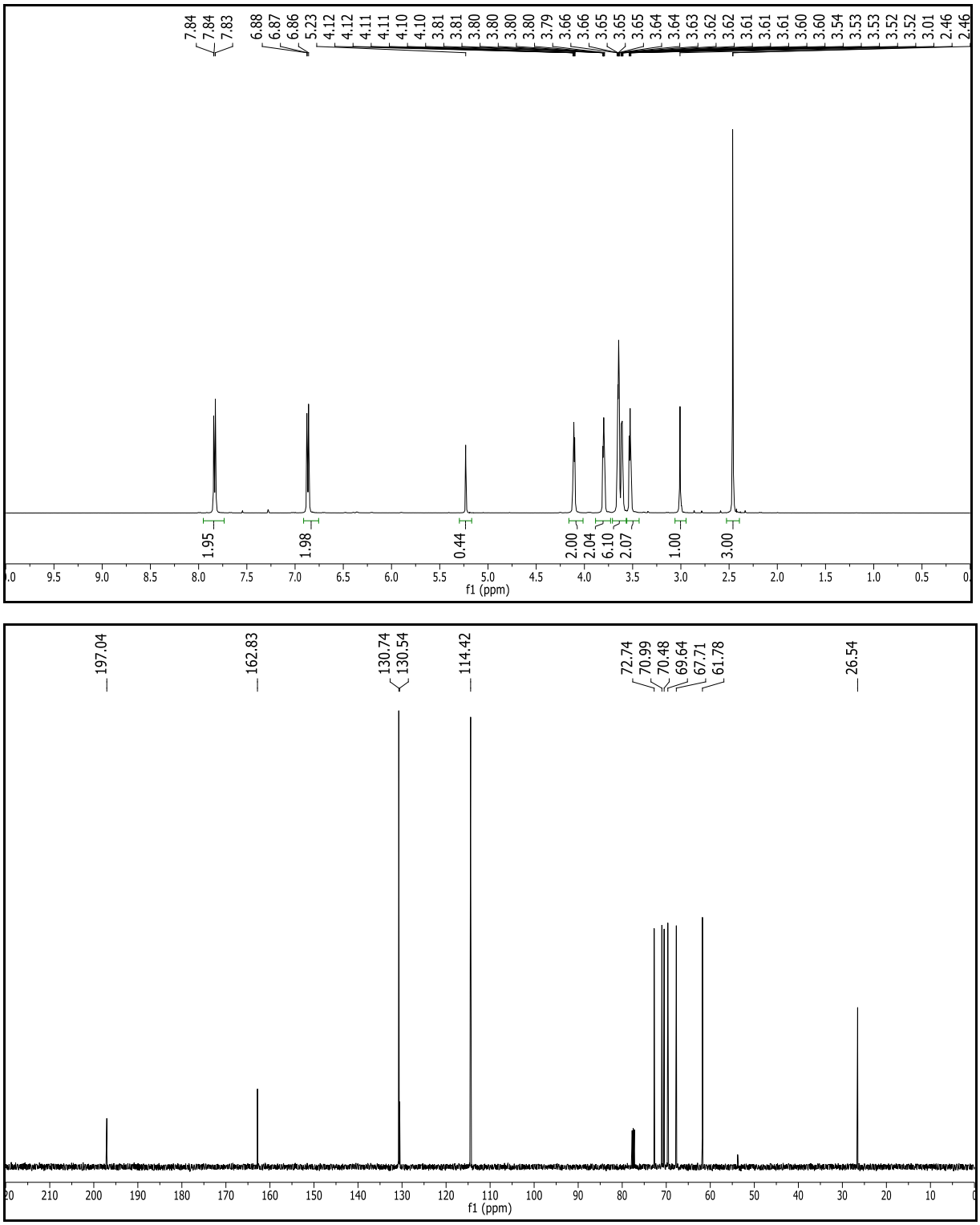

Figure F.21. ^{1}H NMR (400 MHz, $CDCl_3$) and ^{13}C NMR (100 MHz, $CDCl_3$) spectra of **24**.

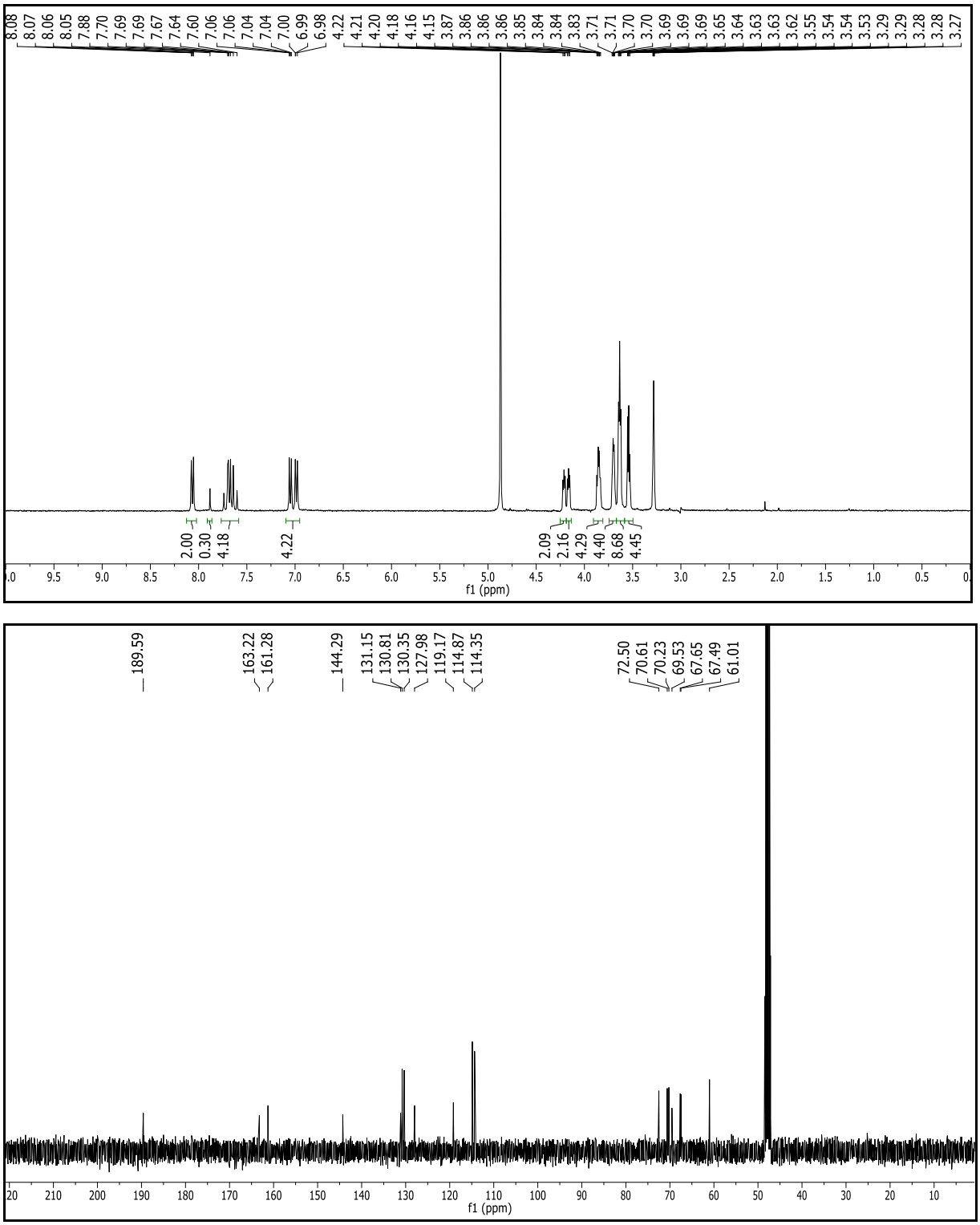

Figure F.22. ^{1}H NMR (400 MHz, MeOD) and ^{13}C NMR (100 MHz, MeOD) spectra of **25**.

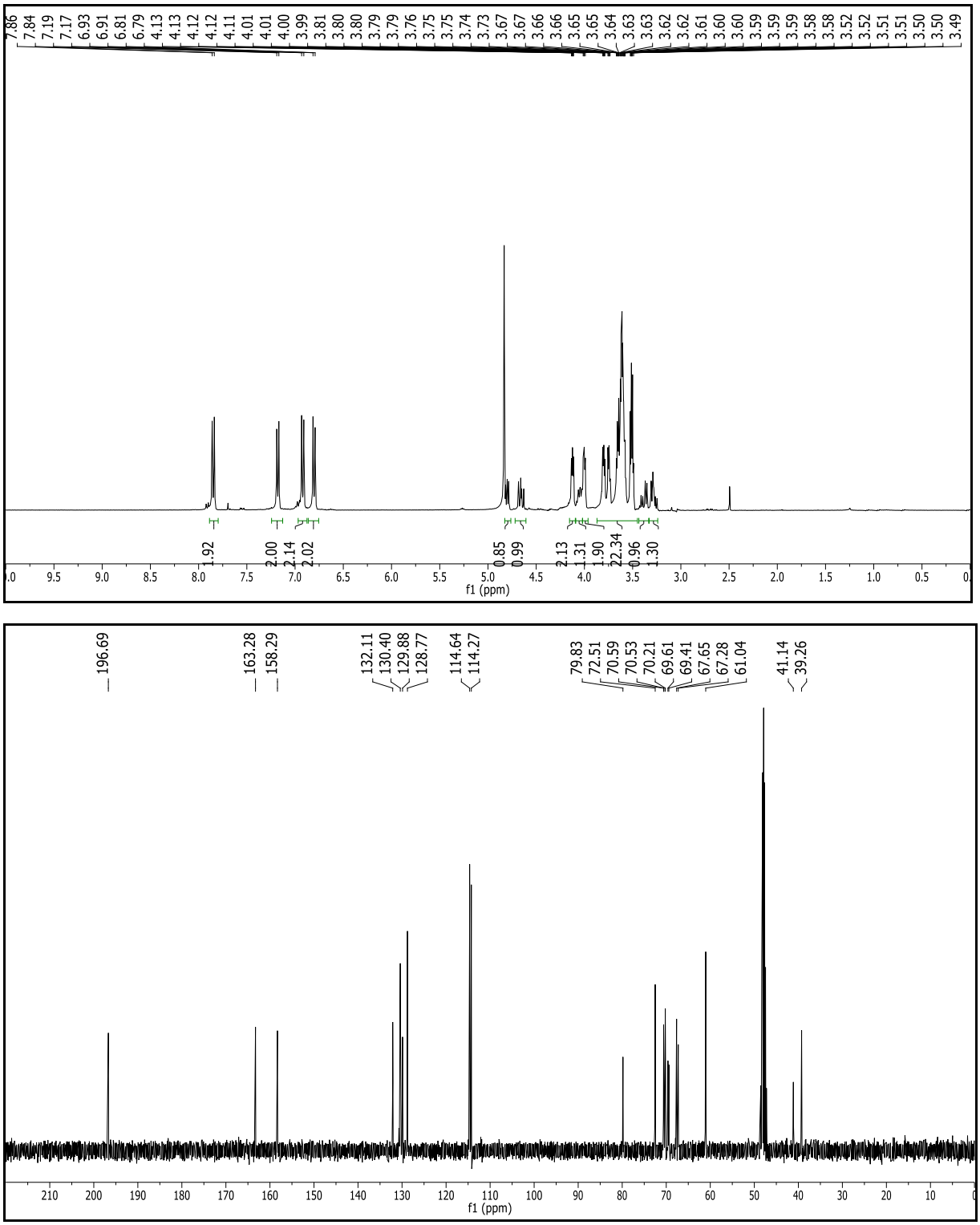

Figure F.23. ^{1}H NMR (400 MHz, MeOD) and ^{13}C NMR (100 MHz, MeOD) spectra of **26**.

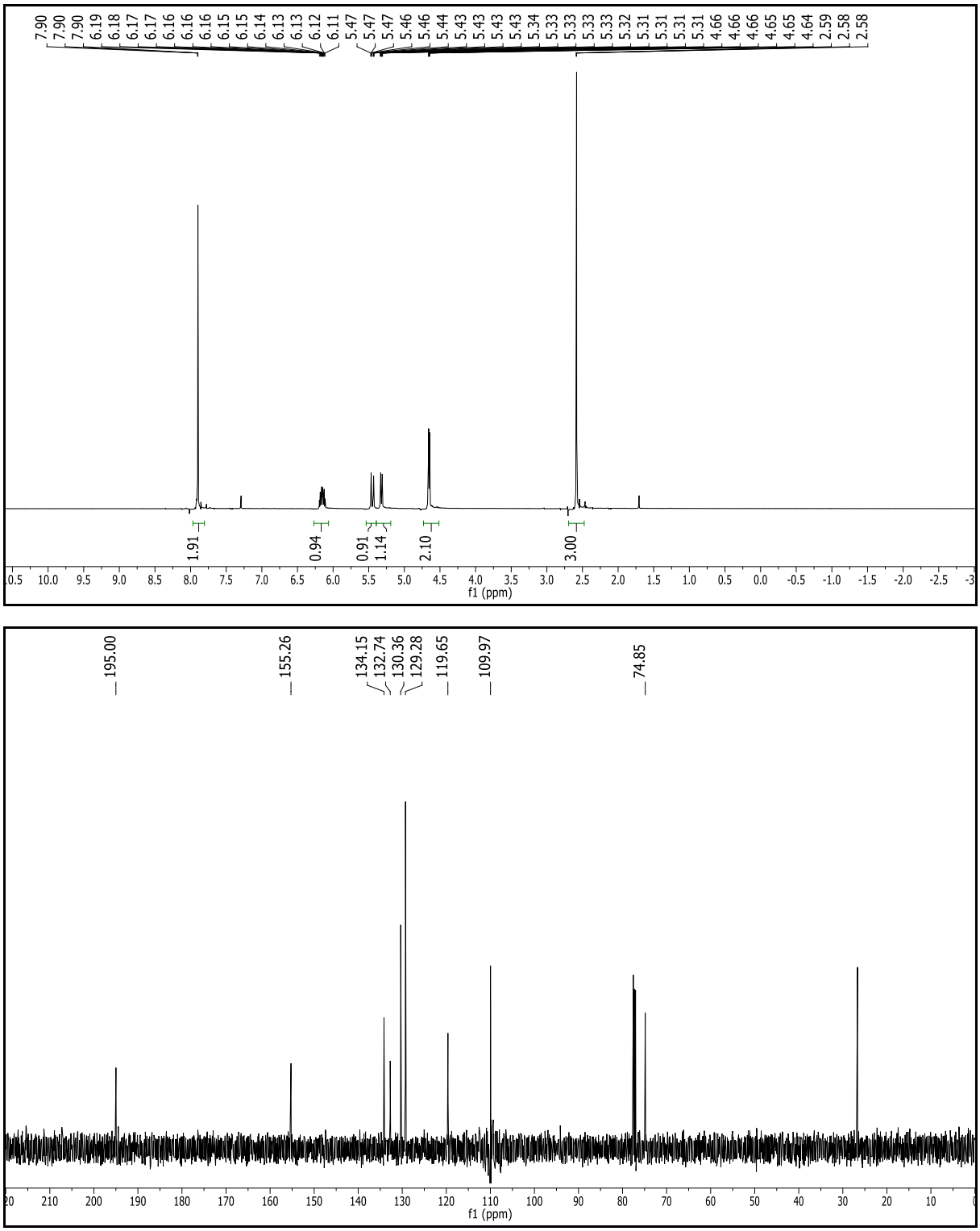

Figure F.24. ^{1}H NMR (500 MHz, $CDCl_3$) and ^{13}C NMR (125 MHz, $CDCl_3$) spectra of **27**.

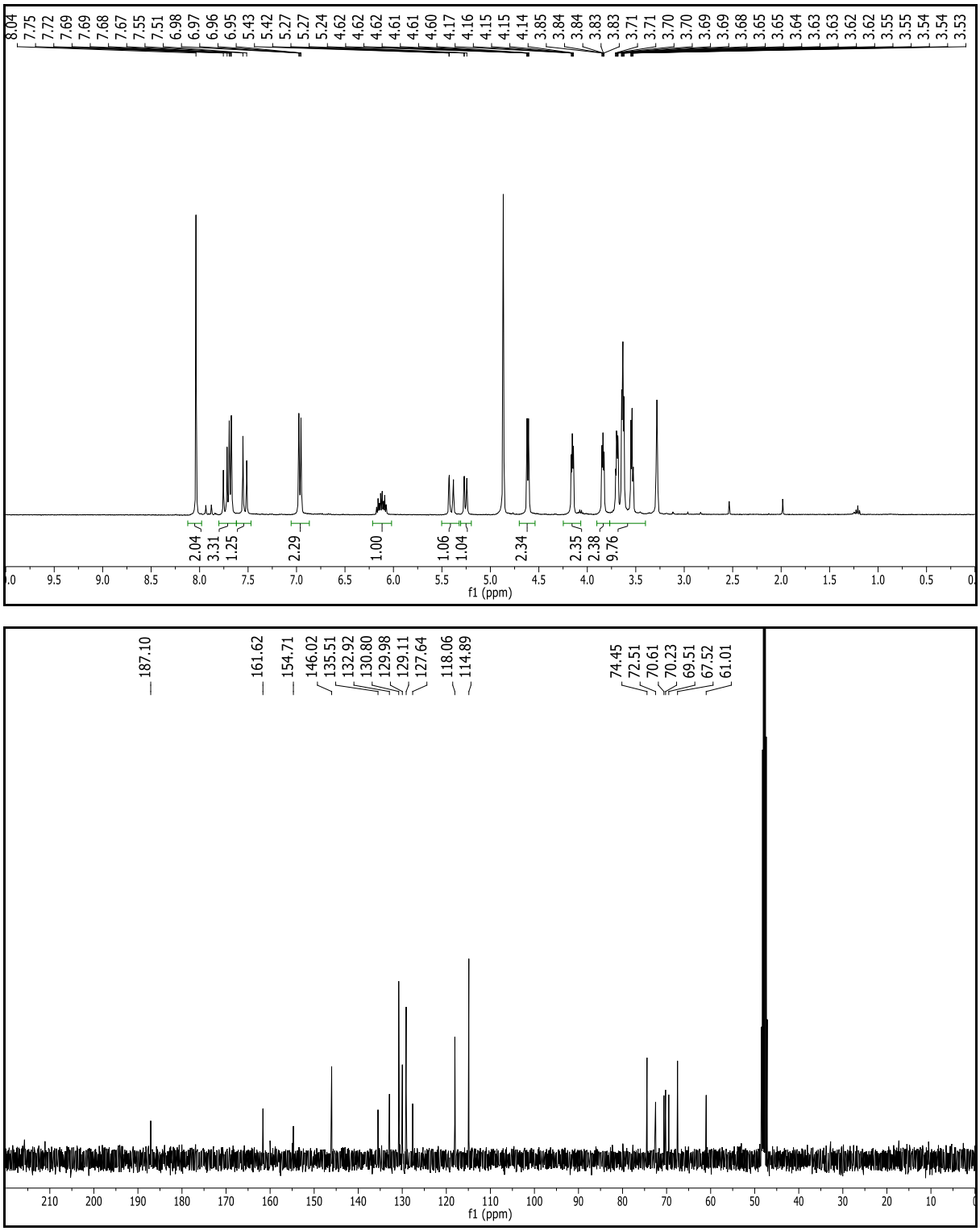

Figure F.25. ^{1}H NMR (400 MHz, MeOD) and ^{13}C NMR (100 MHz, MeOD) spectra of **28**.

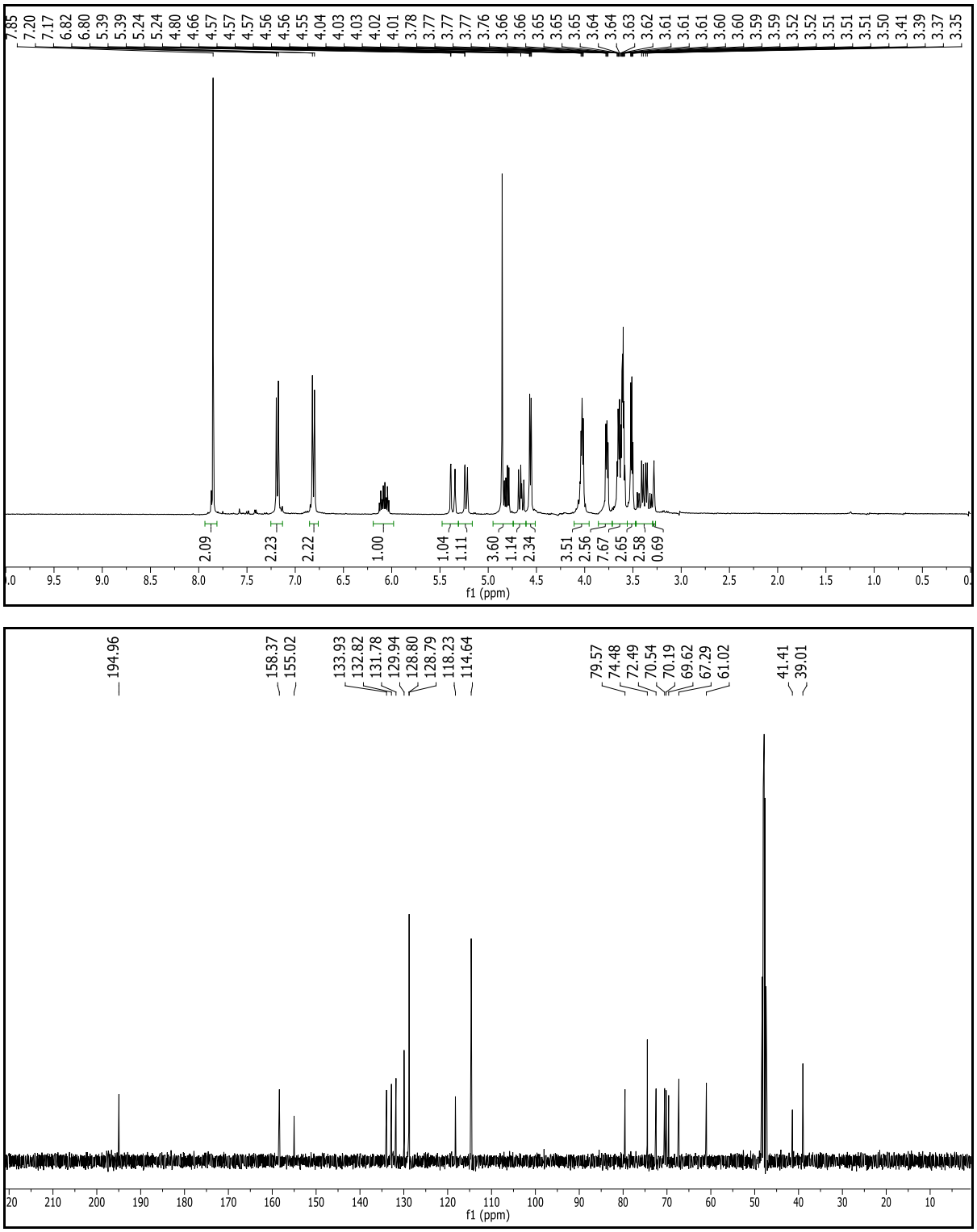

Figure F.26. ^{1}H NMR (400 MHz, MeOD) and ^{13}C NMR (100 MHz, MeOD) spectra of **29**.

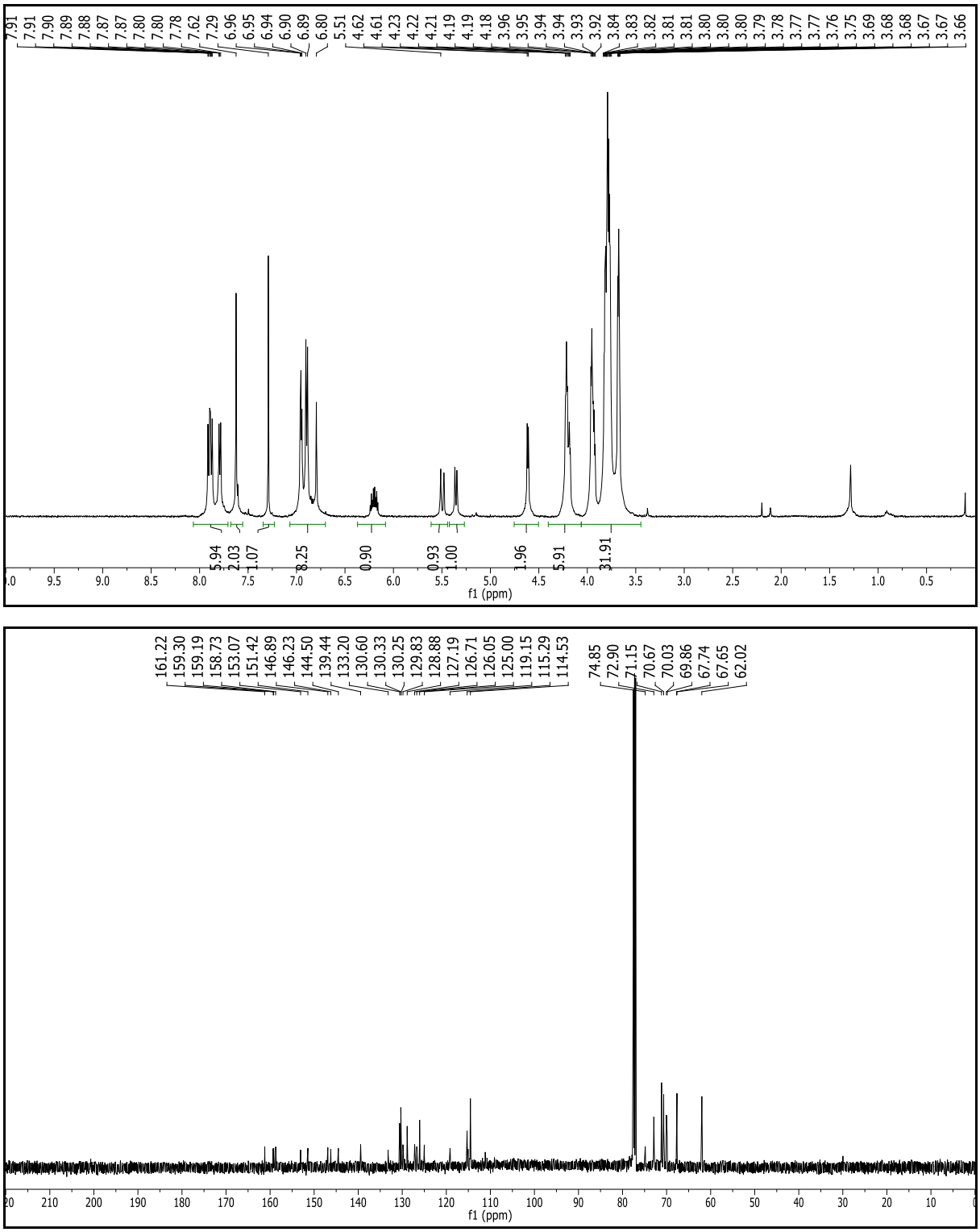

Figure F.27. ^{1}H NMR (500 MHz, $CDCl_3$) and ^{13}C NMR (125 MHz, $CDCl_3$) spectra of **30**.

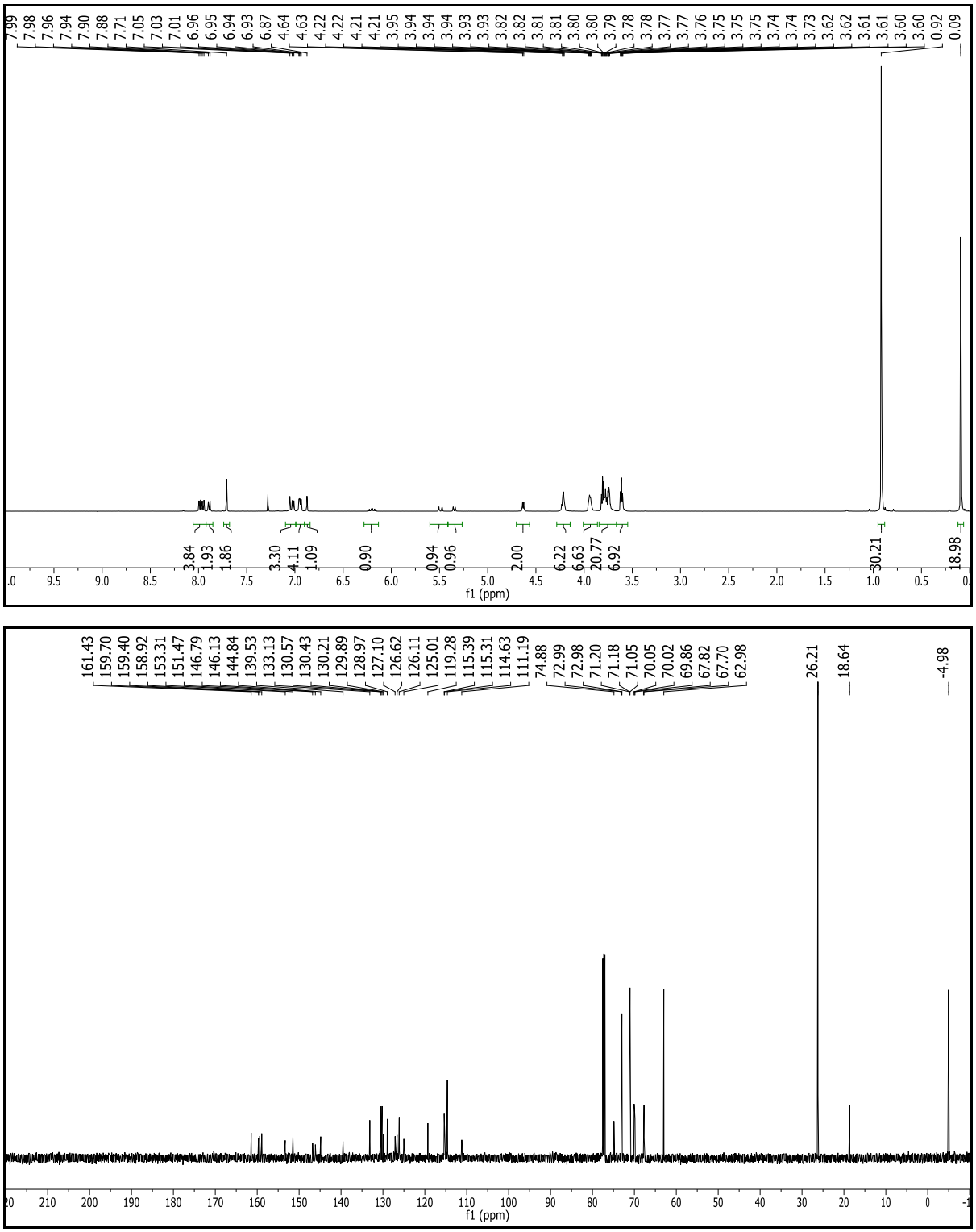

Figure F.28. ^{1}H NMR (500 MHz, $CDCl_3$) and ^{13}C NMR (125 MHz, $CDCl_3$) spectra of **31**.

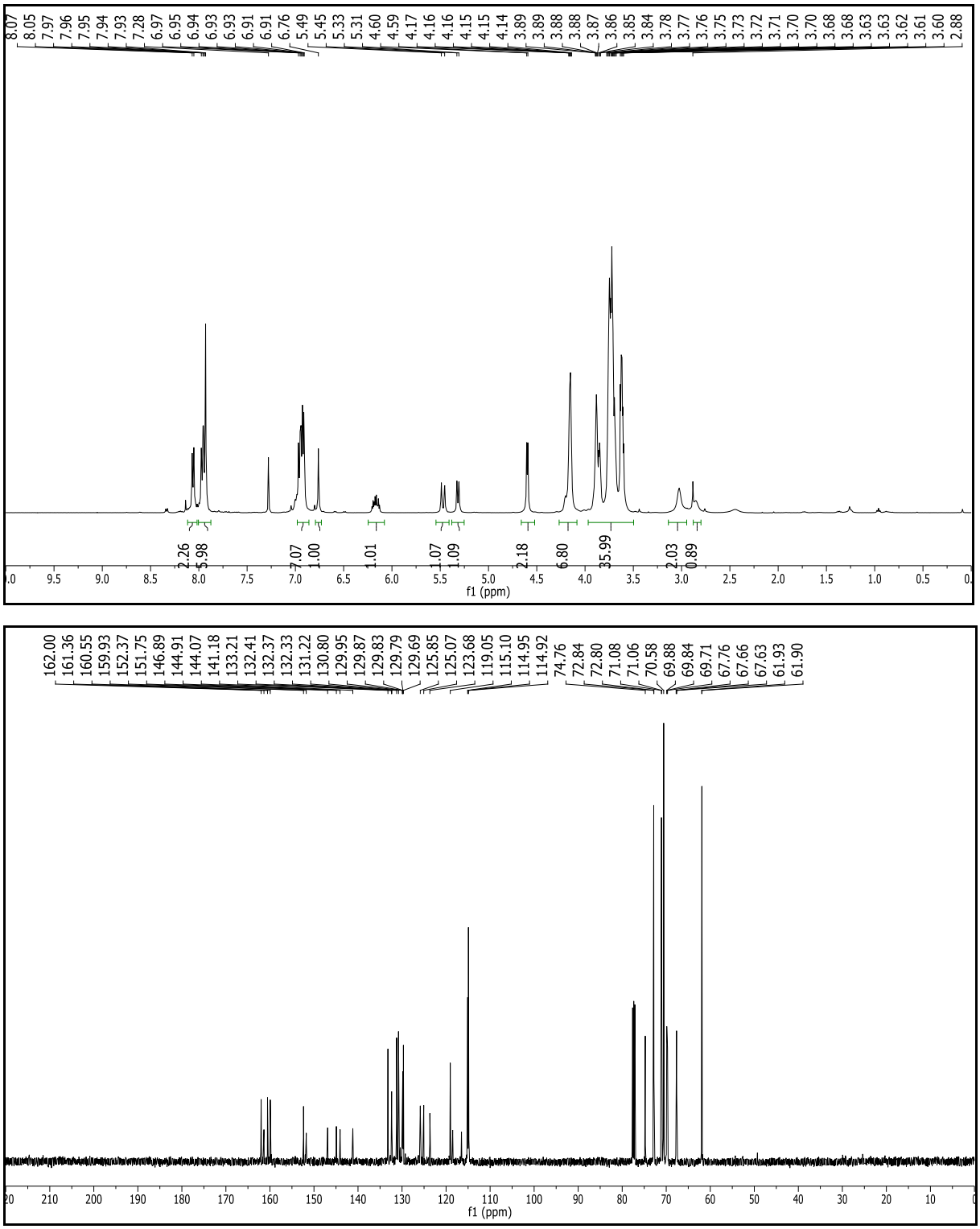

Figure F.29. ^{1}H NMR (500 MHz, $CDCl_3$) and ^{13}C NMR (125 MHz, $CDCl_3$) spectra of **32**.

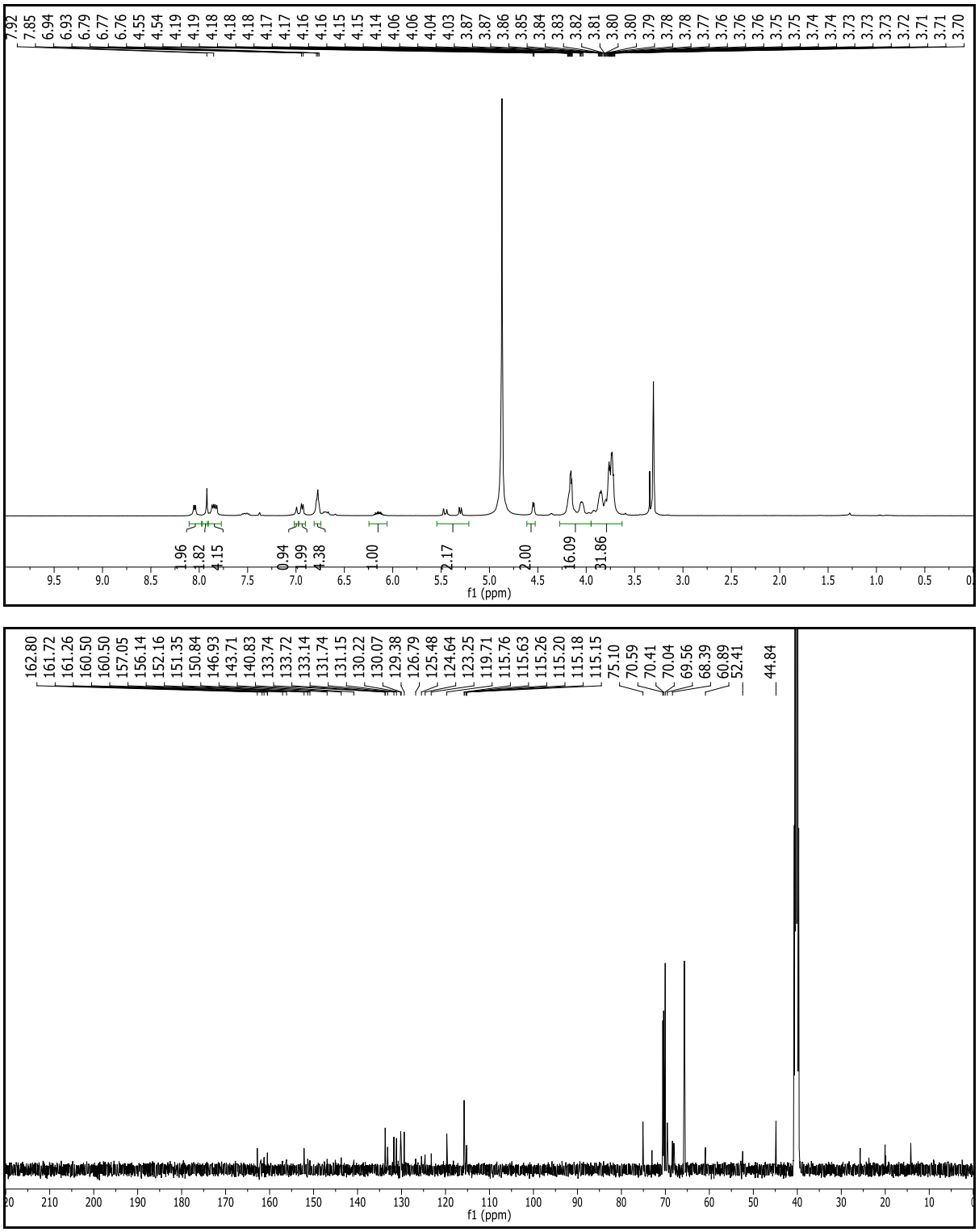

Figure F.30. ^{1}H NMR (500 MHz, $CDCl_3$) and ^{13}C NMR (125 MHz, $CDCl_3$) spectra of **33**.

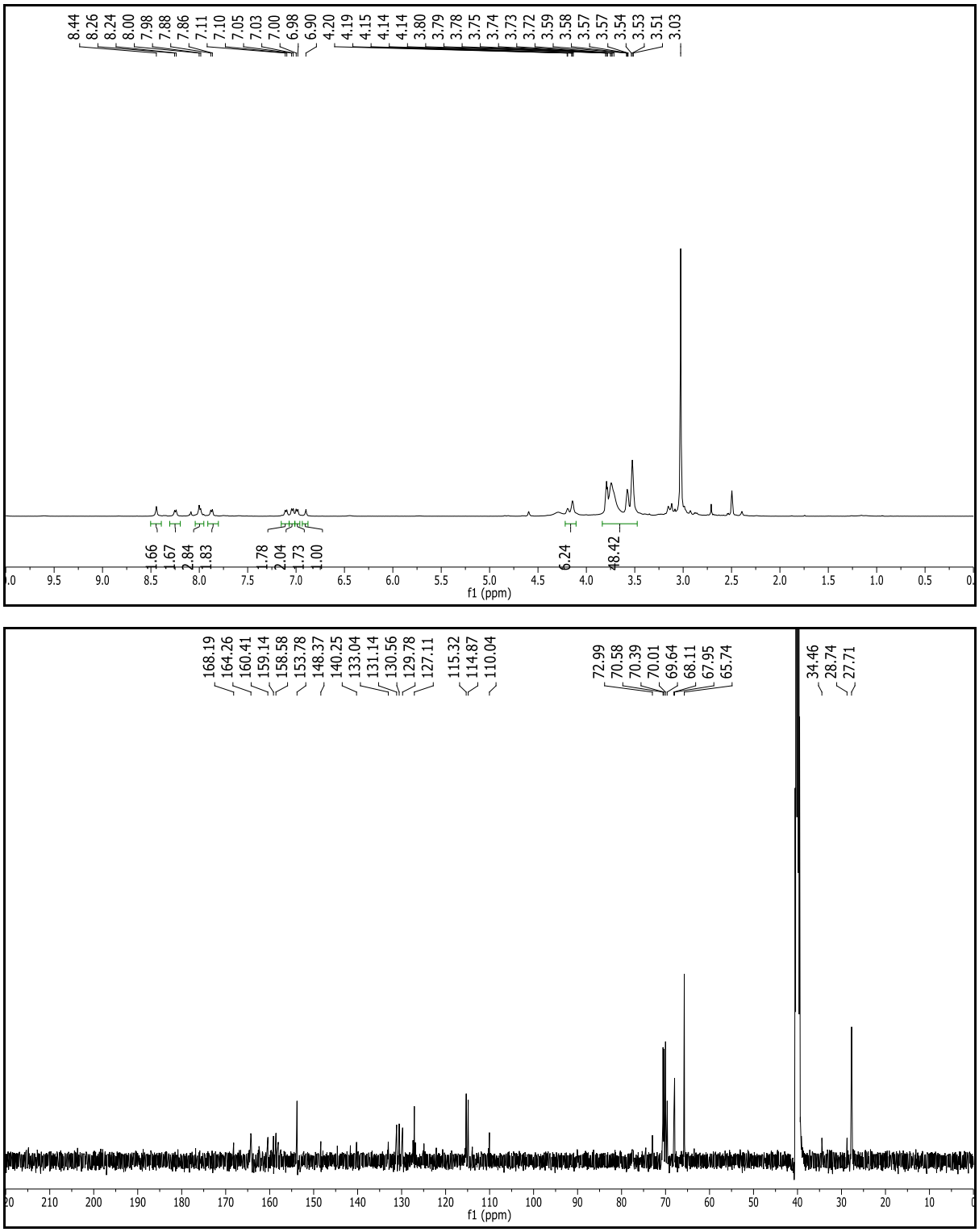

Figure F.31. ^{1}H NMR (500 MHz, DMSO-d6) and ^{13}C NMR (125 MHz, DMSO-d6) spectra of **34**.

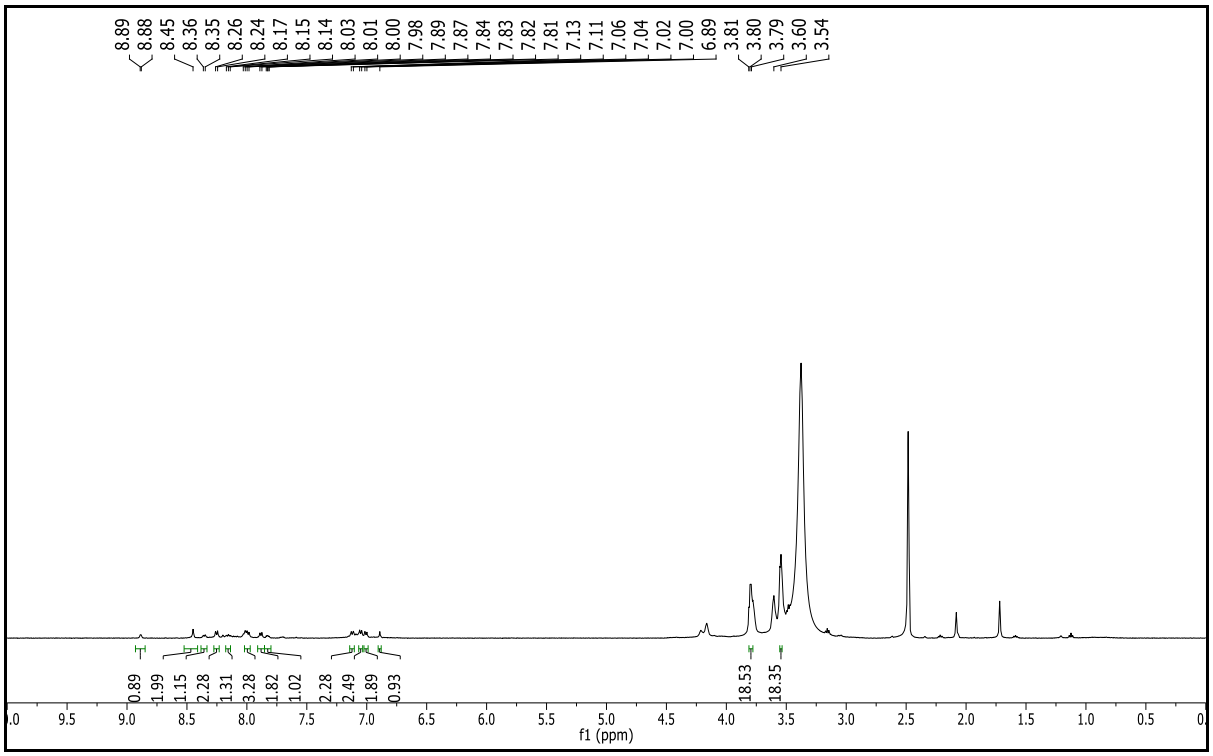

Figure F.32. ^{1}H NMR (500 MHz, DMSO-d6) spectrum of APC-2.